UNIVERSITY OF SOUTHAMPTON

FACULTY OF NATURAL AND ENVRIONMENTAL SCIENCES

Ocean and Earth Sciences, National Oceanography Centre Southampton

A LAB-ON-CHIP SENSOR FOR *IN SITU* SPECTROPHOTOMETRIC MEASUREMENT OF SEAWATER pH

by

Tianya Yin

Thesis for the degree of Doctor of Philosophy

September 2017

子曰：学而不思则罔，思而不学则殆。

——《论语·为政》

Learning without reasoning leads to confusion,

Thinking without learning is effort wasted.

— Confucius

UNIVERSITY OF SOUTHAMPTON

ABSTRACT

FACULTY OF NATURAL AND ENVIRONMENTAL SCIENCES

Ocean and Earth Sciences

Thesis for the degree of Doctor of Philosophy

A Lab-on-Chip Sensor for in situ Spectrophotometric Measurement of Seawater pH

Tianya Yin

Accurate and high precision measurements of seawater pH are important for monitoring of ocean acidification and to fully understand the dynamics of the oceanic carbonate system. An optimisation and field testing of an *in situ* pH sensor, based on lab-on-chip technology, offers potential to address to this problem. The sensor employs a spectrophotometric method, with high precision (0.001 pH units) and accuracy (0.005 pH units) within the range of a certified TRIS buffer. In addition, it is a compact miniaturised field analyser that consumes minimal power (3 W) and uses low reagent consumption (2.2 µL per analysis). A newly developed Absorbance-Derivative method is used to eliminate indicator-induced pH perturbation; automatically correcting approximately ±0.08 pH units perturbation for each individual analysis. Another R-correction calibration method is also studied, resulting an accuracy of ±0.005 pH units, thereby providing an easy but also sufficiently accurate way to calibrate pH sensors. A recipe for preparing TRIS buffer with any pH value between 7.4 and 8.4, and with any salinity between 20 and 40 psu

is resented, with initial verification suggesting an accuracy of ±0.004 pH units. The sensor has been field tested under various conditions, including vertical profiling, a brackish water moored deployment and a seawater moored deployment. A three-month pontoon deployment was performed, with an accuracy of ±0.003 pH units recorded over a 2 week period. However, biofouling in the inlet filter caused a diurnal offset up to 0.1 pH units, indicating that the next version of this pH sensor should focus on anti-biofouling technology.

Table of Contents

List of Figures

List of Tables

Declaration of Authorship

I, Tianya Yin, declare that this thesis entitled “A Lab-on-Chip Sensor for in situ Spectrophotometric Measurement of Seawater pH” and the work presented in it are my own and has been generated by me as the result of my own original research.

I confirm that:

1. This work was done wholly or mainly while in candidature for a research degree at this University;
2. Where any part of this thesis has previously been submitted for a degree or any other qualification at this University or any other institution, this has been clearly stated;
3. Where I have consulted the published work of others, this is always clearly attributed;
4. Where I have quoted from the work of others, the source is always given. With the exception of such quotations, this thesis is entirely my own work;
5. I have acknowledged all main sources of help;
6. Where the thesis is based on work done by myself jointly with others, I have made clear exactly what was done by others and what I have contributed myself;
7. None of this work has been published before submission.

Signed: .....

Date: 25/09/2017 .....

Graduate School of the National Oceanography

Centre Southampton

This PhD dissertation by Tianya Yin has been produced under the supervision of the following persons:

Supervisors

Prof. Matthew Mowlem

Prof. Martin Palmer

Chair of Advisory Panel

Dr. Douglas Connelly

Acknowledgements

First, I would like to thank my supervisors Prof. Matt Mowlem and Prof. Martin Palmer for giving me the opportunity to work on this thesis. I would like to thank Matt for all his advises in technique, which I learnt so much from, and his firm support when I was in need. I would like to thank Martin for his encouragement and guidance throughout my PhD study, for showing me what a true scientist is.

I would like to thank my advisory panel chair Dr Doug Connelly, for his encouragement, and his management of the SenseOCEAN project which gave me the chance to participate.

I would like to thank Dr Socratis Loucaides for his questions and insight that have been brought to my attention through our discussion of results from the optimisation and the research of new methods. I am grateful to Socratis for his help in the XPRIZE competition.

I would like to thank Victoire Rérolle for designing the sensor and teaching me the spectrophotometric method. I would like to thank Dr Martin Arundell for the assembling and maintaining of the sensors and the help in pontoon deployment at NOCS.

I am grateful to Dr Christopher Cardwell for continuously providing the electronics boards. I thank Dr Ed Waugh for his version of software to control the sensor in the early stage of this study, and John Walk for the later “WetChem” software that significantly improves the controlling. I thank Gregory Slavik for the fabrication of the sensors’ chips. I thank Dr Andrew Morris for calibrating the thermometer I used on spectrophotometer. Special thanks go to Dr Sebastian Steigenberger, our

chemistry lab manager, for his management and help in the laboratory's instrumentation. I thank Dr Alexander Beaton for his advises in sensor deployment.

Thanks go to Dr Jennifer Clarke for teaching me how to prepare TRIS buffer.

Thank you to the NOC sensor group for sharing experience and tips in sensor development.

My special thanks go to my fantastic officemates for their company. You are among the truly treasure I have earned from my PhD.

This work was supported by China Scholarship Council (CSC) (certificate no. 201306320178). Gratitude to the Wendy Schmidt Foundation and the XPRIZE Foundation for sponsoring the Wendy Schmidt Ocean Health XPRIZE, results from which directed the improvement of the sensor.

Finally I would like to thank my parents for their sacrificial love and support in the past four years, 5,600 miles away. I love you too.

Chapter 1 Introduction

1.1 Atmospheric CO_2 and ocean acidification

Since the beginning of the industrial revolution, the consumption of fossil fuels and the change of land-use by human activity have poured massive amounts of carbon dioxide (CO_2) into the Earth's system. As a result, the atmospheric CO_2 concentration has increased from 280 parts per million (ppm) to 405 ppm in August 2017 (Figure 1-1) and is predicted to rise to 950 ppm by 2100 under the Intergovernmental Panel on Climate Change (IPCC) business-as-usual emission scenario (PCR8.5) (Ciais et al., 2013). Approximately 30% of total anthropogenic CO_2 emissions are taken up by the ocean (Le Quéré et al., 2015), shifting the ocean's carbonate system equilibrium, with a reduction in seawater pH. It is estimated that the average surface-ocean pH has decreased by 0.1 pH units since its preindustrial level (Caldeira and Wickett, 2005) and will reach a level between 7.6 (Arctic) and 7.8 (tropics) by end of this century under PCR8.5 (Ciais et al., 2013). The phenomenon of the reduction of seawater pH is termed ocean acidification, indicating that the concentration of the hydrogen ion ($[H^+]$) increases.

Ocean acidification reduces the concentration of carbonate ion (See section 1.2), decreases calcium carbonate ($CaCO_3$) saturation states and increases its dissolution rates, hence can affect shell formation for marine animals such as corals, plankton, and shellfish (Byrne et al., 2011; Nakamura et al., 2011). This process could affect fundamental biological and chemical processes of the sea in coming decades (Pörtner et al., 2014; Wong et al., 2014). The changes in the marine-carbonate system would also

reduce the ocean's capacity to absorb future atmospheric CO_2 emissions, which means that the increase in atmospheric CO_2 levels would be accelerated (Canadell et al., 2007).

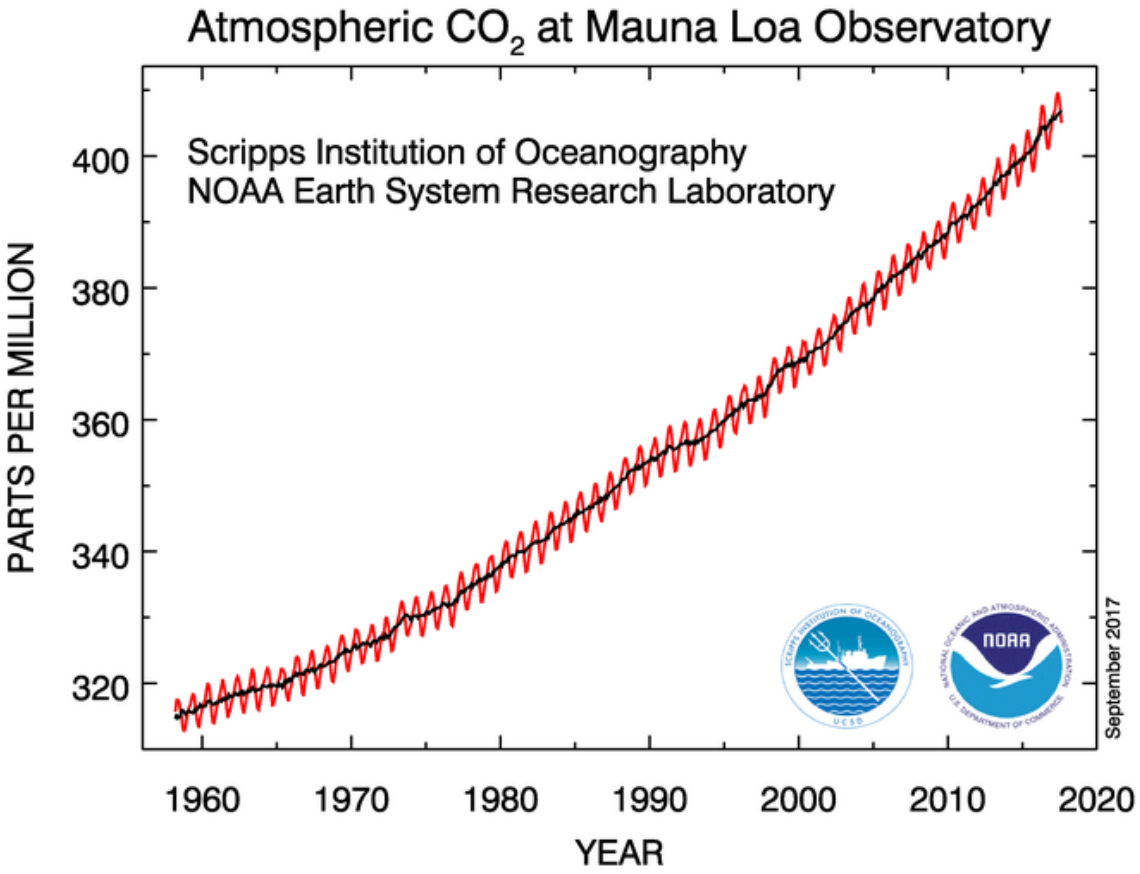

Figure 1-1: Time series of atmospheric CO2 level at Mauna Loa, data from NOAA/ESRL.

Reports estimate that the ocean's pH is presently decreasing with a rate of -0.0017 pH units per year by from an analysis of time-series measurements covering several decades (Bates et al., 2012; Dore et al., 2009; Feely et al., 2009; Gonzalez-Davila et al., 2010). However, the vastness, remoteness and complex nature of the ocean means that the spatial and temporal resolution of pH measurements is currently still insufficient (Takahashi et al., 2009). Widespread measurements, particularly on small platforms as part of a global observing system, will only be possible with the use of low-cost sensors featuring low power and resource (e.g. reagent) consumption. Miniaturized pH systems with high analytical precision and accuracy

would be optimal for deployment on oceanic moorings and small vehicles to allow large scale monitoring of ocean acidification.

1.2 Marine carbonate chemistry

Once CO_2 has dissolved, it exists in three main forms: free aqueous carbon dioxide ($CO_2(\text{aq})$), bicarbonate (HCO_3^-) and carbonate (CO_3^{2-}) ions. A minor form is true carbonic acid (H_2CO_3) with a concentration of less than 0.3% of $[CO_2(\text{aq})]$. The sum of $[CO_2(\text{aq})]$ and $[H_2CO_3]$ is denoted as $[CO_2]$. The equilibrium can be expressed as below: (Gattuso and Hansson, 2011)

$$CO_2(g) \overset{K_0}{\Leftrightarrow} CO_2 \tag{1-1}$$

$$CO_2 + H_2O \overset{K_1^*}{\Leftrightarrow} H^+ + HCO_3^- \tag{1-2}$$

$$HCO_3^- \overset{K_2^*}{\Leftrightarrow} H^+ + CO_3^{2-} \tag{1-3}$$

where the parameter K_0 is the solubility coefficient of the CO_2 in seawater. The concentration of dissolved CO_2 and the fugacity of gaseous CO_2, fCO_2, obey the equation

$$[CO_2] = K_0 \times fCO_2 \tag{1-4}$$

The fugacity is practically equal to the partial pressure, pCO_2 (within ~1%). The first and second dissociation constants of carbonate acid are given by

$$K_1^* = \frac{[H^+][HCO_3^-]}{[CO_2]} \tag{1-5}$$

$$K_2^* = \frac{[H^+][CO_3^{2-}]}{[HCO_3^-]} \tag{1-6}$$

$pK_1^*(= \log_{10} K_1^*)$ = 5.94 and pK_2^* = 9.13 at temperature $T = 15$℃, salinity $S = 35$, and surface pressure $P = 1\ atm$ on the total pH scale (Lueker et al., 2000). At a

typical surface-seawater pH_T of 8.2, the speciation between $[CO_2]$, $[HCO_3^-]$ and $[CO_3^{2-}]$ is 0.5%, 89%, and 10.5%, showing that most of the dissolved CO_2 is in the form of HCO_3^- and not CO_2.

1.3 Definition of pH and pH scales

pH is a numeric scale used to specify the acidity or basicity of an aqueous solution. It is defined as the decimal logarithm of the reciprocal of the hydrogen ion activity. a_{H^+}, in a solution.

$$pH = -\log a_{H^+} \approx -\log[H^+] \quad (1\text{-}7)$$

where the hydrogen ion concentration is expressed in moles per kilogram of solution (Dickson et al., 2007). The symbol 'log' in this thesis is the abbreviation of $\log_{10}$.

In chemical oceanography, different pH scales have been used. The use of different pH scale may cause errors between different data set (Table 1-1), therefore it is important to make clear which pH scale is used before comparing reported pH values. There are four pH scales that are mostly commonly used: the IUPAC NBS pH scale, the free hydrogen ion scale, the total pH scale and the seawater pH scale. The IUPAC NBS pH scale is based on low ionic strength buffer standards from the US National Bureau of Standards (NBS) and is universally used in laboratories. However, this scale is not suitable for seawater pH measurement, because the high ionic strength of seawater will introduce additional significant liquid junction potential error (Chen, 2009). The free hydrogen ion scale only takes into account the free hydrogen ions (Bates and Culberson, 1977), whereas the total pH scale also considers sulphate (Hansson, 1973), and the seawater pH scale includes sulphate and

fluoride complexes. In oceanic carbonate chemistry research, the total hydrogen ion scale is recommended (Dickson et al., 2007). In the total pH scale, pH is defined by

$$pH = -\log([H^+]_F + [HSO_4^-]) = -\log[H^+]_T \quad (1\text{-}8)$$

The use of this scale avoids problems associated with uncertainties in the stability constants for fluoride complexes which are required for the seawater pH scale, or the measurement of sulphate concentration as well as dissociation constant for the free hydrogen scale. Importantly, a certified pH buffer based on the total pH scaleis now available from the laboratory of Prof. A.G.Dickson, Scripps Institution of Oceanography, San Diego (DelValls and Dickson, 1998; Nemzer and Dickson, 2005). This buffer is made of 2-amino-2-methyl-1,3-propanediol (TRIS) in artificial seawater. There is no certified reference material available based on the other seawater pH scales.

Table 1-1: The offset in pH value applying with different pH scales.

pH scale	Application	Standard material	pH_F-pH_i (pH units)
pH_{NBS}	Freshwater	Pure water	-
pH_F	Seawater	Artificial seawater	-
pH_T	Seawater	Artificial seawater	0.11
pH_{SW}	Seawater	Artificial seawater	0.12

1.4 Analytical techniques for seawater pH measurement

1.4.1 Potentiometric methods

1.4.1.1 Glass electrode

The glass electrode is a classic method for pH measurement, which is still widely used in various fields. The pH of a sample is defined in terms of the electromotive

force (EMF) measured in the sample (E_{sample}) and a standard buffer solution (E_{buffer}) of assigned pH (pH_{buffer}):

$$pH_{sample}=pH_{buffer}+(E_{buffer}-E_{sample})F/(RTln10) \quad (1\text{-}9)$$

where R is the gas constant, T is the measurement temperature and F is the Faraday constant.

The advantages of the potentiometric method are that it is non-destructive, the equipment is relatively cheap and it can achieve a high frequency rate of measurements (>1Hz) (Hemmink et al., 2009). It is also relatively easy to miniaturize. However, because the potentiometric method requires quantification of small electromotive forces, a high input impedance is required and this is sensitive to temperature and humidity and the impedance can be reduced by environment change. Therefore, this method can suffer from significant measurement drift (up to 0.02 pH units per day) (Seiter and DeGrandpre, 2001). Hence regular calibration is required, making autonomous measurements problematic. Other problems include electromagnetic interferences, residual liquid-junction potentials and variations in asymmetry potential. The junction potential is generally attributed to ionic interdiffusion at a direct (liquid-liquid) interface between the measured sample and the junction electrolyte. Potentiometric pH sensors rarely achieve an accuracy of better than 0.01 pH units (Seiter and DeGrandpre, 2001), which are unsuitable for chemical oceanography.

1.4.1.2 ISFET sensors

Briefly, an ion sensitive field effect transistor (ISFET) is a metal oxide semiconductor field effect transistor without a metal gate electrode, but with a reference electrode over the conduction channel (Martz et al., 2010). The conduction

channel is covered by a thin insulating layer of amphoteric material such as silicon nitride, aluminium oxide, yttrium oxide, or tantalum pentoxide (Bergveld, 2003). The concentration of hydrogen ion (pH) of the solution at the insulator/solution interface controls the site-binding protonation/deprotonation state of the insulator material and, hence, the surface charge at the interface. The interfacial charge determines the strength of the electric field in the conduction channel of the FET, located between the source and the drain. The pH value is obtained by the voltage between the reference electrode and the source electrode, which follows a Nernst equation form.

ISFETs have low power consumption of about 2 mV (Martz et al., 2010) and rapid pH response on the scale of 15 seconds (Bresnahan et al., 2016; Briggs et al., 2017) due to the high specific surface area. They also have good potential to be miniaturized (Chou and Weng, 2001) as well as low cost (Hemmink et al., 2009). The stability of ISFET can be better than 0.005 pH units over periods of weeks to months, and short-term precision is about ±0.0005 pH units over several hours, for in situ applications at 1 atm (Martz et al., 2010). Johnson et al. (2016) reported a pressure-tolerant ISFET pH sensor called Deep-Sea DuraFET that performed a profiling down to 1000 m. Products of Honeywell Durafet have been successfully tested over a wide range of environments including dynamic estuary (Gonski et al., 2018) and coastal water (McLaughlin et al., 2017). Efforts were made to integrate two CO_2 parameter measurements, pH and total alkalinity, on the same ISFET in order to reduce the cost and complexity of sensor (Briggs et al., 2017). Despite its rapid and impressive development in recent years, ISFET pH sensor still have some issues needed to deal with, such as hysteresis caused by the reference electrode

(Johnson et al., 2016) and prolonged pre-conditioning prior to deployment (Gonski et al., 2018).

1.4.2 Luminescence method

The luminescence method is based on the variation of luminescent pH indicator dye emission characteristics (intensity, absorbance or lifetime) with hydrogen-ion concentration. Fluorescence is a form of luminescence and it has a relatively short ($<10^{-7}$s) (Hecht et al., 2013) optical response output after excitation is turned off, compared to other luminescence methods.

Luminescence sensors can be divided into absorption-cell-based sensors (Hakonen et al., 2013) and solid-matrix sensors (optodes) (Aigner et al., 2012; Hecht et al., 2013). In the type with an absorption cell, indicator dye and sample are injected by pump and mixed through a channel before being measured in the cuvette. In Hakonen et al. (2013)'s work, the mixture is irradiated by an LED and the luminescence recorded by a camera. This method works on a similar principle to the spectrophotometric method, but employs a camera instead of a spectrophotometer as detector. While in the optode case, the indicator dye is usually prepared as sensor beads with polymer and solvent, and the mixture is coated on to a sensor substrate (Aigner et al., 2013).

Except for absorption-cell-based sensors, optodes have good potential for miniaturisation because they do not require a reference electrode or mixing procedures (Clarke et al., 2015; Fages et al., 2013). They also have a theoretical potential for high resolution (Aigner et al., 2014). Optode pH measurements are highly ironic strength-dependent, especially between salinity 25 and 35, on the scale

of -0.01 pH units per salinity psu (Clarke et al., 2015; Hakonen et al., 2013). Therefore the ironic strength effects should be compensated fit if precise (better than 0.02 pH units) measurement is required. One of the attempts is multi-linear regression of T and S for fluorescent signal conversion to pH yielding a standard error of 0.005 pH units (Clarke et al., 2015).

Optodes have attracted scientific interests because of its potential of miniaturisation and fast response as well as encouraged by the success of oxygen and pCO2 optodes. Nevertheless, further research are still needed to deal with issues such as indicator leaching (Wencel et al., 2014), the mismatch between pK_a and seawater pH and internal temperature measurement in order to approach precise and stable measurements (Clarke et al., 2015).

1.4.3 Spectrophotometric method

Although the use of colorimetric indicator dyes for seawater pH measurement dates back to the early 20th century (McClendon, 1917), it was not until in 1980s when Byrne and his co-workers developed the method (Byrne, 1987; Byrne and Breland, 1989; Robertbaldo et al., 1985) so that it could be used to determine seawater pH with high repeatability, i.e. a precision, of 0.0004 pH units (Clayton and Byrne, 1993). This method is based on the addition of an indicator dye, usually a sulfonephthalein compound, into the seawater sample, and measuring the distinct absorbance at wavelengths where the two forms of the dye – the protonated and the deprotonated terms – absorb the most of light, respectively. The detailed theory of this method is described in Section 1.5.

Spectrophotometric method is currently the most precise and accurate method to determine seawater pH (Okazaki et al., 2017). By using purified indicator dye (Liu et al., 2011; Yao et al., 2007) the accuracy of spectrophotometric pH method can reach 0.004 pH units (Lai et al., 2016), which is much more accurate than the pH electrode, whose accuracy is on the order of 0.10 pH units (Bockmon and Dickson, 2015; Yao and Byrne, 2001).

Automated systems for spectrophotometric seawater pH measurements have been developed ever since (Aßmann et al., 2011; Bellerby et al., 2002; Carter et al., 2013; Martz et al., 2003; Rérolle et al., 2013). They generally consist of a pump for injecting both indicator and sample, a mixer where the indicator and the sample mix well so as to reach a steady temperature (e.g. 25°C), and an absorption cell attached to a light source and a detector (a spectrophotometer) where the absorbance are recorded. Over the years, these systems have tended to become smaller in size, and more affordable. Adornato et al. (2016) developed a portable carbon system sensor comparable in size to a large briefcase. By integrating a low cost system, such as using a light emitting diode as light source (Yang et al., 2014) and a photodiode as the detector (Perez de Vargas Sansalvador et al., 2016), the cheaper price would allow wider and more frequent deployment around the world. Another trend is that the simultaneous measurements of carbonate parameters is increasing benefiting from the development of a compact design. Wang et al. (2007) reported an autonomous multi-parameter flow-through CO_2 system capable of measuring surface seawater pH, carbon dioxide fugacity and total inorganic carbon concentrations simultaneously. An updated version was later reported (Wang et al., 2015). Over-determination of the seawater carbonate system (DIC, TA, pH and fCO_2) help to support the accuracy and precision assessment in comparison to earlier data (Friis et

al., 2004) as well as improving quality control to constrain the accuracy of other carbonate system parameters (McElligott et al., 1998).

More interest in recent years has focused on the long-term *in situ* application of the spectrophotometric pH method. SAMI-pH (Seidel et al., 2008) is one good example. Adapted from a sensor originally developed for freshwater pH measurement, the new SAMI-pH uses a custom made Z-cell, where the flow enters the optical path at a 45° angle, in order to help flush the area in front of the fibre optic input and output. This effective design influenced later sensors such as those described by Rérolle et al. (2013) and Wang et al. (2015). Updated SAMI2 (Spaulding et al., 2011) provides better signal-to-noise ratio and lower power consumption, which makes it capable of being deployed on platforms such as gliders and moorings. The SAMI-pH is now commercialised, and field deployed (Gray et al., 2011), and won the $2 million Wendy Schmidt Ocean Health XPRIZE (Okazaki et al., 2017). The sensor precision was 0.0003±0.0016 pH units (Spaulding et al., 2011) and the measurement frequency was programed as every 15 minutes (Seidel et al., 2008).

In order to recognise existing and promising new commercial technologies, the Alliance for Coastal Technologies (ACT) conducted a verification of in-situ pH sensors during 2013 and 2014. This aimed to characterise performance measures including accuracy and reliability by a series of controlled laboratory studies and field mooring tests in diverse costal environments (www.act-us.info/evaluations.php#ph). These evaluations provide an unbiased, comprehensive investigation into the technologies available on the market. Seven companies participated in the evaluation, which included sensors based on three principles:

spectrophotometric, ISFET and glass electrode methods. SAMI-pH was the only example of a spectrophotometric sensor, whereas ISFET method pH sensors included the SeaFET and Cambell Scientific Instruments pH (CSI-pH). Glass electrode technologies were the Indronaut Ocean Seven 305 Plus CTD (IOS-CTD), EXO2, In-Situ Troll 9500 and Eureka Manta2.

The first verification test was a ten-week laboratory study, which included conditions at three salinities: 35 (salt water), 20 (brackish water) and 0.03 (fresh water). This lab test also included several rapid pH change experiments to test the sensors' performance in dynamic environments. Four moored field deployments involved environments of coastal seawater (Moss Landing Harbour, California), seawater in reefs (Kaneohe Bay, Hawaii), brackish water (Chesapeake Bay, Virginia) and fresh water (Lake Michigan, Michigan). The SAMI-pH performed best on average of all the pH sensors. The SAMI-pH sensorusingmeta-cresol purple (mCP) as the indicator dye obtained an accuracy of the magnitude of 0.01 pH units in the lab tests, -0.014 to 0.04 pH units in field tests when salinity was higher than 20, and -0.162 pH units when the sample was freshwater. The large offset in freshwater originated from the equilibrium constant for the indicator mCP, which was not well known at low salinity. The SAMI-pH prototype with indicator phenol red (PR) gained a better accuracy of 0.021±0.047 pH units in the Lake Michigan deployment, highlighting the importance of the equilibrium constant in the spectrophotometric pH measurement.

In other pH sensor categories, the Satlantic SeaFET performed well too. Due to an electronics problem with one of the circuit boards there was no reportable data for the SeaFET in the lab test. In moored field tests, SeaFET reported -0.008±0.029, -

0.014±0.009, -0.001±0.007 and -0.183±0.040 in coastal seawater, reefs seawater, brackish water and freshwater respectively. Glass electrodes generally produced a precision of ±0.05 pH units, with accuracy varying from -0.05 to 0.1 pH units in different environments. Note that the glass electrodes were calibrated with NBS buffers and the offset between NBS scale and total pH scale, i.e. 0.13 pH units, is considered in this review. Glass electrodes also have to compensate for the exhaustion and depletion of internal electrolyte in the reference electrode. Submersible reference sensors have a limited reservoir of electrolyte.During immersion, the internal electrolyte will be gradually lost over time and possibly replaced with ions from the sample. This will result in an offset due to causing the sensor to lose its ability to maintain a stable liquid junction potential.. This offset cannot not be corrected by re-calibration unless the electrolyte is replaced.

1.5 Spectrophotometric theory

Spectrophotometric pH determination is based on the addition of an indicator dye to a seawater sample which changes its optical properties with pH. The dye selected is usually an acid-base compound with a second dissociation constant that is close to the pH of seawater (Dickson et al., 2007) (typically, ~7.6 to 8.3). The solution (sample with indicator) pH can be calculated from the acid-dissociation constant and the concentration of the protonated (HI^-) and the deprotonated (I^{2-}) forms of the indicator dye.

All sulfonephthalein indicators exist in three forms – H_2I, HI^- and I^{2-} – and each has distinctive absorption characteristics. The chemical equilibria between these three forms can be described by stepwise dissociation constants:

$$H_2I \overset{K_1}{\Leftrightarrow} HI^- + H^+ \quad (1\text{-}10a)$$

$$HI^- \overset{K_2}{\Leftrightarrow} I^{2-} + H^+ \quad (1\text{-}10b)$$

According to Beer-Lambert's law, the absorbance due to dye in solution is described by:

$$A_\lambda = \left(\varepsilon_\lambda^I[I^{2-}] + \varepsilon_\lambda^{HI}[HI^-] + \varepsilon_\lambda^{H_2I}[H_2I]\right)b \quad (1\text{-}11)$$

Where A_λ is the absorbance at wavelength λ, ε_λ^X is the molar absorptivity of species X at wavelength λ, [] denotes concentration, and b is the optical pathlength. The wavelengths of maximum absorption for the three forms of meta-Cresol Purple (mCP) are (Clayton and Byrne, 1993):

λ_0 = 529 nm = wavelength maximum of $\varepsilon_\lambda^{H_2I}$,

λ_1 = 434 nm = wavelength maximum of ε_λ^{HI}, and

λ_2 = 578 nm = wavelength maximum of ε_λ^I

Algebraic manipulation of equation (1-10) and (1-11) can be used to derive the equation to calculate pH (the detailed process is described in Clayton and Byrne (1993):

$$\mathrm{p}H_T = \mathrm{p}K_2 + \log\left(\frac{R - e_1}{e_2 - Re_3}\right) \quad (1\text{-}12)$$

where $K_2 = [H^+]_T[I^{2-}][HI^-]^{-1}$, $R = A_2/A_1$, $e_1 = \varepsilon_2^{HI^-}/\varepsilon_1^{HI^-}$, $e_2 = \varepsilon_2^{I^{2-}}/\varepsilon_1^{HI^-}$, $e_3 = \varepsilon_1^{I^{2-}}/\varepsilon_1^{HI^-}$. The subscript T denotes the total hydrogen ion scale of pH.

Liu et al. (2011) simplified equation (1-12) with fewer parameters as:

$$\mathrm{p}H_T = -\log(K_2^T e_2) + \log\left(\frac{R - e_1}{1 - R\frac{e_3}{e_2}}\right) \quad (1\text{-}13)$$

The e_3/e_2 ratio is obtained directly in synthetic solutions with compositions similar to seawater, at a pH sufficiently high (i.e. 12) that species other than I^{2-} are negligible. The initial estimation of e_1 value can be obtained in a solution at low pH (i.e. 4.5),

where HI^- is the predominant form of mCP. The initial estimation of $pK_2^T e_2$ can be determined as a single parameter by measuring the absorbance ratio *R* in a solution of known pH_T (e.g. Tris buffer solution in synthetic seawater). An iterative procedure is then applied to refine e_1 and $pK_2^T e_2$. This process is described in Clayton and Byrne (1993) and Liu et al. (2011).

At pH = 12, the dye is almost exclusively in the I^{2-} form ($[I^{2-}]/[HI^-]=10^4$), and equation (1-11) can be written as:

$$A_{434} = b\varepsilon_{434}^{I^{2-}}[ind] \tag{1-14a}$$

$$A_{578} = b\varepsilon_{578}^{I^{2-}}[ind] \tag{1-14b}$$

If the absorbance at the two wavelengths is measured in the same sample at the same time, then the indicator concentration and the pathlength are ensured to be identical. When the dye is injected into a long serpentine channel and mixed with the sample (synthetic seawater) that passes slowly through the channel, a Taylor dispersion forms, The change of absorbance with time at any fixed point (the detector) is then due to the changing concentration of $[I^{2-}]$ passing through the optical cell. Hence the ratio of the extinction coefficients can be determined as the slope of the two absorbance at the two wavelengths:

$$e_3/e_2 = \varepsilon_1^{I^{2-}}/\varepsilon_2^{I^{2-}} = A_{434}/A_{578} \tag{1-15}$$

Similarly, at pH=4.5, the dye is >99.8% HI^- and the $\varepsilon_1^{HI^-}$ and $\varepsilon_2^{HI^-}$ are given by;

$$e_1 = \varepsilon_2^{HI^-}/\varepsilon_1^{HI^-} = A_{578}/A_{434} \tag{1-16}$$

We use the spectrophotometric dye mCP as it is well studied, and has an appropriate pK_2 of 8.0 at 25°C, S=35, close to that of mean seawater 8.1. We use purified mCP to avoid the need to characterise each batch of dye (Yao et al., 2007) using the

standard method as described in (Clayton and Byrne, 1993; Liu et al., 2011; Seidel et al., 2008).

The pH indicator characteristics ($K_2^T e_2$, e_1, e_3/e_2) can be described as a function of temperature and salinity by the equations (Liu et al., 2011):

$$pK_2^T e_2 = a + \left(\frac{b}{T}\right) + c \ln T - dT \quad (1\text{-}17)$$

Where

$$a = -246.64209 + 0.315971S + 2.8855 \times 10^{-4} S^2$$

$$b = 7229.23864 - 7.098137S - 0.057034S^2$$

$$c = 44.493382 - 0.052711S$$

And

$$e_1 = -0.007762 + 4.5174 \times 10^{-5} T \quad (1\text{-}18)$$

$$e_3/e_2 = -0.020813 + 2.60262 \times 10^{-4} T + 1.0436 \times 10^{-4} (S - 35) \quad (1\text{-}19)$$

This characterization is appropriate for temperatures of 278.15 K$\leqslant T \leqslant$308.15K and 20 $\leqslant S \leq$40, using purified meta-cresol purple (mCP).

1.6 Thesis objectives

The Ocean Technology and Engineering Group (OTEG) at National Oceanography Centre has experience of developing autonomous sensors for marine research for more than fifteen years. As part of the group projects, a bench-top autonomous microfluidic spectrophotometric system for seawater pH measurement was developed in 2012 (Rérolle et al., 2013). In 2013 the group decided to transfer the

bench-top system to a lab-on-chip platform. A prototype had been designed, manufactured and assembled in early 2014. My aim was to optimise the prototype in order to produce a system that can work with an accuracy of 0.005 and a precision of 0.001 pH units. The sensor should be able to work on moorings and floats for months without service. It needs to be robust, stable, yield precise data, have low power consumption and be calibration-free.

The performance of the sensor was assessed by a short-term deployment for the accuracy and precision, as well as a long-term deployment for the stability and robustness.

1.7 Thesis outline and novelty claim

Chapter 2 describes the construction of the sensor and its measurement protocol. All the sensors used in this thesis were originally designed by Vicotire Rérolle and manufactured in the Ocean Technology and Engineering Group (OTEG), National Oceanography Centre Southampton, with contribution of Gregory Slavik (chip manufacturing), Christopher Cardwell (electronics), Martin Arundell (assembling) and John Walk (firmware and user interface). The measurement protocol (Chapter 2.3) is based on the previous bench-top version (Rérolle et al., 2013), with optimised flow rate and updated data processing procedures which are my work.

Chapter 3 focuses on the error reduction of the sensor. It starts with the error analysis that reveals the source of measurement error and indicates the methods developed to eliminate them. Then an optimised thermistor calibration protocol is presented.

Finally a novel method to eliminate indicator-introduced pH perturbation is explained.

Chapter 4 presents two ways of calibration of the pH sensor and discusses the results. The first method is the conventional characterisation of the m-cresol purple indicator and the second is known as the R-adjusting method. This chapter also discusses the preparation of the non-equal mole TRIS buffer in synthetic seawater. This part of the work can also be transferred to wider applications in both marine chemistry and general analytical chemistry.

Unless otherwise mentioned, Chapter 3 and 4 are my work.

Chapter 5 presents the results of field deployments from the XPrize competition, the SenseOCEAN project and in the dock at NOCS. The XPRIZE competition (Chapter 5.1) was completed by Socratis Loucaides and myself, while I processed the data. The deployment in SenseOCEAN project and at the dock, along with the data process, was carried out by me, unless others' contribution are mentioned in the chapter.

Finally, Chapter 6 discusses potential future improvements in the sensor and possible methods to achieve these goals.

Chapter 2 Instrument

2.1 Introduction of lab-on-chip sensors

Since its introduction in the 1990s, Lab-on-Chip technology has attracted interest in its application to many fields. This interest largely arises because the technology allows miniaturization of analytical systems that are usually metre-scale (laboratory scale) to the square centimetre scale by development of specially designed microfluidic manifolds, integrated mini valves, pumps and other features. In aquatic environmental measurement and monitoring, microfluidic Lab-on-Chip platforms have been developed since the beginning of 21st century. Applications have included the determination of concentrations of nitrate (Beaton et al., 2012), nitrite, phosphate, lead (Jung et al., 2011), cadmium (Zou et al., 2009), reduced and oxidised iron species and manganese (Milani et al., 2015). Relatively few microfluidic sensors have, however, been developed to determine dissolved carbonate parameters. Rérolle et al. (2013) produced a microfluidic sensor for determination of pH, although this is a bench-top system, not designed for *in situ* use. Perez de Vargas Sansalvador et al. (2016) developed an autonomous microfluidic pH sensor platform (using a light-emitting diode, abbreviated LED, as the light source and a photodiode as the detector), yet it still contained a large syringe pump and was thus too large to be used for portable deployments.

The need for reliable in situ sensors of the marine carbonate systems arises because the oceans play an important role in global CO_2 system. For example, seawater absorbs approximately 25% of anthropogenic CO_2 emissions (Gattuso and Hansson, 2011). While the oceanic sink mitigates climatic changes, the oceans have become

more “acidic” by an estimated 0.1 pH units since the onset of the industrial revolution (Caldeira and Wickett, 2005), or 0.002 pH units per year on average. It is therefore important to monitor this change, preferably with precision and drift <0.002 pH, so that we can better understand how it affects the marine ecosystem and the global climate, both today and in the future. Unfortunately, the cost of mounting ship-based campaigns to monitor marine carbonate parameters means that at present most parts of the oceans are poorly sampled. Thus, there is an increasing demand for cheaper, faster and larger scale sampling. A promising approach is the development of low-cost, reliable and robust sensors than can be deployed easily throughout the oceans, especially in remote areas. Lab-on-Chip technology can provide a solution to this requirement.

Here, I describe the transfer of microfluidic technology from the bench top to *in situ* application, to measure the pH of seawater. The sensor is based on a tinted poly(methylmethacrylate) (PMMA) chip, assembled with controlling valves, pumps and processing electronic boards using similar componentry to nutrient sensors developed at the NOC (Beaton et al., 2012; Ogilvie et al., 2011). It is a field-deployable platform with: dimensions of ϕ120 mm × 120 mm (excluding the indicator dye reservoir and the power supply); low power consumption (3 W); low reagent consumption (2.2 μL per measurement); and low waste generation (1.3 mL per measurement). It can measure pH at a frequency of up to one analysis every 10 minutes with an accuracy of ±0.004 pH units and precision ±0.0005 pH units. The system is spectrophotometric-based, and thus is self-calibrated, and can yield results for deployments of several months.

2.2 NOC-pH sensor overview

2.2.1 Construction

The *in situ* pH sensor is derived from a previously developed bench-top pH system (Rérolle et al., 2013) and utilizes components developed for *in situ* nutrient analysers (Beaton et al., 2012). The *in situ* core system integrates a three-layer microfluidic chip, a syringe pump, two syringes, three controlling electronic boards, four controlling valves and two temperature-monitoring thermistors. The completed system also includes the housing, the batteries (optional) and reagent bags. The core system can be contained within a cylinder with dimensions of ϕ130 × 140 mm and has a weight in air of 920g. When housed together with external batteries, the complete system has dimensions of ϕ150 × 1000 mm and an air weight of 8000g, with the bulk of the volume and weight comprised of the batteries.

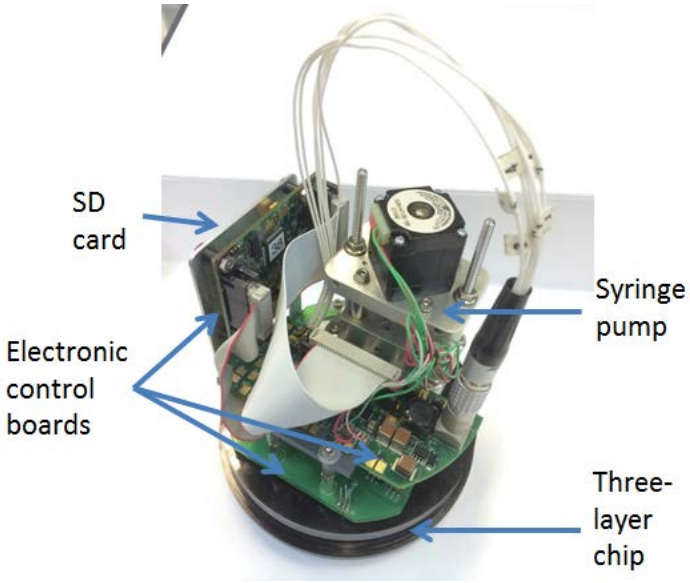

Figure 2-1: The pH sensor. The dimension of the chip is ϕ130 mm and the height from the bottom of the chip to the top of the pump is 140 mm. The white wire shown in the figure can be bend into the housing.

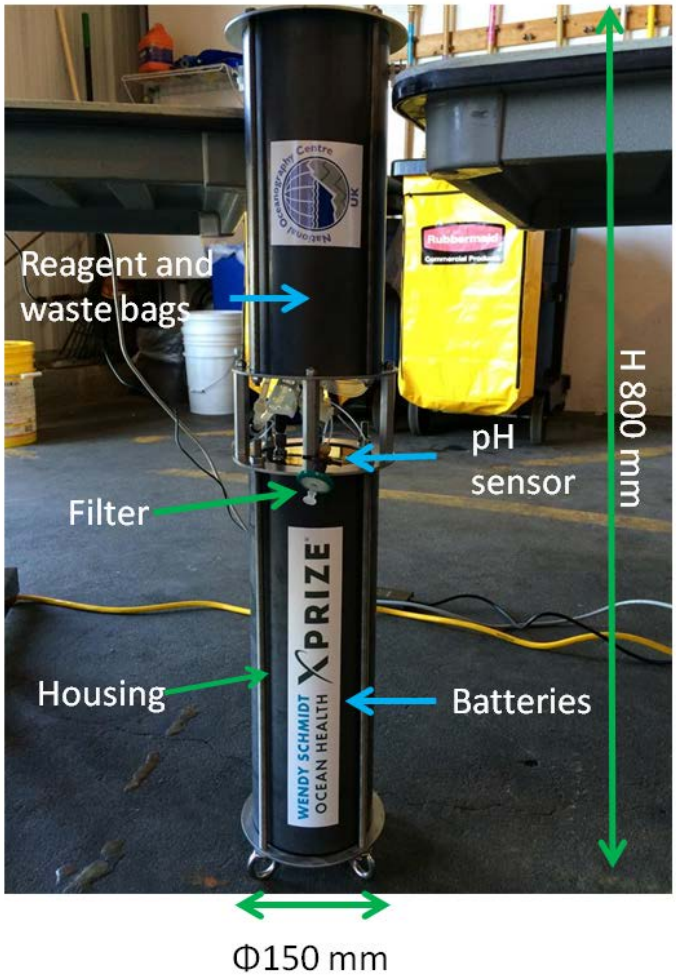

Figure 2-2: Integrated pH system, placing inside a housing with batteries, and reagent and waste bags. Blue colour implies the parts is inside the housing and green means outside.

2.2.2 Microfluidic chip

The three-layer microfluidic chip is the most important component of the system. It is made of tinted PMMA, which can be easily machined and the colouration prevents stray ambient light emitted by the LED that has not passed through the full absorption cell from entering the optical detector (Ogilvie et al., 2010). A 1300 mm-long, 250 μm × 250 μm-wide serpentine mixing channel was milled in the middle layer, along with the 10 mm-long, 300 μm × 300 μm-wide optical cell and probe holes for the thermistors. The upper and bottom layers were bonded to the middle layer using a solvent vapour bonding method (Ogilvie et al., 2010). The LED and

photodiode were then fixed into the pre-milled holes in the upper layer using glue (Opti-tec 5012, Intertronics). Subsequently, a custom-designed pump and other attachments (valves, boards and thermistors) were fixed into the upper layer. The detailed manufacturing process can be found in previously published papers (Beaton et al., 2012; Perez de Vargas Sansalvador et al., 2016).

The thermistors are used as internal temperature probes, with an accuracy better than ±0.03 K and precision better than ±0.005 K (for further information, see Chapter 3.2).

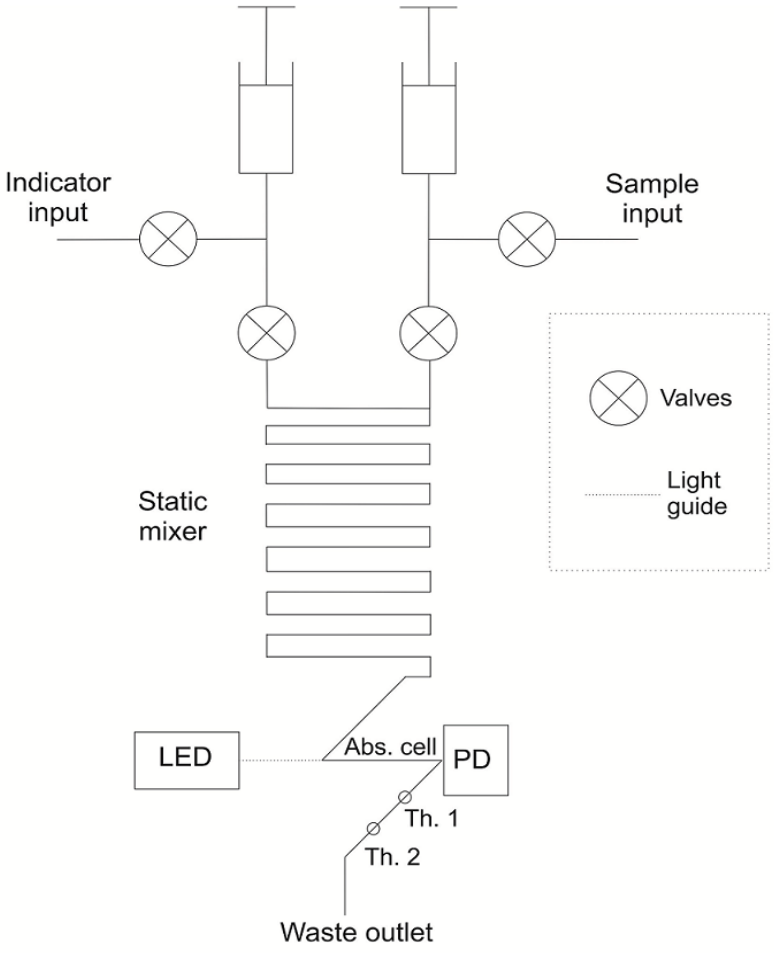

Figure 2-3 Schematic fluidic path diagram indicating the two syringes, four valves, absorption cell, LED, the light-to-voltage converter (photodiode or PD for short) and two thermistors. The two syringes are driven by the same pump.

2.2.3 Optical set up

The light source used in the sensor is a multi-wavelength light-emission diode (LED) containing two light sources whose peak wavelengths are 426 nm (with a width at half maximum, or FWHM, of 15 nm) and 590 nm (FWHM=15 nm), respectively. Compared to the indicator dye meta-Cresol Purple (m-CP) maximum absorbance wavelengths of 434 nm and 578 nm, the light source are slightly mismatched. This is due to the lack of a more appropriate LED on the market when the sensor was designed. However, by integrating the errors caused by wavelength offset into R-adjusting (see Chapter 4.2), this mistake can be taken into account.

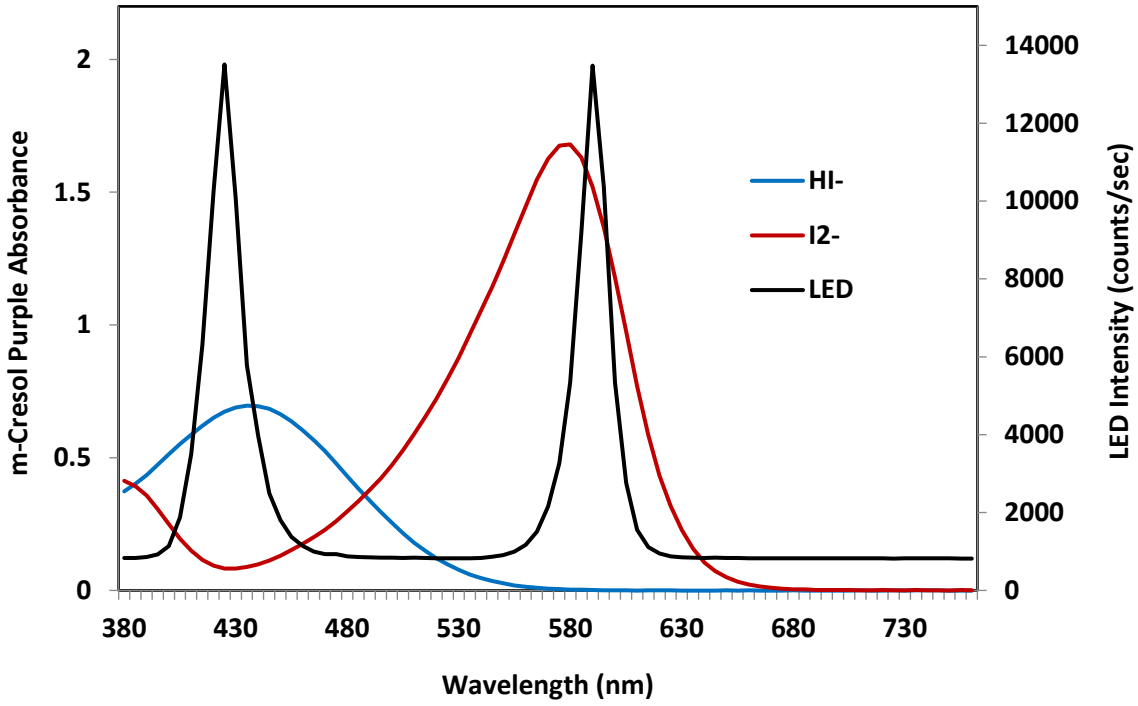

Figure 2-4: The spectrum of the LED comparing to the absorbance spectrum of the dye species: protonated HI^- and deprotonated I^{2-}

A light-to-voltage converter (TSL257, Texas Advanced Optoelectronic Solutions Inc., USA), consisting a photodiode and a transimpedance amplifier on a single monolithic complementary metal–oxide–semiconductor (CMOS) integrated circuit, is used in the sensor as the detector. The LED is modulated based on time-division multiplexing, which means the two light sources, 434 nm and 578 nm, switch on and off alternatively in a defined frequency that can be demodulated by the detector. Hence, although the detector only receives one light-intensity signal at a time, it can distinguish the intensity at two wavelengths respectively, and then send the two intensity readings to the build-in data storage for later pH calculation (Section 2.4).

2.2.4 Indicator stock solution

A 4 mmol/L lab-purified m-CP indicator stock solution in 0.7 mol/L NaCl is used for all measurements. The pH of the stock solution is adjusted to 8.1±0.1 pH units (room temperature, or 20°C) by addition of 1 M NaOH or 1 M HCl solution and verified with a glass electrode. The stock solution is stored in a gas tight blood bag wrapped in aluminium foil to protect from photo-bleaching. The purification of m-CP was carried out by Prof. Eric Achterberg's group following the procedure described by Patsavas et al. (2013). The purified m-CP powder is stored in dark cupboard and, when required, a calculated amount of powder is dissolved into solution. The stock solution can be stable on the shelf for several months (Adornato et al., 2016).

2.3 Measurement protocol

2.3.1 Software

The operation of the sensor is controlled by home-made software WetChem (unpublished; credit to John Walk) written in C language. The software allows the user to program the analysis steps including, but not limited to, parameters of sample volume, dye volume, flow rate, etc. It also provides visualisation of the data (intensity, temperature, pump position, measurement time, etc. The software can be updated.) and calculated pH once one measurement is completed. The calculation is based on parameters that are entered prior to the analysis. The user can also choose to download .csv files which contains both the settings and raw data, and subsequently process them in Matlab or other programming language.

2.3.2 Principles of operation

The analysis of seawater samples can be performed automatically and requires no manual intervention once the software is set up. A typical automatic operation of this pH sensor comprises four steps:

1. *Rinse.* Seawater is drawn into the pump barrel via the inlet filter (Figure 2-2), before being injected into the serpentine mixing channel (Figure 2-3) at a flow rate of 350 μL/min.
2. *Injection of indicator.* After two rinses of the barrel and the channel, a third withdrawal of the pump is undertaken, then a small pulse (2 seconds of 50 μL/min) of indicator dye is injected into the channel.
3. *Form of the diffusion curve.* A diffusion curve (Figure 2-5) is obtained by slowly pushing the seawater sample into the channel (57 μL/min), in order to

generate a gradient between the indicator concentration and the absorbance ratio of two wavelengths measured in the optical cell. Intensity data of this step is recorded in a build-in SD card.

4. *Discard.* After reception of the diffusion curve signal is completed, the remaining sample in the barrel is discarded by a rapid (570 μL/min) injection.

All four of the steps described above takes approximately 10 minutes to complete.

When the sensor is out of working status for a long period (>1 week), it is rinsed with mili-Q water to prevent salt precipitation that may block the channel.

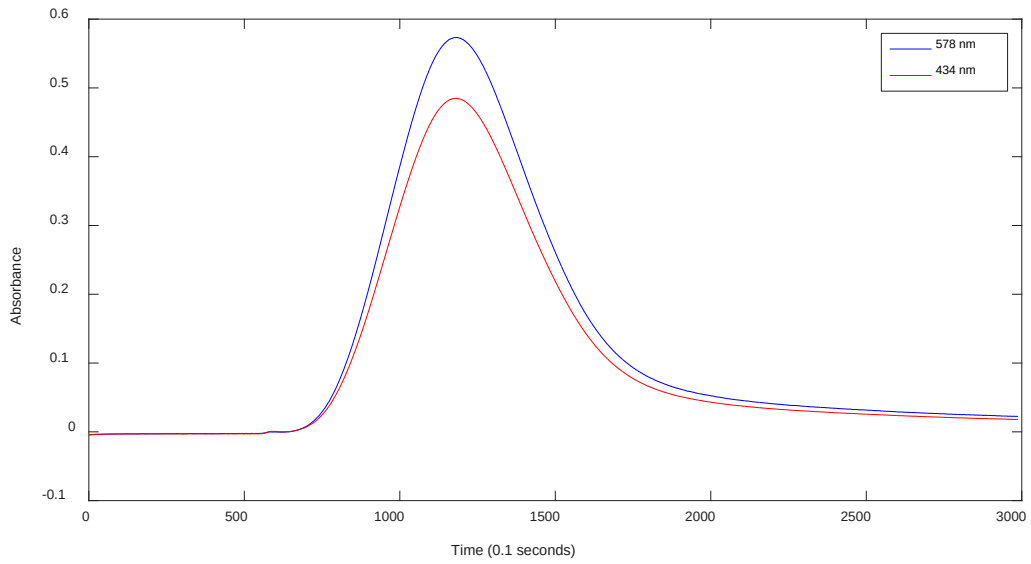

Figure 2-5: Absorbance transient showing broadening of a slug (short injection) of indicator dye by Talyor-Arris dispersion to give a range of dilutions that can be used to quantify perturbation of measured pH due to dilution and the effects of the acid-base dye.

2.4 Data processing

The data process covers four parts: The measurement of blank intensity; the calculation of absorbance; the elimination of indicator-induced pH perturbation; and the calculation of pH.

1. *Blank intensity.* The intensity recorded between 40 seconds and 60 seconds in Step 4 (Section 2.3.2, Figure 2-5) is taken as the blank intensity, I^0, in every pH measurement. This frequent blank measurement ensures that the intensity shift caused by variation of conditions can be compensated, e.g. due to varieties in sample composition, intensity shift of light source due to temperature change, etc.
2. *Absorbance.* The absorbance at two wavelength is calculated following the equation:

$$A_\lambda = \log\left(\frac{I_\lambda^0}{I_\lambda}\right) \tag{2-1}$$

Where λ represents 434 nm and 578 nm. I_λ is the intensity measured at wavelength λ. Because the sensor takes 3000 intensity readings (one of every 0.1 seconds, or in a frequency of 10 Hz) in one measurement, A_λ is a 3000×1 matrix.

Normally the value of A_λ falls between 0 and 1. The data points after the maximum absorbance ("crest" of Figure 2-5) where both A_{434} and A_{578} are between 0.1 and 0.6 are used to calculate R_m. This range of data is called the "data to be processed".

3. *Obtaining R_0.* For each data point, the ratio of the two absorbance values is expressed as:

$$R = A_{578}/A_{434} \tag{2-2}$$

However, the indicator dye, as an amphoteric compound, impacts the sample's pH. Thus it is important to account for this such impact. Here, the method is briefly given to calculate indicator-free *R*, or known as R_0 in this pH sensor, the subscript 0 indicates that no dye in present.

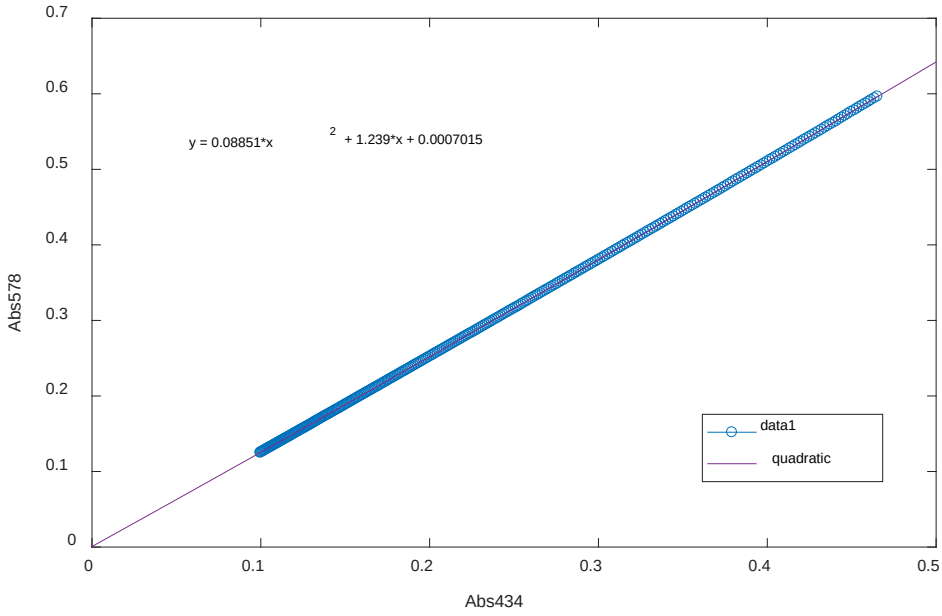

Figure 2-6: Absorbance at 578 nm (Abs578) plotted against absorbance at 434 nm (Abs434) in a typical pH measurement. The quadratic fitting matches the data very well.

In the range of data to be processed, a quadratic fitting is obtained through the absorbances at 578 nm and 434 nm (Figure 2-6). From the polynomial fitting, the coefficient for the term of the7 first degree is saved as R_0. In the case shown in Figure 2-6, R_0 equals 1.239. For a theoretical explanation, please see Chapter 3.3.

4. *Adjustment of R and calculation of pH.* Due to the sensor's calibration method (Chapter 4.2) the R_0 obtained by the sensor needs to be adjusted into R_{th}, subscript "th" meaning "theoretical", following the equation below:

$$R_{th} = aR_0 + b \tag{2-3}$$

Where *a* and *b* are adjustment coefficients obtained through sensor's calibration stage, and vary from sensor to sensor.

Then R_{th} is used to calculate pH following the equation described in Liu et al. (2011)

$$\mathrm{p}H_T = -\log(K_2^T e_2) + \log\left(\frac{R_{th}-e_1}{1-R\frac{e_3}{e_2}}\right) \quad (2\text{-}4)$$

Where $-\log(K_2^T e_2) = pK_2^T e_2 = a + \left(\frac{b}{T}\right) + c\ln T - dT$,

$a = -246.64209 + 0.315971S + 2.8855 \times 10^{-4}S^2$

$b = 7229.23864 - 7.098137S - 0.057034S^2$

$c = 44.493382 - 0.052711S$

And $e_1 = -0.007762 + 4.5174 \times 10^{-5}T$,

$e_3/e_2 = -0.020813 + 2.60262 \times 10^{-4}T + 1.0436 \times 10^{-4}(S-35)$.

Here salinity S is either provided by CTD (conductivity, temperature and depth device) real time or estimated by the user prior to analysis. Temperature T is obtained from the thermistors (for further details of temperature adjustment, see Chapter 3.2).

The above four steps can be processed by Matlab programming. Appendix A gives the script used for this propose. The original Matlab script has also been translated into C language for WetChem to provide processed pH values on its graphical user interface (GUI) for instant check of measurement. The user can also save the processed pH value along with other information, e.g. date, time, salinity, etc., in a single .csv file.

The next two chapters will explain the optimisation and calibration of the sensor in details.

Chapter 3 Optimisation for error reduction

This chapter is describes optimisation of the sensor for error reduction. It contains an uncertainty analysis of the pH system for error identification, the temperature measurement quality control (thermistor calibration) and a discussion about the dye effect on the pH measurement, i.e. perturbation and dilution.

3.1 Uncertainty analysis of the pH system

The uncertainty analysis aims to identify the error sources within the pH system, and quantify the effect of each error source on the final pH measurement, so as to assist the developers in deciding the priority for improvement of each part of the sensor and to identify which factors only have a negligible effect. The analysis involves error propagation, based on mathematic analysis and experimental data. The equations and data are processed in Matlab.

3.1.1 Method

The error in measured pH is calculated as the square root of the sum of the squares of the estimated uncertainties of the method (the indicator dissociation constants and molar absorptivities, the accuracy of the temperature, salinity and absorption measurements).

$$pH_T = -\log(K_2^T e_2) + \log\left(\frac{R_{th}-e_1}{1-R\frac{e_3}{e_2}}\right) \quad (3\text{-}1)$$

Alternatively, this equation can be written as:

$$pH_T = pK_2' + \ln\left(\frac{R_{th}-e_1}{1-Re_4}\right)\cdot\frac{1}{\ln(10)} \quad (3\text{-}2)$$

Where K_2' is short for $K_2^T e_2$, e_4 short for e_3/e_2, and R_{th} is the R measured on a narrow-band spectrophotometer (See Chapter 4). The values of the characteristics of mCP ($K_2^T e_2$, e_3/e_2 and e_1) are from literature(Liu et al., 2011). In the equations below, R_{th} is written as R for abbreviation.

The pH is a function of four parameters: pK_2', R, e_1, and e_4. The initial hypothesis is that the four parameters are independent of each other (i.e. covariance = 0), hence the equation below can be obtained:

$$u_{pH} = \sqrt{\left(\frac{\partial pH}{\partial pK_2'}\cdot u_{pK_2'}\right)^2 + \left(\frac{\partial pH}{\partial R}\cdot u_R\right)^2 + \left(\frac{\partial pH}{\partial e_1}\cdot u_{e_1}\right)^2 + \left(\frac{\partial pH}{\partial e_4}\cdot u_{e_4}\right)^2}$$

$$= \sqrt{\left(D_{pK_2'}\cdot u_{pK_2'}\right)^2 + (D_R\cdot u_R)^2 + \left(D_{e_1}\cdot u_{e_1}\right)^2 + \left(D_{e_4}\cdot u_{e_4}\right)^2}$$

With

$$D_{pK_2'} = 1$$

$$D_R = \frac{1}{\ln(10)}\cdot\frac{1-e_1e_4}{(1-R_{th}e_4)(R_{th}-e_1)}$$

$$D_{e_1} = -\frac{1}{\ln(10)}\cdot\frac{1}{R_{th}-e_1}$$

$$D_{e_4} = \frac{1}{\ln(10)}\cdot\frac{R_{th}}{1-R_{th}e_4}$$

Error on pK_2' ($u_{pK_2'}$):

$$pK_2' = a + \frac{b}{T} + c\ln T - dT$$

With

$$a = -246.64209 + 0.315974S + 2.8855 \times 10^{-4}S^2$$

$$b = 7229.23864 - 7.098137S - 0.057034S^2$$

$$c = 44.493382 - 0.052711S$$

$$d = 0.0781344$$

Then

$$u_{pK_2'} = \sqrt{\left(\frac{\partial pK_2'}{\partial T} \cdot u_T\right)^2 + \left(\frac{\partial pK_2'}{\partial S} \cdot u_S\right)^2} = \sqrt{(D_T \cdot u_T)^2 + (D_S \cdot u_S)^2}$$

With

$$D_T = -\frac{b}{T^2} + \frac{c}{T} - d$$

$$D_S = \left(5.771 \times 10^{-4} - 0.114068\frac{1}{T}\right)S + 0.315974 - 7.098137\frac{1}{T} - 0.052711 \ln T$$

u_T and u_S are the uncertainties in the salinity and temperature. These equations also indicate that $u_{pK_2'}$ is only related to the temperature and salinity measurements.

Error on the absorbance ratio (u_R):

R is the ratio of absorbances at 578 nm (with the subscript 2) and 434 nm (subscript 1). In the R-correction method, an R is measured by the sensor, called R_m, and then is used in a linear relationship to obtain a theoretical R (R_{th}) from which pH will be calculated.

$$R_{th} = AR_m + B$$

Where R_m refers to the R measured by the sensor, and A and B are experimental constants with associated errors of uA and uB. Then:

$$u_{R_{th}} = \sqrt{\left(\frac{\partial R_{th}}{\partial A} \cdot u_A\right)^2 + \left(\frac{\partial R_{th}}{\partial R_m} \cdot u_{R_m}\right)^2 + \left(\frac{\partial R_{th}}{\partial B} \cdot u_B\right)^2}$$

$$= \sqrt{(D_A \cdot u_A)^2 + \left(D_{R_m} \cdot u_{R_m}\right)^2 + (D_B \cdot u_B)^2}$$

With

$$D_A = R_m$$

$$D_{R_m} = A$$

$$D_B = 1$$

Error on sensor calibration

The linear regression of the calibration data of pH sensor (See Chapter 4.2 for the linear regression) produces an uncertainty of

$$u_A = 0.00074$$

$$u_B = 0.0013$$

Error on intensity

Because:

$$R_m = \frac{A_2}{A_1} = \frac{\log\left(\frac{I_2^{ref}}{I_2}\right)}{\log\left(\frac{I_1^{ref}}{I_1}\right)} = \frac{\ln\left(\frac{I_2^{ref}}{I_2}\right)}{\ln\left(\frac{I_1^{ref}}{I_1}\right)}$$

which contains four variables that requires experimental determination, namely I_2^{ref}, I_2, I_1^{ref}, and I_1, we have

$$u_{R_m} = \sqrt{\left(\frac{\partial R_m}{\partial I_2^{ref}} \cdot u_2^{ref}\right)^2 + \left(\frac{\partial R_m}{\partial I_2} \cdot u_2\right)^2 + \left(\frac{\partial R_m}{\partial I_1^{ref}} \cdot u_1^{ref}\right)^2 + \left(\frac{\partial R_m}{\partial I_1} \cdot u_1\right)^2}$$

$$= \sqrt{\left(D_1 \cdot u_2^{ref}\right)^2 + (D_2 \cdot u_2)^2 + \left(D_3 \cdot u_1^{ref}\right)^2 + (D_4 \cdot u_1)^2}$$

With

$$D_1 = \frac{1}{\ln\left(\frac{I_1^{ref}}{I_1}\right)} \cdot \frac{1}{I_2^{ref}}$$

$$D_2 = -\frac{1}{\ln\left(\frac{I_1^{ref}}{I_1}\right)} \cdot \frac{1}{I_2}$$

$$D_3 = -\ln\left(\frac{I_2^{ref}}{I_2}\right) \cdot \frac{1}{I_1^{ref} \cdot \left[\ln\left(\frac{I_1^{ref}}{I_1}\right)\right]^2}$$

$$D_3 = \ln\left(\frac{I_2^{ref}}{I_2}\right) \cdot \frac{1}{I_1 \cdot \left[\ln\left(\frac{I_1^{ref}}{I_1}\right)\right]^2}$$

The error in reference intensity is calculated as the standard deviation of the recorded reference intensity :

$$u_1^{ref} = std\left(I_1^{ref400} : I_1^{ref600}\right)$$

$$u_2^{ref} = std\left(I_2^{ref400} : I_2^{ref600}\right)$$

The intensity errors are calculated using the equations based on the estimated data

$$u_1 = 0.00005I_1 + 0.0003$$

$$u_2 = 0.00005I_2 + 0.0003$$

Error on the extinction coefficients ratios (u_{e_1} and u_{e_4})

e_1 and e_4 are calculated following the equation of (Liu et al., 2011) :

$$e_1 = -0.007762 + 4.5174 \times 10^{-5}T$$

$$e_4 = -0.020813 + 2.60262 \times 10^{-4}T + 1.0436 \times 10^{-4}(S - 35)$$

Then

$$u_{e_1} = 4.5174 \times 10^{-5}u_T$$

$$u_{e_4} = \sqrt{\left(\frac{\partial e_4}{\partial T} \cdot u_T\right)^2 + \left(\frac{\partial e_4}{\partial S} \cdot u_S\right)^2}$$

$$= \sqrt{(2.60262 \times 10^{-4}u_T)^2 + (1.0436 \times 10^{-4} \times u_S)^2}$$

3.1.2 Result and discussion

Single point result

The CTD (SBE 37-SM MicroCAT C-T(P), Sea-Bird Scientific) used for the deployment has an initial salinity accuracy of ±0.002 psu. If the temperature uncertainty lies between 0.001 K to 0.1 K (i.e. the accuracy of temperature measurement is no better than 0.001 K, but no worse than 0.1 K), and the temperature step size is every 0.005 K, the Matlab script can produce a plot of the accuracy of temperature measurement versus the total error propagated in pH measurement, as show in Figure 3-3. The plot indicates that the contribution to the

total pH uncertainty comes from three major factors: 1) the uncertainty in the pK_2e_2 measurement (with a set salinity error, it is almost linearly related to the temperature error), 2) the errors in e_1 and e_4 (they are small and negligible), and 3) the error from the R measurement. This final error source is a combined error from both the intensity measurement and the calibration precision. Because the calibration quality is set, an improvement in the intensity measurement uncertainty (especially the reference intensity) would reduce the pH error significantly.

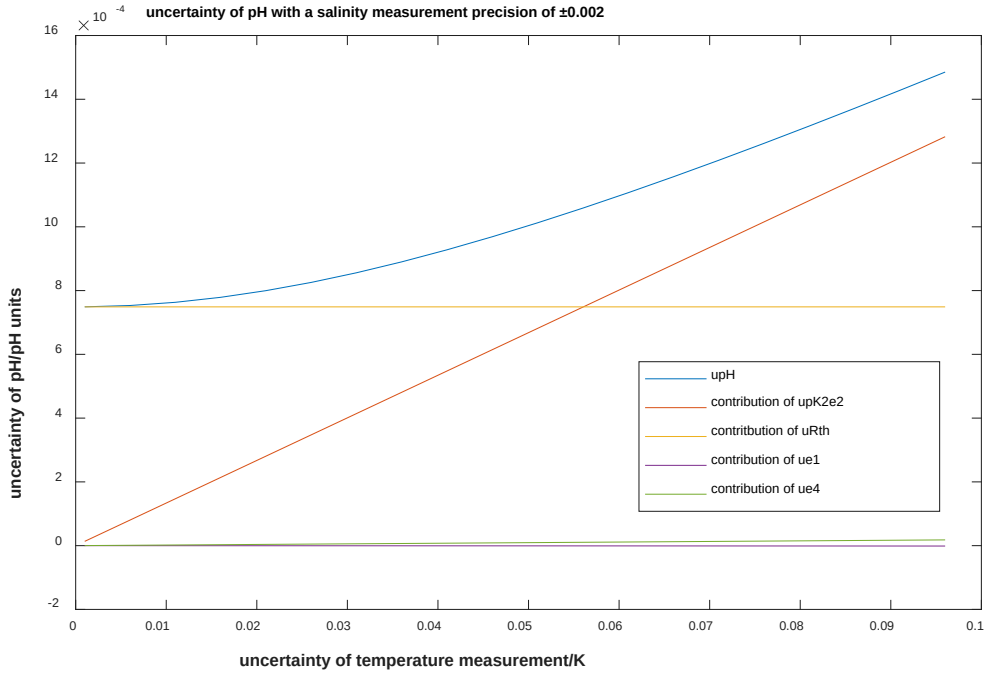

Figure 3-1: The source of errors for pH measurement. Coloured lines repreesents the different sources.

Figure 3-1 indicates that an error in the temperature measurement of 0.05 K would yield an acceptable uncertainty of 0.001 pH units. Taking into account the other sources of error in practical measurements (i.e. systematic errors and pressure uncertainties), a 0.03 K accuracy is achievable for this pH system, and would yield a theoretical accuracy of better than 0.001 pH units.

Deployment result

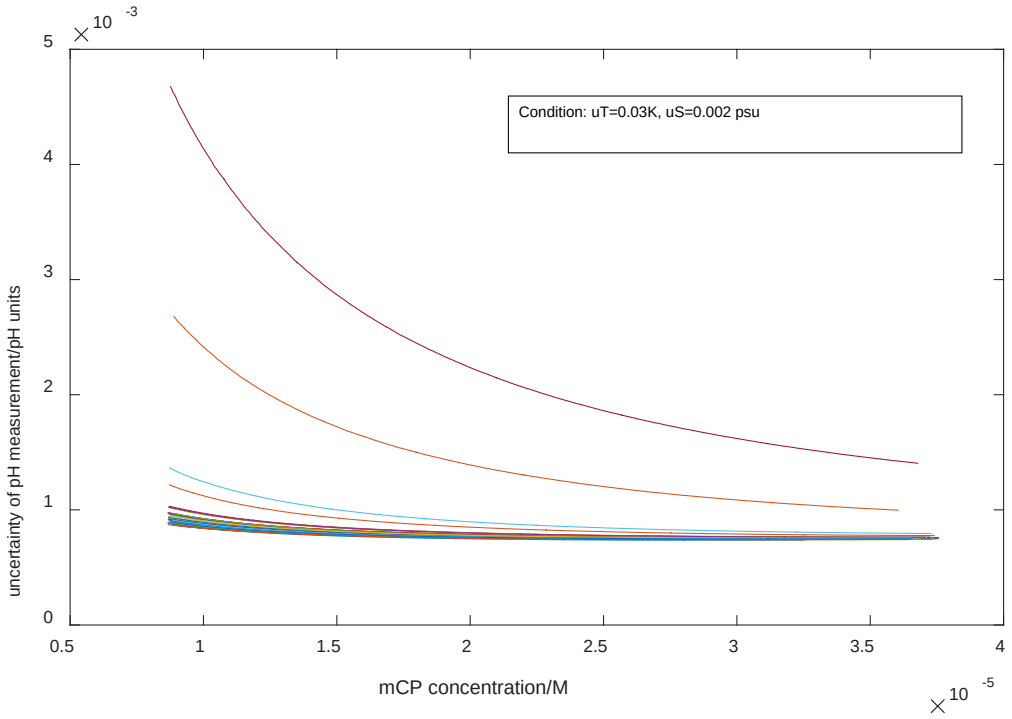

Figure 3-2: The uncertainty of pH measurements in dock deployment.

Figure 3-2 shows the result of uncertainty analyses of 50 pH measurements in a deployment. Each line represents one measurement. *x* axis presents mCP concentration calculated from Liu et al. (2011)'s characteristics and salinity and temperature data. *y* axis shows the theoretical uncertainty at that mCP concentration. For each measurement, the mCP concentration passing through the optical cell decreases as the measurement progress, causing the uncertainty in the pH measurement to increase. This is because the ratio of signal/noise decreases at low absorbance. Therefore, it is important to carefully choose which part of mCP concentration should be applied to gain the most precise pH data. Most of the fifty measurements have accuracies better than 0.0015 pH units, and many are better than 0.001 pH units. The higher the mCP concentration, the more accurate the pH determination. Two out of the fifty analyses show an uncertainty of more than 0.002

pH units. This was because their reference intensity was more disrupted than the others; probably due to the presence of small air bubbles or particles that interfered with the pH determination. The result indicates that the stability of the blank intensity is the key to reducing systemic errors in the pH sensor.

3.2 Thermistor calibration

Experiments observe that there is a significant temperature difference (up to 4°C, see Chapter 5.3) between the sample in the absorption cell and the sample bag, mainly due to the pump movement (for further explanation, see Chapter 3.2). Because pH is highly temperature dependent (c.a. -0.016 pH units/K for seawater), accurate temperature measurement is important for the NOC-pH sensor. As discussed in the uncertainty analysis, the aim for the accuracy of temperature measurement is 0.03 K. Thermistors were first installed on the pH sensors during the XPRIZE competition (Chapter 5.1), but the quality of both the thermistors and the linear regression of data were not good enough. Thus a cubic polynomial fitting was introduced to improve the performance of thermistors.

The thermistors convert the temperature signal into voltage. The calibration is performed in a thermostatic environmental chamber, where the thermistors to be mounted on the sensor chip are suspended in air next to a reference SBE 56 temperature logger (Sea-Bird Scientific). The environmental chamber remains at each temperature for at least 2 hours before the reading of the thermistors are taken. Because for an n-th polynomial model, it needs n+1 data points to solve the equations, at least four data points are needed for the cubic fitting. In the case of

Figure 3-3, sixteen temperatures were measured in total in three temperature cycles (i.e. from 5°C to 25°C, and then back to 5°C).

The precision is defined as how precisely the thermistor can measure at the same temperature. It is calculated as the standard deviation of the thermistor's reading in ten minutes' of time, when the SBE 56 determines the temperature fluctuation in the environmental chamber is ±0.003 K. Figure 3-3-B presents sixteen data points for determining the precision, the majority of which are within ±0.01 K, but yet some can show discrepancies as large as -0.03 K. Such a large deviation is probably due to the uneven of temperature inside the chamber because it is full of air, instead of water. The accuracy is not the residuals of the fitting, because residuals only tell how close an equation fits the actual curve, but the accuracy is deviation between the theoretically calculated temperature and the true measured temperature. Thus the accuracy is determined as the difference of the predicted temperature using the fitting obtained from the first cycle of temperature measurements, to the "true" temperature measured by the SBE 56 in the second or third cycle of temperature measurement. Figure 3-3-C shows the average accuracy of this thermistor is better than ±0.02 K, which is adequate for the pH sensor.

Note, that although the fitting obtained from the first temperature cycle is used for the accuracy estimation, the final equation used to convert from voltage to temperature the fitting of all sixteen data points. This yields a better accuracy.

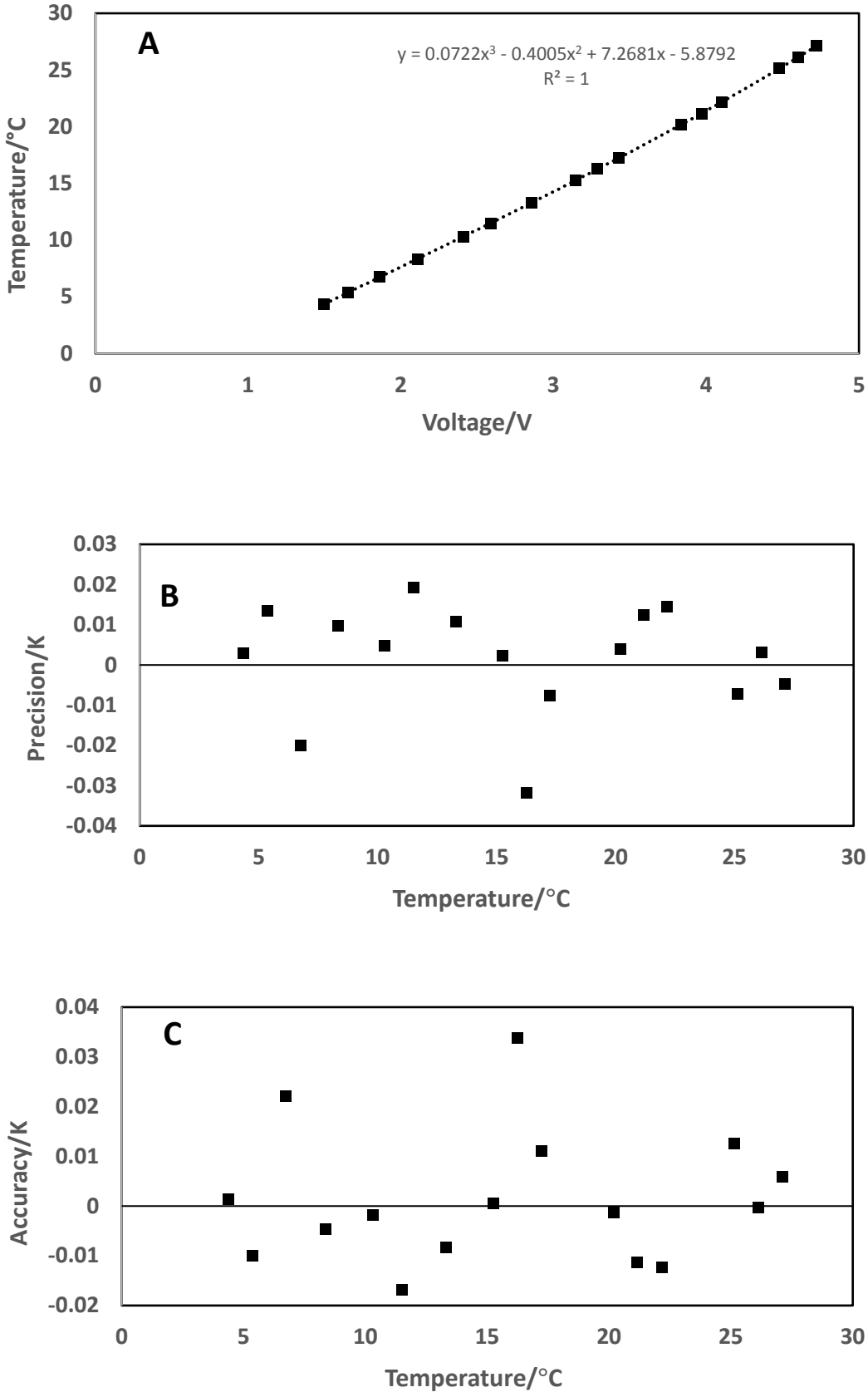

Figure 3-3: Calibration of thermistors. A. The 3-order polynomial fit of SBE 56's temperature reading and the thermistor's voltage reading. B. The residuals of the fit are scattered randomly.

3.3 Perturbation correction

The indicator dye mCP is amphoteric and dissociates in solution to generate hydrogen ions, and thus changes the pH of the solution. This effect is known as indicator-induced perturbation. The error caused by this process is on the order between 0.002 pH units (Yang et al., 2014) and up to 0.07 pH units (Gabriel et al., 2005; Martz et al., 2003; Seidel et al., 2008) depending on the sensor's construction. The NOC-pH sensor's perturbation correction order is approximately 0.04 pH units because it uses an approximately ten times higher indicator concentration ($3\text{-}5*10^{-5}$ M) than used in many other flow-injection-spectrophotometric pH systems ($3*10^{-6}$ M) (Nakano et al., 2006; Wang et al., 2015). At these higher indicator concentrations, the impact on the measured pH cannot be ignored, especially for a pH sensor designed to operate at high precision.

Seidel (2006) used a linear regression to correct for the perturbation. They plot pH against the total indicator concentration in the optical cell (termed as [dye]), and the intercept is the pH value when no dye is present. However, this method requires a sufficient concentration of indicator stock solution (1 mM mCP), otherwise the pH-[dye] plot in the pH measurement would deviate from linearity at lower dye concentration (<30 µM) (Figure 3-4). The NOC-pH sensor records the same shape of deviation at low dye concentration as shown in Figure 3-5-C. In addition to the deviation, the calculation based on the linear part of different concentration also gives different intercept (Seidel, 2006), which indicates that the linear regression might not be the correct way to calculate the dye-free pH value.

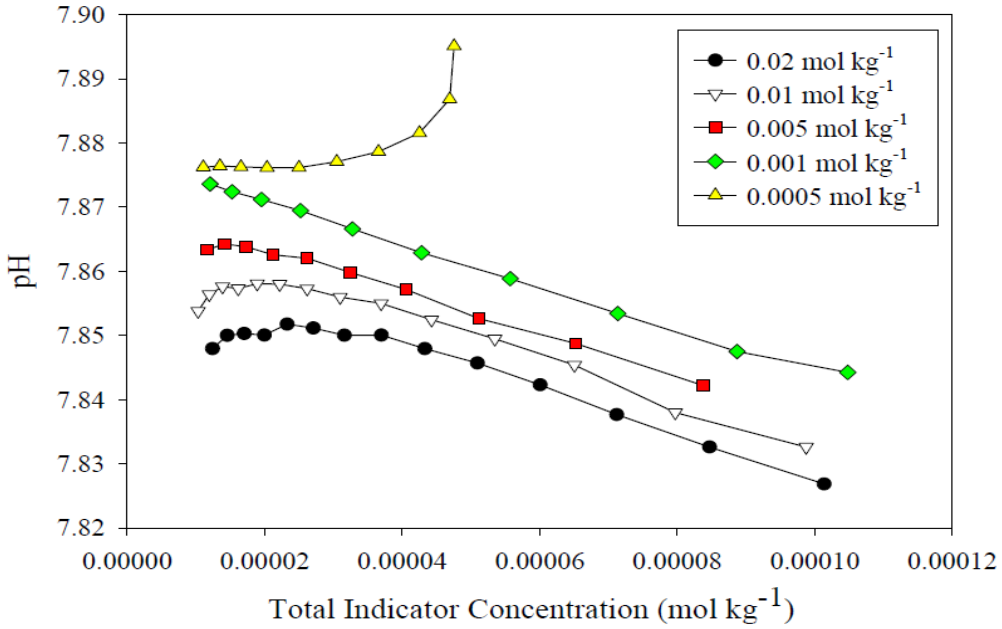

Figure 3-4: pH plot against total indicator concentration for five indicator stock solutions, on the sensor of SAMI-pH. Figure comes from the PhD thesis of Seidel (2006). The linear part of the five curves were used for calculation of the indicator-free pH.

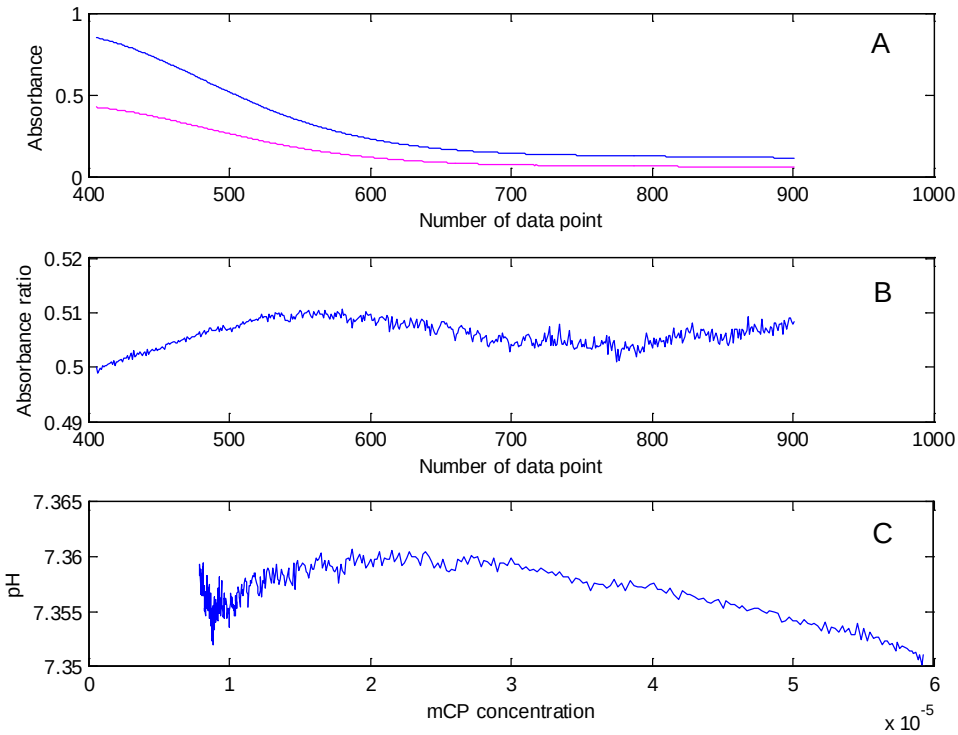

Figure 3-5: The pH changes as the dye concentration increases, on the sensor of NOC-pH. **A.** The absorbance plot against the number of data point. Each data point represents 0.1 seconds after the indicator was injected into the serpentine. The blue line is the absorbance at 434 nm while the red line is at 578 nm. **B.** The ratio of the two absorbance (*R*) plot against the time. **C.** The time is converted into total indicator concentration. The pH is calculated based on the *R* value.

Here, a novel method to correct for the indicator-induced pH perturbation is described. As a matter of fact, the value of *R* represents ratio of absorbance at two wavelengths when the dye equilibrium transforms due to the change of hydrogen ion concentration:

$$R = \frac{\partial y}{\partial x} \tag{3-3}$$

where *y* represents absorbance at 578 nm and *x* absorbance at 434 nm. If we plot *y* against *x* in a second-degree polynomial fit,

$$y = ax^2 + bx + c \tag{3-4}$$

the changing of slope (*R*) would be the first derivative of *y*. It is understandable that the slope changes, because the more indicator that is added to the sample, the more the pH is changed.

The value of *R* without any indicator present is the slope of the two absorbances when the indicator concentration approaches zero:

$$R_0 = y'|_{\lim_{x\to 0} y} = b \tag{3-5}$$

where R_0 is the *R* value at zero indicator concentration. Then the R_0 is used to calculate pH when no dye presents. Figure 3-6-B gives an example of the calculation procedure.

Figure 3-6 in fact provides two ways of approaching the quadratic fitting. Both pairs of parameters show a good match, however, the R-[mCP] pair represents more fluctuation, while the Abs78-Abs434 pair yields perfect match. This is likely because the absorbance-vs-absorbance method directly reflects the fundamental chemical reaction between the indicator dye and the solution, while the R-[mCP] pair may be prone to environmental interferences, such as the light signal-to-noise ratio, small temperature fluctuations, etc.

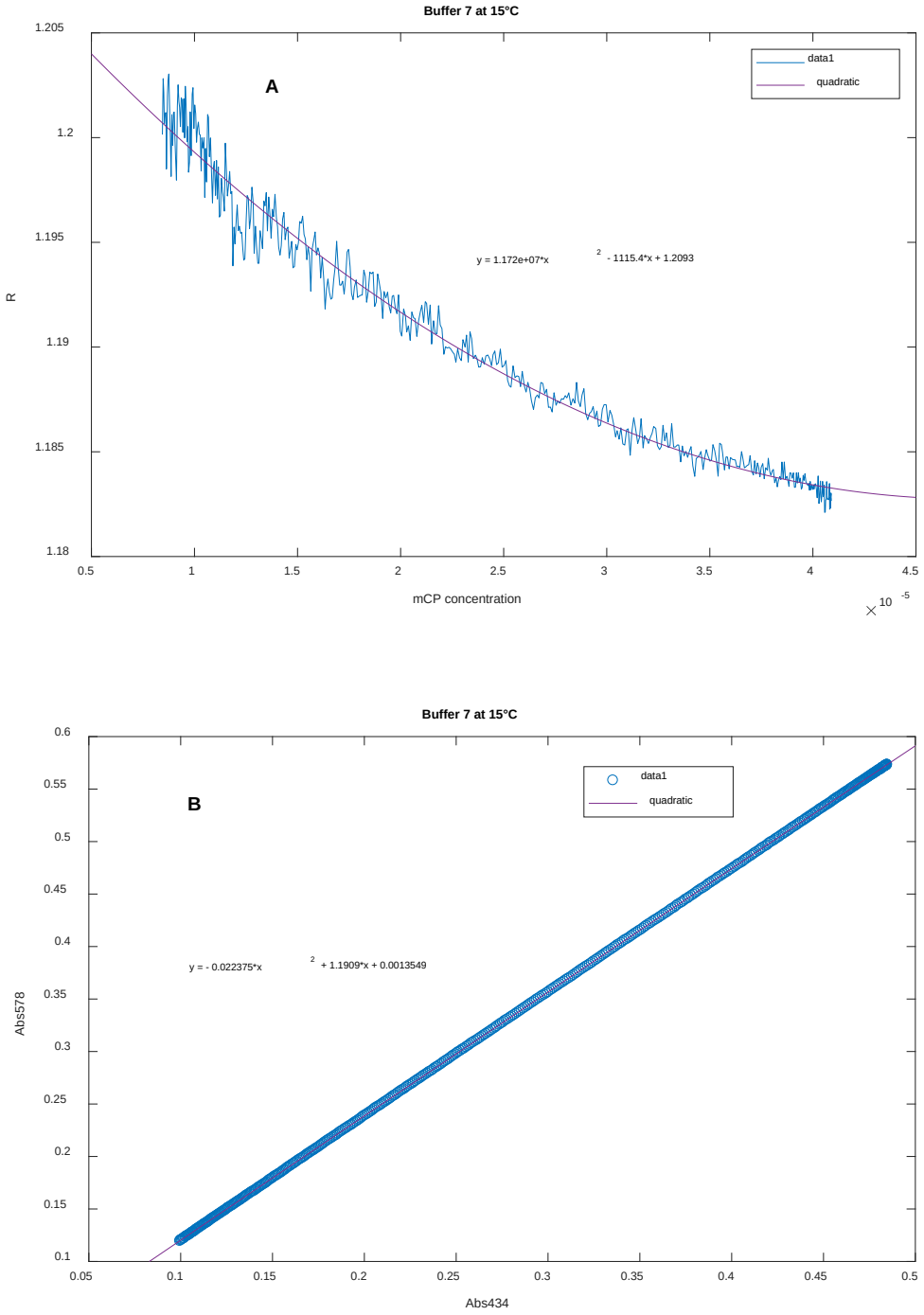

Figure 3-6: The comparison of quadratic fitting for two pair of parameters for the same buffer under the same conditions: **A.** Plot R vs. [mCP]. **B.** Plot absorbance at 578 nm (Abs578) vs. absorbance at 434 nm (Abs434).

Further analysis reveals that the imprecision introduced by the calculation of the R-[mCP] pair is on the order of ±0.00085 pH units, which would be insufficient for the

desired precision of ±0.001 pH units. However, the precision of Abs578-Abs434 pair is $\pm 6*10^{-6}$ pH units, which is negligible.

3.4 Dilution effect

3.4.1 Estimation of dilution effect

Because the indicator dye stock solution usually contains a different carbonate concentration compared to most samples, the dilution of sample caused by the addition of the dye solution will affect the sample pH. For the pH sensor described here, which uses a dye concentration in the absorption cell of between 10 to 35 µM and a 4 mM indicator stock solution, the dilution ratio of the sample to the indicator solution is between about 100 to 400 folds.

To investigate and remedy the perturbation effect, a theoretical simulation was constructed and used to test mitigation methods. The simulation used an example sample of the Batch 128 of Seawater Reference Materials (Scripps Institution of Oceanography of the University of California, San Diego). The salinity of Batch 128 is 33.442, total alkalinity 2240.28 µmol/kg, total phosphorus 0.3 µM and total silica 3.7 µM. The indicator solution salinity is 35 and the pH 8.1. Because the dilution effect only takes into account the solution impact without dye perturbation, the total alkalinity can be regarded as 0. Hence, for a 100-fold dilution, the salinity changes from 33.442 to 33.4576 (because the dye solution is more salty), while total alkalinity decreases to 2217.88 µmol/kg. Instead of the Batch 128 DIC, the calculation uses pCO_2 as one of the parameters. Both the sample and the diluted sample after indicator addition are considered air-CO_2 balanced, so the pCO_2 are

both estimated as 400 µatm. With these parameters defined, the CO2Sys_v2.1.xls calculator (Pierrot et al., 2006) is used to calculate the pH of the original sample and the diluted sample with added indicator solution, respectively.

3.4.2 Result

The pH of the example sample is 8.038 (25°C), while the diluted sample pH is 8.035 (°C). In other words, the dilution effect caused by the addition of indicator solution is -0.003 pH units. Because the TA of the indicator stock solution is regarded as 0, if the salinity of the sample is equal or greater than that of the indicator the dilution always reduces pH. However, when the sample salinity is lower than the indicator solution salinity (35), the dilution will increase the pH, regardless of whether the indicator solution pH is higher than the sample pH. Considering all of these factors, the dilution with indicator solution may decrease the sample pH when the salinity and pH of the sample are both lower than these of the indicator solution, is an extent which is of the order of a few mpH units.

One method to reduce the dilution effect that can be taken, is to increase the extent of indicator solution dilution with the sample. Simulation of a 1000-fold dilution suggests that the effect could be less than -0.0005 pH units, consistent with literature reports (Martz et al., 2003). Another measure that reduces the impact of dilution is the R-adjusting method. Because synthetic seawater is used in the process of sensor calibration (i.e. close to real samples encountered in field work) the dilution effect is inherently adjusted by R. We have observed a deviation of Rm-Rth from linear regression (Figures 3-4, 3-5). The dilution by indicator solution may also play a role in the error.

3.5 Temperature gradient in the chip

The temperature gradient in the chip is a particular problem for the microfluidic pH sensor. This is mainly because the heat generated by the pump is transported by the fluid. The PMMA is a good heat-insulation material that restricts the heat within the microfluidic channel. The heat gradient along the channel can be 0.15°C per centimetre, which is significant for pH measurement (equivalent to 0.0048 pH units for Tris buffer). Wrong measurement of the temperature would lead to inaccurate and imprecise pH measurements which has been verified in lab tests (data omitted) and field deployment (Chapter 5.1; data are omitted). Ideally the exact temperature is either measured directly in the middle of the absorption cell, or is done by two thermistors before and after the cell and then a mean is taken. This version of the sensor was designed to have two thermistors both after the absorption cell as the temperature gradient was only discovered after the sensor was designed. Therefore a temperature correction method was applied for this version of the sensor.

As shown in Figure 3-7, the temperature gap widens gradually throughout several measurements as the heat accumulates, until it reaches steady (approx. after nine measurements) thermal balance. Assuming that the heat gradient is constant along the channel, at least in the last few centimetres, the actual temperature in the absorption cell is related to its distance from the thermistors. The distance between the end of the absorption cell and the closest thermistor is 1 cm, the two thermistors are 1 cm apart from each other, and the length of the optical cell is also 1 cm. Thus, the average temperature in the absorption cell is obtained following the equation below:

$$\Delta T = T_1 - T_2 \tag{3-6a}$$

$$T = \frac{T_1+T_2}{2} + 2\Delta T \quad \text{(3-6b)}$$

where T_1 refers to the thermistor closer to the absorption cell and T_2 to the further one. T is the estimated temperature in the middle of the absorption cell, representing the mean in the whole cell.

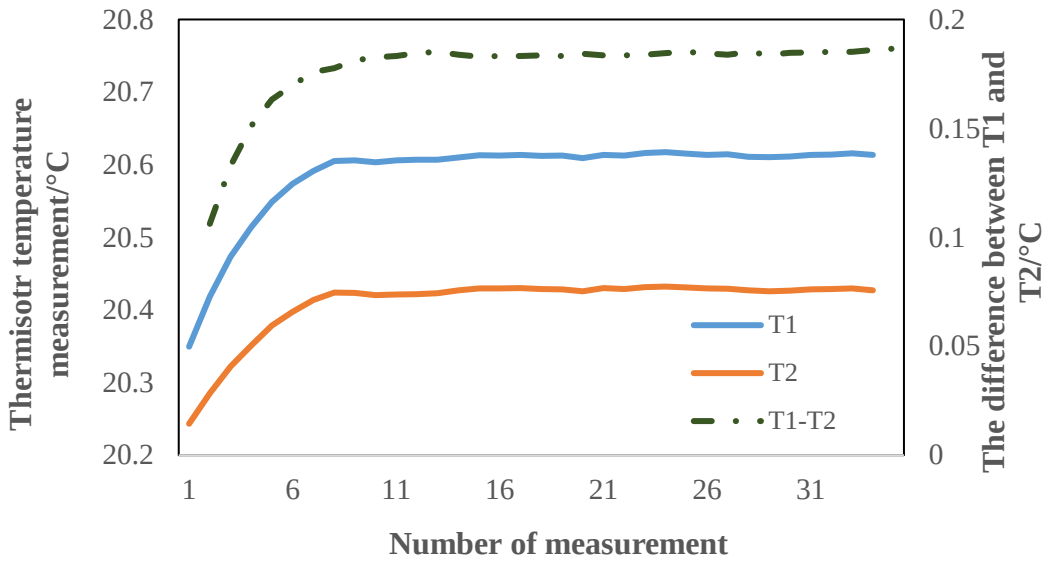

Figure 3-7: The blue and red line show the temperature recorded by the two thermistors (T1 and T2) separately. The dash grey line shows the difference between T1 and T2 growing bigger and bigger until it reaches a thermal balance after about nine measurements.

When the sensor is on a one-measurement-per-hour schedule such as in a field deployment (Chapter 5), it will never get the chance to form a steady temperature gap. To deal with this, the sensor always takes temperature measurements of both thermistors and applies Equation 3-8 to obtain a real-time estimation of the T before calculating the pH. In most cases, the assumption of a linear temperature gradient is sufficiently accurate, but a future version of the pH sensor would be able to measure the temperature inside the absorption cell directly and reveal if this assumption is correct or not.

Chapter 4 Calibration of the pH system

In this chapter, two methods of pH sensor's calibration are implemented. The first method is to characterise the indicator dye for each sensor, and the other one, known as the *R-adjusting method*, is to apply the same characteristics for every sensor but adjust the *R* to fit each sensor. Both methods have their advantages and disadvantages, and the author recommends that users should choose either of them based on the specific requirement for a pH sensor.

4.1 meta-Cresol Purple indicator characterisation

The success of spectrophotometric pH method depends on the accurate determination of characteristics of the sulfonephthalein indicator dye, namely the extinction coefficients (εs) and apparent dissociation constants (K_1, K_2) (For theory details, see Chapter 1.5). Although characteristics of meta-Cresol Purple (m-CP) indicator can be found in literature (Clayton and Byrne, 1993; Liu et al., 2011), it is necessary to determine these characteristics individually for each of the sensors (Rérolle et al., 2013; Seidel et al., 2008). This is because usually a sensor's structure is not as ideal as high-quality bench-top spectrophotometers. A typical sensors detection optics have a spectral full width at half maximum (FWHM) of the order of ±12 nm in wavelength (Martz et al., 2003;Rérolle, 2013;Yang et al., 2014) which compares to spectrophotometers' ±2 nm (Liu et al., 2011; Zhang and Byrne, 1996). Besides, sensors' light source may not provide precisely the maximum absorbance wavelength of the dye due to a variety of reasons, such as the availability or cost of light sources and/or filters with maxima at these specific wavelengths. As a result,

the absorbance of the dye measured are often termed ‘apparent’ absorbance, and are a mixture of absorbance at maximum and other wavelengths. Meanwhile, the literature reports only the extinction coefficients at the maximum absorbance wavelength, but the extinction coefficients of the dye are not constant across the spectral emission bands of the LEDs. Therefore, the ‘apparent’ extinction coefficients on the integrated wavelength bands need to be determined individually for each sensor due to the small manufactural variations. Otherwise the discrepancy could induce inaccuracies as large as 0.015 pH units (Rérolle, 2013).

4.1.1 Materials and method

The characterisation of mCP follows the method described by Liu et al. (2011) and Clayton and Byrne (1993). The theory can also be found in Chapter 1.5. Based on Equation 1-13, three characteristics need to be determined: $-\log(K_2^T e_2)$, e_1 and e_3/e_2. Three solutions are used to determine e_1 and e_3/e_2: the purified mCP stock solution; the acidic solution for determination of e_1; the basic solution for determination of e_3/e_2. The recipes are listed as below:

1. *mCP stock solution.* 100 ml 4 mM purified m-CP in I=0.7 NaCl: 4.0908 g NaCl, 0.1618 g m-CP, made up to 100 ml using MQ water, adding drops of 1M NaOH to increase the pH to 8.0±0.1. (Chapter 2.2.4)

   The dye of mCP characterised is purified. Impurities in the indicator may also affect the extinction coefficients, resulting in an offset of up to 0.01 pH units (Yao et al., 2007). Although theoretically these offset could be eliminated by characterisation anyway, it requires the sensor always uses the same batch of dye. For the consistent of sensor’s measurement for different

batches of dye, as well as to compare the deviation of the sensor's performance from literature reports, the purified mCP is chosen.

2. *Acidic solution.* 250 ml pH 4.5 acetate buffer solution: 168 µl 97% acetic acid, 0.1805 g NaAc, 10.115 g NaCl, made up to 250 ml using MQ water. Under these conditions, the dye is 99.8% HI^-.
3. *Basic solution.* 250 ml pH 12 artificial seawater-NaOH solution at 0.7 M ionic strength: 9.3895 g NaCl, 0.2657 g KCl, 0.0385 g KBr, 0.0103 g H_3BO_3, made up to 250 ml with MQ water, adding drops of 1 M NaOH to adjust to pH 12. Under these conditions, the dye is almost exclusively in the I^{2-} form ($[I^{2-}]/[HI^-] \approx 10^4$).

Three sensors are characterised (serial numbers SN1, SN2, and SN4). The calibrations are undertaken at four temperatures (5, 10, 15, and 20°C) in an environmental chamber, so that the temperature-dependent relationship can be obtained. The procedure used in the sensor operation was carried out automatically under control of a custom electronics package (Sensor Controller II (NOC, UK), based on a SAM4L microprocessor (ARM, UK)). After two sample flushes, a small amount of indicator dye solution (1.65 µL) was injected into the serpentine channel. Then a total amount of 0.3 ml of buffer solution was slowly injected into the same channel at a rate of 57 µL/min, in order to produce an indicator concentration gradient (by Taylor-Arris dispersion, see above). The absorbance at the two wavelengths after the maximum absorption point and their relationship can be calculated using standard Taylor-Arris theory implemented a Matlab manuscript (See Appendix A). The low absorbance range (0-0.5) was used in order to minimise the indicator perturbation (See Chapter 3.3). A typical plot is shown as Figure 4-1.

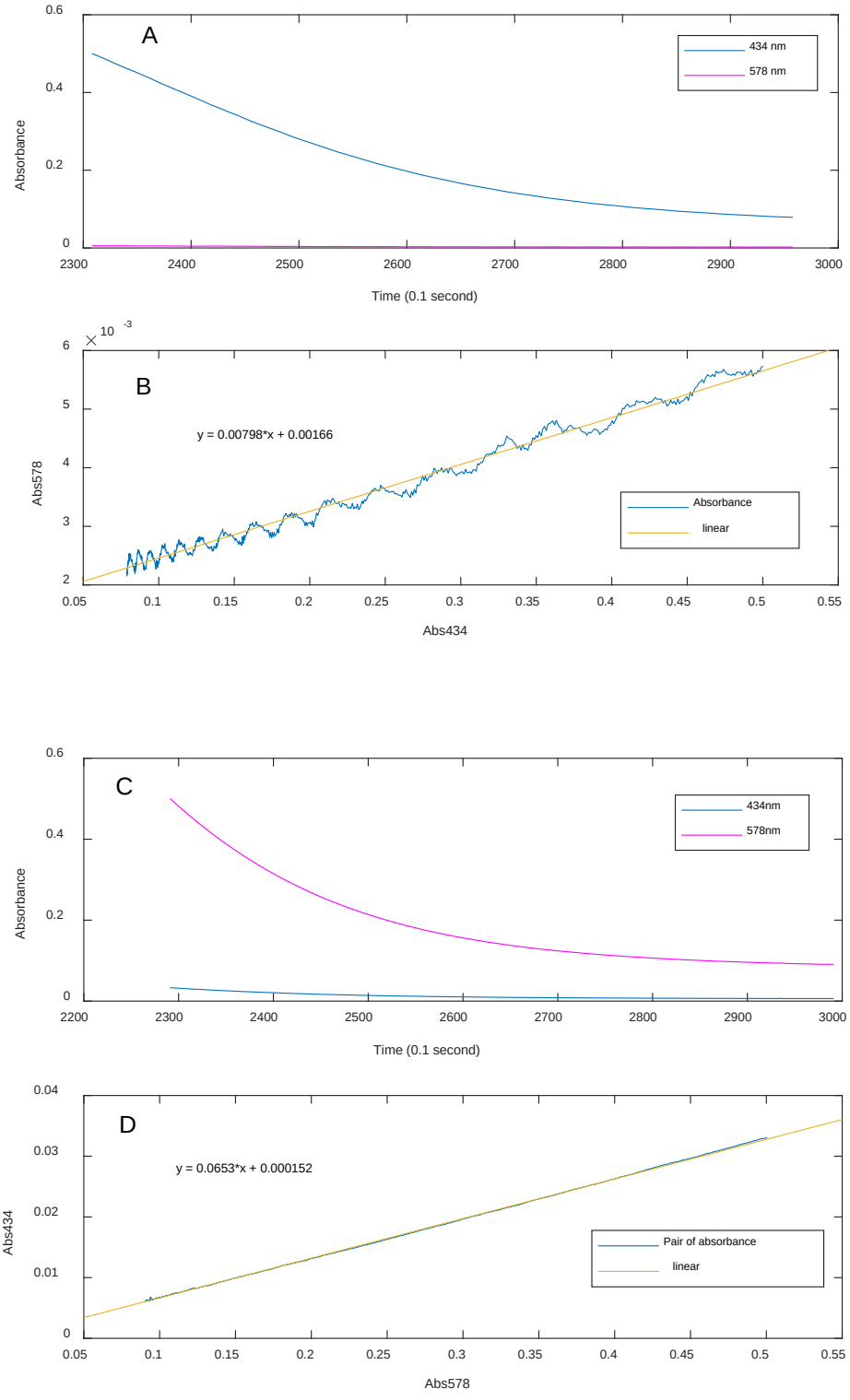

Figure 4-1: **A.** When determining e_1, the absorbance at wavelengths 434 and 578 nm is a function of time (0.1s) as the indicator slug passes through the optical cell. **B.** e_1 is the slope between A_{578} and A_{434}. **C.** When determining e_3/e_2, the absorbance is measured at wavelengths 434 and 578 nm as a function of time (0.1s) as the indicator slug passes through the optical cell. **D.** e_3/e_2 is the slope between A_{578} and A_{434}.

4.1.2 Result and discussion

The temperature dependent e_1 of Sensor No.1, No.2 and No.4 are shown as Figure 4-2.

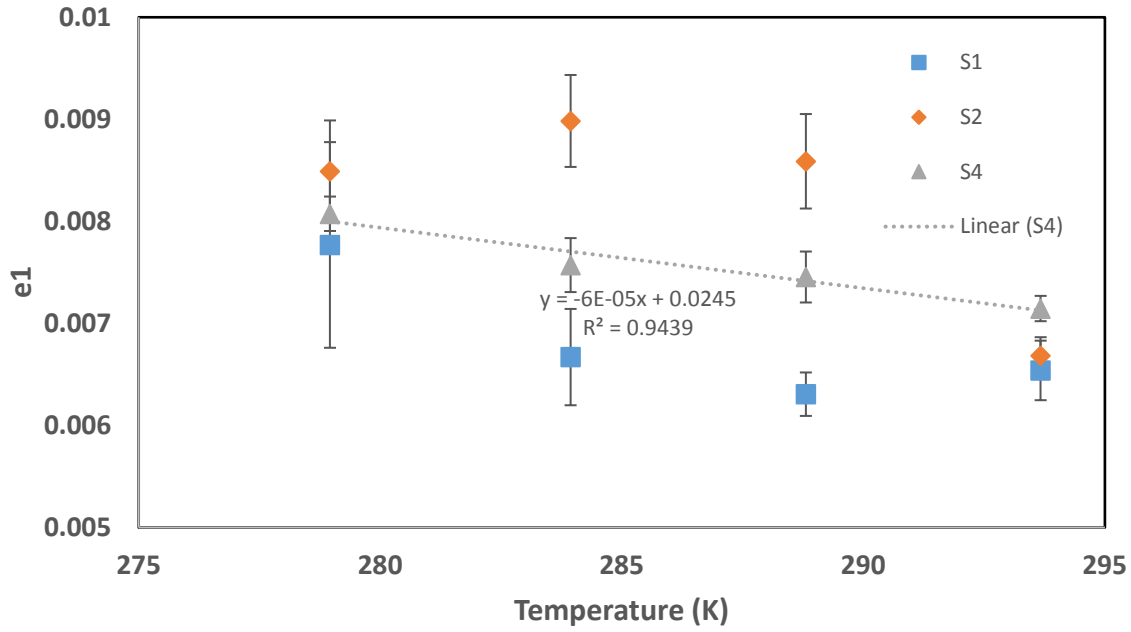

Figure 4-2: The temperature dependence of e1, with Sensor No.1, No.2 and No.4.

Only Sensor No.4 showed a linear relationship between e_1 and temperature. The other sensors' mCP characterisation resulted in large errors (up to 13%) and non-linear relationship with temperature. There are several factors that caused the non-linear relationship. First, the temperature measurement was not precise. The sensor did not have a thermistor installed within the housing at that time. After this characterisation, all the pH sensors were then equipped with calibrated thermistors to record temperature inside the chip. Second, the absorbance at the minor species' maximum absorption wavelength was very low (0.05 to 0.15 absorbance units, comparing to normally 0.1 to 1 absorbance units), which resulted in a large measurement error. This was due to the experimental design that the pair of

absorbance at the two wavelengths should be measured at the same time. According to equation 1-14, when *b*, the path length is short (1 cm), the indicator concentration needs to be high in order to get descent absorbance of the minor species. However, the absorbance of major species would exceed determination limit (i.e. optical signal saturates). The solution to this particular problem is to use a 10 cm path length, as Liu et al. (2011) and Clayton and Byrne (1993) did. Therefore re-design the sensor's microfluidic chip in order to include a 10 cm optical cell was discussed in meetings, but later it was decided that the *R-adjusting* method would be worth trying, and the success of *R-adjusting* method (See the next section) made the re-design never happen.

The inaccuracy and imprecise of e_1, induced by the highly-uncertain (Figure 4-2) characterisation, alone would generate an error in pH measurement of ±0.001 pH units, in both accuracy and precision. Regardless within the accuracy aim of the pH sensor (±0.004 pH units; with a precision of ±0.001 pH units), the precision aim could not be met by applying such data. Considering that the determinations of e_3/e_2 and $K_2^T e_2$ require even higher resolution of absorbance measurements than the determination of e_1 does, they were suspended and never happen.

4.2 R-adjusting calibration method

To calibrate a pH sensor has long been a matter of time-consuming and tricky (Personal communication with peers). The *R-adjusting* calibration method is the method that Yang et al. (2014) presented for an easy-making, low-cost seawater pH analyser with 0.01 unit pH accuracy. Though based on their experiment data Yang et al. regarded that this method would only be appropriate for analysers that require an

accuracy no better than 0.01 pH units, the work done on the NOC-pH sensors suggests that this method actually can achieve a precision of ±0.0004 pH units and an accuracy of ±0.005 pH units. The accuracy result is comparable to the CRM's (certificate reference materials) accuracy of ±0.004 pH units, making it capable for marine environmental monitoring and global carbonate study where accuracy is concerned. This calibration method, besides its high precision and accuracy, is quicker and easier to implement, comparing to characterising dyes for each sensor. Efficient and low-cost, the *R-adjusting* method is promising to be applied on sensors particularly when large scale of deployment is needed, for example on Argo floats.

4.2.1 Principles

The key point of *R-adjusting* method is that for every *R* value (the absorbance ratio) measured with the sensor (known as R_m), there is a corresponding *R* value (termed as R_{th}, subscript *th* for theoretical) that a narrowband spectrophotometer would report for the same sample at the same temperature. An experimentally determined transform function converts R_m to R_{th}. Thus applying sample's temperature (*T*) and salinity (*S*), along with R_{th}, the sample's pH can be calculated, following Equations 1-13, 1-17, 1-18 and 1-19.

To determine the R_m-R_{th} function, well-buffered synthetic seawater samples over a range of pH_T are measured on the sensor and a bench-top spectrophotometer (Carry 60 UV-Vis, Agilent Technologies) using the same mCP stock solution. Detailed procedures are described in the following sections.

4.2.2 Preparation of non-equimolar Tris buffers

The mostly used Tris buffer in synthetic seawater is sometimes known as equimolar Tris buffer, indicating that the species of Tris and Tris·HCl in the buffer have a molality ratio of 0.04: 0.04. The pH of an equimolar Tris is 8.0935 at 25°C. Therefore to obtain different pH values, a set of non-equal-molar Tris buffers in artificial seawater with a constant salinity 35 psu are made following the procedure described in the paper of Pratt (2014). In brief, a concentrated artificial seawater (CASW) is made from NaCl, Na_2SO_4, KCl, $MgCl_2$ and $CaCl_2$. Then a set of concentrated buffer (CB) are made from 2-amino-2dydroxymethyl-1,3-propanediol (Tris), hydrogen chloride and sodium chloride, and mixed with the CASW to obtained the final product – Tris buffer in artificial seawater. The pH of these Tris buffers are adjusted by the ratio between Tris and HCl that added in the CB. The sodium chloride in the CB is used to adjust the final salinity to 35 psu. Jennifer Clark (GEOMAR, Kiel, Germany) made the spreadsheet that help to make non-equal molar Tris buffer in the range of pH 7 to 8.4 (25°C). All the chemicals used are purchased from Sigma-Aldrich, analytical grade, and oven-dried at 110°C for at least 2 hours.

Another non-equal-molar Tris buffer with pH 7.6 (25°C) and salinity 20, numbered as S20_B7, is also made for salinity effect check. First, a recipe of pH 7.6 and salinity 35 is made following the method above. Then the chemicals used are reduced proportionally following equations in T.A. DeValls and A.G.Dickson's paper (DelValls and Dickson, 1998) in order to adjust the salinity to 20. A spreadsheet is made to help do the calculation.

Finally, a certificated equal-molar TRIS buffer purchased from A.G.Dickson's laboratory (Scripps Institution of Oceanography, UC San Diego, California, USA) is used to verify the calibration's accuracy.

4.2.3 Determination of the Tris buffers' pH correction

Six non-equimolar Tris buffers are used in the calibration of NOC-pH sensor S/N 16, which are known as Buffer #4, #6, #7, #8, #9 and #10. All the buffers are salinity 35. Their pH are determined with a bench-top spectrophotometer (Carry 60 UV-Vis, Agilent Technologies), which has a thermostatic 10 cm cell attached to a water bath, at 15 °C and 25°C, following the standard procedure (Dickson et al., 2007), using purified mCP stock solution and a Fisher thermometer (Serial number 80614977) to determine the temperature. Buffer #6 and #10 are further measured at 10°C. The measured absorbance ratio is used to calculate the non-equimolar Tris buffers' pH applying the reported characteristics of purified mCP (Liu et al., 2011) at the measured temperature.

The pH of equimolar Tris buffer can be calculated from the equation below (DelValls and Dickson, 1998) :

$$pH_T(equimolar\ tris) = (11911.08 - 18.2499S - 0.039336S^2)/T - 366.27059 + 0.53993607S + 0.00016329S^2 + (64.52243 - 0.084041S)\ln T - 0.11149858T \quad (4\text{-}1)$$

where T is in K.

The offset of pH value of a non-equimolar buffer from the equimolar buffer at the same temperature is used as the *pH correction* of the non-equimolar buffer.

4.2.4 R_m-R_{th} linear regression

The samples are measured at several temperatures in order to obtain more than one R_m-R_{th} data pairs. The pH value of the sample at the sensor's temperature is calculated as:

$$pH_{th}(T,S) = pH_T(equimolar\ tris)(T,S) + correction \quad (4\text{-}2)$$

Hence the absorbance ratio that a spectrophotometer would report is calculated as:

$$R_{th} = 10^{(pH_{th}-pK_2e_2)+e_1}/(1 + e_3/e_2 \times 10^{pH_{th}-pK_2e_2}) \quad (4\text{-}3)$$

R_{th} is the output along with the R_m that the sensor actually records. The data processing is performed by Matlab programming (Appendix A).

A total of 488 measurements or data pairs, are collected on S/N 26. Temperatures were between 5 and 26 °C, covering pH from 7.3 to 8.5. In the range between 0.3 and 3.5, R_m and R_{th} are linearly related, with the fitting degree (R^2) of 0.9998 (Figure 4-1). Root mean square (RMS) of the residuals is 0.0126, which can lead to a pH uncertainty less than ±0.003 pH units (See Chapter 3.2 for error propagation) when R_m=2.

Due to the limit of time before deployment, in this work only one buffer with salinity 20 (S20_B7) was used to test if this method could be used for a wider salinity range. Figure 4-1 shows that data of S20_B7 can be interpolated by the data of buffers with salinity 35. The RMS of R_m is 0.0045, or equivalent to ±0.002 pH units of error, within the uncertainty of this R-adjusting method. The result is promising, because this indicates that this calibration method is insensitive to salinity, i.e. a calibration at S=35 can be used for 20<S<35. This will make future calibrations free from

consideration of salinity effect. In my future work, I would like to add more data with a variety of salinity to have this conclusion more solid, as well as widen its range to 15<S<45.

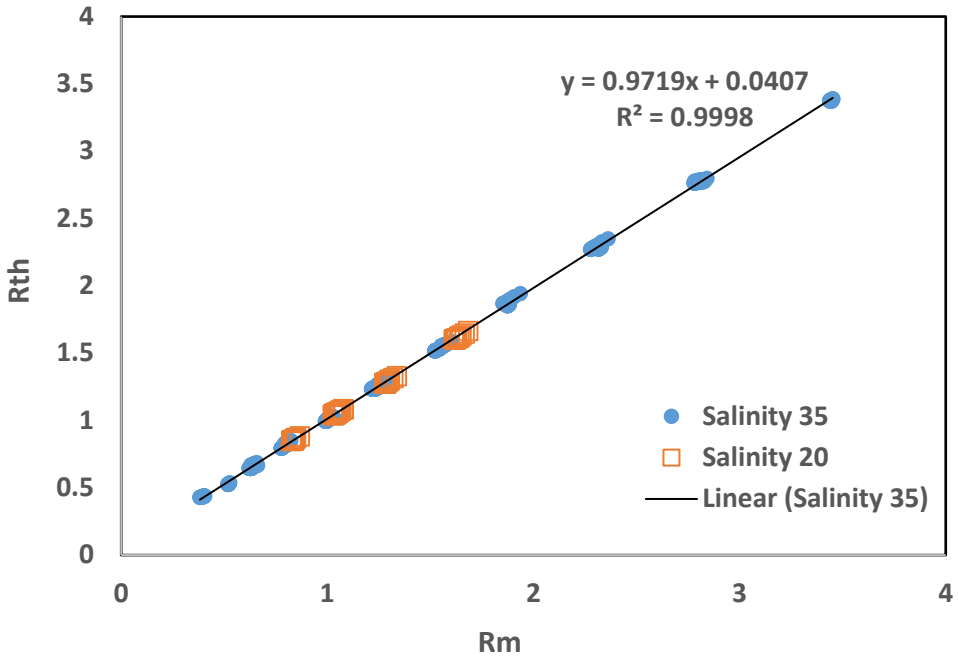

Figure 4-3: The linear relationship between Rm and Rth. Blue points are salinity 35 and red are salinity 20.

The calibration experiment was designed to have different buffers resulting in similar R values, in order to compare how agree they are. Figure 4-5 provides two examples. Figure 4-5-A shows that when R_m is about 0.8, buffer #4, #7 and S20_B7 are consistent, within ±0.002 R units, or ±0.001 pH units. The disagreement between #4 and S20_B7 is ±0.012 R units, or ±0.005 pH units. Figure 4-5-B compares buffer #6, #7, #8, #9 and S20_B7 around R=1.28. However, an up to 0.02 R units or 0.007 pH units disagreement is observed between them.

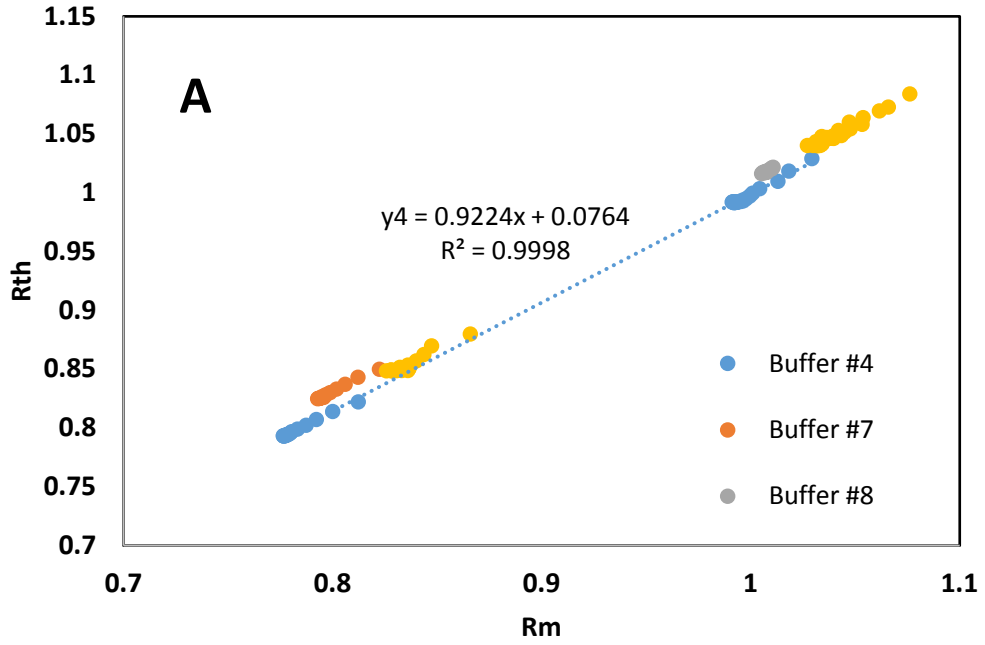

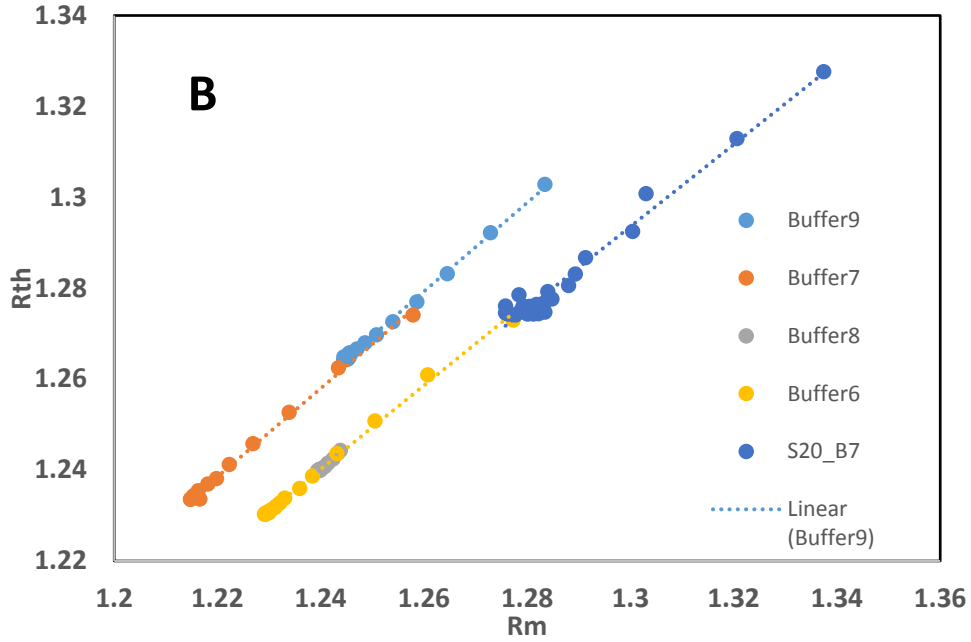

Figure 4-4: Comparison between TRIS buffers. A) Buffer #4, #7, #8 compare with Buffer S20_B7. B) Buffer #6, #7, #8, #9 compare with Buffer S20_B7.

Nevertheless, the result still indicates that a single buffer calibration is practicable, if the buffer is carefully made and determined on a high quality spectrophotometer. This simplicity would make calibration of spectrophotometric pH sensors much

easier than before, when an accuracy of better than 0.005 pH units can also be achieved.

4.2.5 Assessment of accuracy and precision

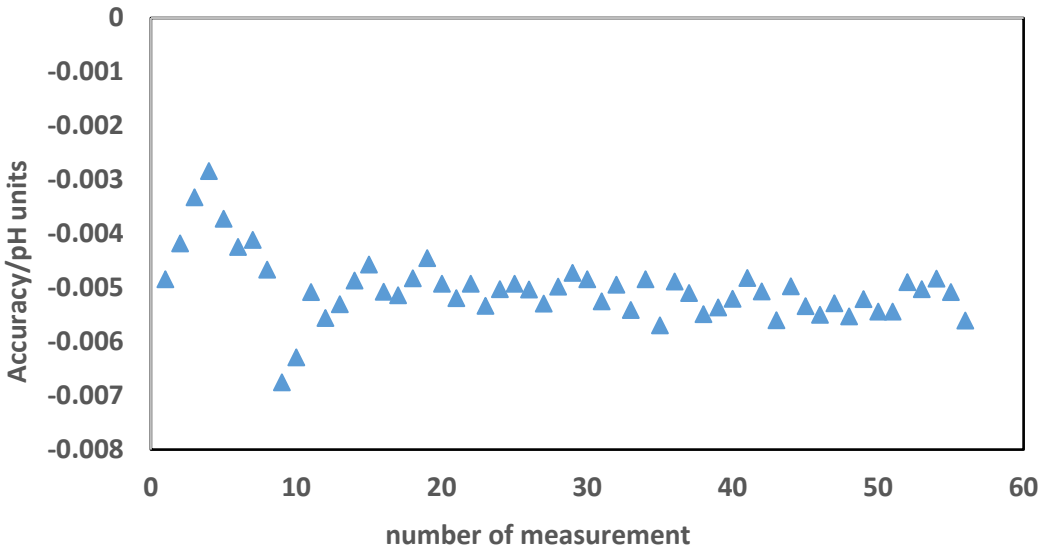

Figure 4-5: The accuracy assessment of Sensor S/N16.

The accuracy of the pH sensor was determined by comparing the sensor's measurement with the theoretical pH value of certificated Tris buffer calculated using Equation 4-1. 55 measurements were made in total, in two sets: firstly, 8 measurements are made in a frequency of one measurement every ten minutes; then, stopped for 1 hour, before another 47 measurements are made at the same frequency. The conditions of the two sets are the same except one element: the LED is always on between measurements in the first set, while off in the second set. The results show that the average offset of the measured pH from the calculated value is -0.004 pH units for the first set, -0.0052 for the second set, and -0.0050 for the average of both. The fact that the first measurement in the second set sees an offset of nearly -0.007 pH units, the second measurement -0.0063 and the third -0.0051, indicates that

the LED-off operation effects the accuracy of the sensor's pH measurement. This is likely to be caused by the LED's wavelength shift when it is heated up, resulting an error on the measurement (The calibration process is done when the LED always on, hence an offset of wavelength is introduced). The stand deviation of the second set is 0.0004 pH units, which can be regarded as the sensor's precision, as they are measured under the same condition, using the same sample and in a continuous test.

4.2.6 Quality verification of the preparation of non-equimolar TRIS buffer

A non-equal molar TRIS buffer of salinity 20 was made, whose recipe is list as Table 4-1.

Table 4-1: Composition of buffer solution in synthetic seawater of salinity 20

Component	mol/(kg H_2O)	Weight (g)
NaCl	0.180557	5.18335
Na_2SO_4	0.016466	1.14896
KCl	0.005953	0.21799
$MgCl_2$	0.030801	14.765[a]
$CaCl_2$	0.006049	3.16037[b]
HCl	0.06	29.8965[c]
Tris	0.08	4.75864

a The concentration of MgCl2 solution is 1.0139 mol/kg-solution

b The concentration of CaCl2 solution is 0.9303 mol/kg-solution

c The concentration of HCl solution is 0.9852 mol/kg-solution

The predicted salinity and pH of the buffer solution are 20 and 7.598 (25°C), respectively. The actual pH measured using the spectrophotometer at 25°C is 7.594.

The -0.004 pH deviation possibly comes from the TRIS salt, which was not dried due to the lack of a proper oven. The insufficient quantity of TRIS would result in a decrease of pH of the buffer solution as TRIS salt is alkaline.

4.3 Summary and future work

The sensor has an accuracy of -0.005 pH units, a precision of ±0.0004 pH units. By employing the *R-adjusting* method, spectrophotometric pH sensors can be calibrated in an easier, cheaper and faster way. This method provides a solution for issues in spectrophotometric pH measurements, such as dye perturbation, dilution effect and optical construction, on top of its simplicity. The convenient calibration method benefits not only this particular type sensor, but also provides a new way to view or to improve other sensors or instruments who use spectrophotometric method.

Chapter 5 Field Deployment

In this chapter the results of several field deployments of the pH sensors are discussed. The timeline runs from the year of 2014 to 2017, during which the sensors were improved after each deployment. The purpose of this exercise is to document the method by which problems were defined and solved.

5.1 The competition of Wendy Schmidt Ocean Health XPRIZE

The pH sensor was entered into the Wendy Schmidt Ocean Health XPRIZE, a worldwide competition of high quality *in situ* pH sensors. The competition contains four phases – Phase 1, the registration; Phase 2, the lab trials; which included accuracy (2a) and stability (2b) tests; Phase 3, the coastal trial; and Phase 4, the ocean trial. The OTEG sent three entries (sensors, #1, #2 and #3) to the competition.

5.1.1 Phase 2a Accuracy Trial

Phase 2a took place in a temperature-constant (approx. 13°C) laboratory at Monterey Bay Aquarium Research Institute (MBARI), California, USA. In Phase 2a, the three sensors were immersed in three containers separately filled with TRIS buffer; the sample to be analysed. The sample was pumped through the filter assembled on the inlet to the sensor. After several measurements, the competition organisers added acid into the vessels to change the pH of the buffer, and several more measurements

were taken. During this time, water samples were taken from the containers by the XPRIZE staff for analysis by a bench-top spectrophotometer. The data obtained by the spectrophotometer were regarded as “the standard” and the data obtained by the sensors were compared against these standards. A Science Advisory Board and Judges then decided if the sensors met the standard of accuracy or not.

Table 1 and Table 2 show the results obtained from the OTEG sensor. The “accuracy” was calculated as the difference between the sensor data and the spectrophotometer data, and the standard deviation of a single measurement was regarded as the “precision”.

Table 5-1: Before the injection of acid.

Unit	Sample Number	T (ºC)	S	Spectrophotometer pH	Sensor pH	Standard Deviation	Difference (pH unit)
#1	1	13.350	35	8.2439	8.24265	0.001028	-0.001
	2	13.356	35	8.2424		(n=18)	-0.0002
#2	1	12.907	35	8.2582	8.193561	0.000959	-0.064
	2	12.930	35	8.2651		(n=18)	-0.072
#3	1	13.270	35	8.2412	8.131221	0.002246	-0.110
	2	13.550	35	8.2358		(n=18)	-0.105

Table 5-2: After the injection of acid.

Unit	Sample Number	T (ºC)	S	Spectrophotometer pH	Sensor pH	Standard Deviation	Difference (pH unit)
#1	1	13.375	35	7.9155	7.986446	0.007564	0.071
	2	13.390	35	7.9177		(n=13)	0.069
#2	1	13.272	35	7.9536	7.888777	0.008091	-0.065
	2	13.273	35	7.9530		(n=13)	-0.064
#3	1	13.407	35	7.9283	7.792854	0.000515	-0.135
	2	13.407	35	7.9271		(n=13)	-0.134

From the data in Table 1 and Table 2 it is apparent that Sensor #1 gave a good accuracy of within 0.001 and 0.0002 pH units during two separate measurements, whereas Sensors #2 and #3 only had accuracies of about 0.07 and 0.1 pH units, respectively. However, after the acid addition, the accuracy of #1 degraded to 0.07 pH units, while the accuracies of #2 and #3 remained the same. As for precision, prior to the addition of acid #1 and #2 yielded precisions of ±0.001 pH units (Table 1), while the precision of #3 was ±0.002 pH units. After the addition of the acid, the precisions of #1 and #2 degraded to ±0.008 pH units (almost 10 times increase in error), while the precision of #3 remained the same. The reason for the degradation in precision was because the sensors were not proper calibrated at that stage of competition – the calibration in described in Chapter 4 was done after Phase 2a was completed. The sensors were only calibrated using one TRIS buffer over a range of temperatures, but once the pH of the sample went beyond the range of this TRIS buffer, the calibration was no longer accurate.

5.1.2 Phase 2b Stability Trial

In Phase 2b, one of the three sensors (#1), together with entries from the other teams, was immersed (hung on a mooring line) in a tank filled with filtered seawater (ozonised regularly to kill microorganisms) at 3-meter depth to perform the stability test. During this time, the initial frequency of measurements was every two hours. The intended duration of the measurement period was 12 weeks, from 24th September to 8th December 2014, but because of corrosion of some of the sensors in the tank during the test, the Science Advisory Board and Judges decided to halt Phase 2b on 12th November.

Sensor #1 suffered some corrosion on one of the screws on the housing, but no damage to the functional sensor itself. A total of 407 measurements were made over 34 days of operation. The length of operating time was shorter than it was expected to be, based on the batteries power capacity. This was because the sensor needs a minimum voltage to operate, but the voltage of the batteries dropped below this required level before the batteries ran out of power.

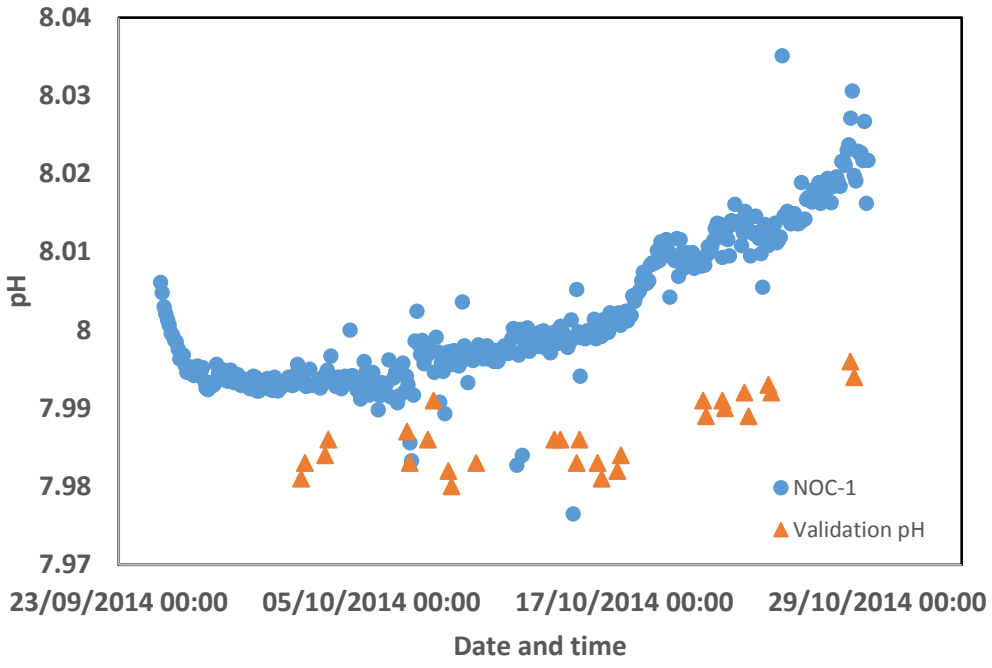

Figure 5-1: XPRIZE Phase2b_NOC-1_MBARI_September 2014, with Liu's characteristics (Liu et al., 2011)

Figure 5-1 shows the data calculated using CTD-determined temperature and salinity. Because the thermistors had not yet been assembled on the sensor at the time of deployment, there was no temperature data from inside the chip. The CTD temperature and salinity data were provided by the test organiser, but were not made available until after the trial. Hence, the temperature was estimated to be 15°C and the salinity as 35 psu. Once these CTD data were received in October 2015, the true result of the sensor was calculated.

On average, the OTEG sensor measurement is 0.015 pH units higher than the pH values validated by discrete samples. At the beginning of the trial, the offset was smaller than 0.010 pH units. During the evening of 7th of October 2014, the rope from which the sensor was hung slipped, causing the sensor to fall to the bottom of the 10 metre-deep tank. Although the sensor was designed to operate at a pressure of up to 4000m by filling the chamber with oil, the sensor was not oil-filled for XPRIZE trial because trial was designed to test deployment in surface water. Nevertheless, staff of XPRIZE rescued the sensor quickly, and during the night the sensor was returned to the surface. While there was no apparent damage to the sensor and all the connections were still tightly closed and the sensor was fully functional, the data quality was impacted. The accuracy drifted to 0.016 pH units deviation from the true value, and then gradually to 0.02 pH units over the next three weeks. It is not clear whether the drift was caused by the impact of the sensor with the bottom of the tank, or simply because of indicator degradation or other instrument drift.

This deployment was the first time that the pH sensor had been run for more than a month. The test proved that the sensor is capable of long-term automatic pH measurements with no calibration required, but the drift in accuracy required further investigation.

5.1.3 Phase 3 Coastal Trials

Phase 3 took place at Seattle Aquarium in Seattle, Washington, USA, on 7th February 2015, over a period of 28 days. All the teams' sensors were submerged no deeper than 1m from the surface in a bespoke tank on Pier 59 and were separated from the other sensors to avoid any potential interference. Water from Elliott Bay

(Puget Sound) was pumped into and out of the tank throughout the testing period. Validation samples were collected from multiple locations in the tank, twice per day, to confirm that the tank was sufficiently homogenous.

Sensor #2 was entered into this Phase because its thermistors were still functioning. However, Sensor #2 failed to inject indicator dye into the chip from the beginning of Phase 3, so the sensor could not produce any meaningful data during this stage of competition.

5.1.4 Conclusion

Table 5-1 and 5-2 show the final rankings of all teams.

This was the first international competition for the NOC pH sensor, although it was still under development. In particular, the temperature-monitoring (thermistors) was lacking for most of the competition and it was not known at this time that the pumping would heat up the chip significantly. This meant that it was not possible to cancel out the perturbation effect on the indicator and set up a true calibration procedure. Nevertheless, the sensor still showed its potential to be an easy-use stable device for ocean study. This is evidenced by the fact that during Phase 3 (the Ease-of-Use Section), the sensor ranked third, only finishing behind the Optode developed by an Austrian team, and the SAMI-pH sensor developed by Sunburst, the commercial company who were the ultimate winners of this competition. Overall, the accuracy, precision and stability of the NOC sensor were good considering that the sensor had not been properly calibrated. These issues were solved later in the project, as described in Chapter 4.

Table 5-3: Final rankings of Phase 2.

TEAM	Phase 2a Accuracy	Phase 2b Stability	Phase 2b Precision	Overall Phase 2
ANB Sensors	3	6 - tied	6 - tied	6
Blue Devil	6 - tied	6 - tied	6 - tied	13 - tied
Cross Strait	6 - tied	5 - tied	1 - tied	9
Durafet 1 - Deep Sea Durafet	1 - tied	3	1- tied	3
Durafet 2 – SeaFET	4	6 - tied	6 - tied	7
Durafet 3 – SeapHOx	2	6 - tied	6 - tied	5
HpHS	6 - tied	4	3	11
NOC-UK	5	5 - tied	4	8
Optode Team Austria	6 - tied	5 - tied	5 - tied	12 - tied
OSU Fabe Sastry	6 - tied	6 - tied	6 - tied	13 - tied
pHFineScale	6 - tied	5 - tied	2	10
SEAS	1 - tied	5 - tied	5 - tied	4 - tied
SINDEN	1 - tied	5 - tied	5 - tied	4 - tied
SmartpHin	6 - tied	5 - tied	5 - tied	12 - tied
Sunburst 1 – tSAMI	1 - tied	1	1 - tied	1
Sunburst 2 – iSAMI	1 - tied	2	1 - tied	2
Xylem	6 - tied	5 - tied	5 - tied	12 - tied

Table 5-4: Final rankings of Phase 3.

TEAM	Phase 3 Ease of Use	Phase 3 Cost - Accuracy Purse	Phase 3 Precision - Accuracy Purse	Phase 3 Stability - Accuracy Purse	Overall Phase 3
ANB Sensors	8 - tied	1 - tied	--	--	--
Blue Devil	6 - tied	1 - tied	--	--	--
Cross Strait	6 - tied	1 - tied	--	--	--
Durafet 1 - Deep Sea Durafet	8 - tied	2 - tied	2 - tied	3 - tied	3
Durafet 2 - SeaFET	8 - tied	2 - tied	3	4	6
Durafet 3 - SeapHOx	8 - tied	4	1 - tied	3 - tied	4
HpHS	5	6	1 - tied	2- tied	5
NOC-UK	3 - tied	5 - tied	--	--	--

Optode Team Austria	1	1 - tied	--	--	--
OSU Fabe Sastry	7	1 - tied	--	--	--
pHFineScale	8 - tied	1 - tied	--	--	--
SEAS	8 - tied	7	--	--	--
SINDEN	8 - tied	5 - tied	--	--	--
SmartpHin	4	1 - tied	--	--	--
Sunburst 1 - tSAMI	2 - tied	3 - tied	1 - tied	1	2
Sunburst 2 - iSAMI	2 - tied	1 - tied	2 - tied	2 -tied	1
Xylem	3 - tied	3 - tied	--	5	--

5.2 Dock deployment at NOCS

Two pH sensors were tested *in situ* at the NOCS dockside for separate two periods, in December 2015 and February-May 2017. The first deployment in the winter of 2015 was carried using Sensor NOC-pH-14, while the second deployment in the spring of 2017 used Sensor NOC-pH-16. The first deployment lasted for one week before the sensor failed to inject indicator dye into the chip, probably due to a manufacturing flaw. However, the second deployment lasted for three months until the primary productivity of the dock water became so high that abundant algae blocked the sensor intake within a short period.

Between the SenseOCEAN deployment (See Section 6.3) and the second dock deployment the temperature gradient between the optical cell and the thermistors was noticed and corrected (See Chapter 3 and Chapter 4 for the correction method). The temperature correction improved the accuracy of the sensor from ±0.010 pH units to ±0.003 pH units, as described below.

5.2.1 Location

The two dock deployments were both performed on the pontoon at NOCS. NOCS lies at the head of Southampton Water, a tidal estuary between the south coast of Hampshire, UK and the Isle of Wight. Three rivers (the Test, the Itchen and the Hamble) flow into Southampton Water, bringing particularly high fluxes of freshwater after extended periods of rain. The busy port shipping and urban environment also bring disturbances to the seawater environment.

The pontoon is located in a dock outside the building of NOCS, five meters away from bank. The pontoon is normally used to moor research boats.

The sensor was suspended from the pontoon, approximately one meter below the surface. A CTD recorder was co-located at the same depth. The sensor was powered by a service box fixed on the pontoon, for the convenience of providing a stable power supply during the test period.

5.2.2 Equipment and settings

The pH sensor is described in Chapter 2. In the first deployment, Sensor S/N #14 was not oil-filled and the measurments were undertaken every hour. Sensor S/N #16 was oil-filled during the second deployment and the measurements were initially undertaken every 10 minutes, but were reduced to half-hourly after five days.

Two different CTD recorders were used for the two deployments: an EXO2 Multiparameter Sonde (YSI Inc. USA) for the first deployment and a SBE 37-SM MicroCAT C-T (P) Recorder (SBE 37 for short) for the second deployment. The

CTD recorders provided temperature, salinity and depth measurements for the pH calculation.

Figure 5-2: Dock deployment: the sensor and the CTD.

The service box was a black plastic box (made by OTEG) that was connected to the domestic 230V AC electricity supply, and was also fitted with RS232 and USB connectors. The sensor was connected to the box with a waterproof cable. Raw data was transferred to a laptop computer from the sensor and the CTD manually every week. During these two deployments the pH was calculated after transfer of the data.

5.2.3 Discrete samples

Discrete water samples were collected to provide comparison pH measurements using a bench-top spectrophotometer, as well as using pH values calculated from DIC and TA measurements. The discrete sample collections followed the procedure

for DIC and TA samples in “Guide to Best Practices for Ocean CO_2 Measurements” Chapter SOP 1(Dickson et al., 2007). pH samples were also collected in glass bottles, leaving 1% of headspace and poisoned by 0.05% saturated mercuric chloride. The pH samples were analysed immediately after collection.

Because the data process involves temperature correction back to *in situ* conditions, which may cause errors that exceed the desired accuracy, the thermostat of the bench-top spectrophotometer was set as close to the *in situ* temperature as possible. Typically, this was between 10°C to 15°C; which is a compromise between the *in situ* temperature (7°C to 11°C) and the laboratory room temperature (20°C). A Fisher Thermometer S/N #80614977 was used to determine the temperature inside the 10 cm optical cell, with an accuracy of 0.02°C.

A bench-top spectrophotometer was used to analyse the pH samples. It contains a 10 cm cell, using the same dye as used in the sensor. Some samples were collected in more than one bottle, and were analysed at various temperatures, in order to determine the temperature dependence of pH measurements in the seawater of Southampton Water.

5.2.4 Result

5.2.4.1 The temperature dependence of pH in Southampton seawater

Four measurements were made during the second deployment. Table 5-4 shows the results.

An average of the measurements (except No.2) was taken as the mean value, or -0.0146 pH units per °C change in temperature. Measurement No.3 was regarded as an abnormal point. This value from temperature-pH dependence is smaller than

literature reports of other coastal water in the world (Hunter, 1998). This discrepancy is probably because of a fresh water dilution effect that reduces the buffer capacity of seawater.

Table 5-5: The temperature dependence of seawater pH of Southampton Seawater

Measurement Number	pH	T in the thermostat	T dependence (pH/°C)
1	7.9316	10.577	-0.01477
	7.8633	15.200	
2	7.9450	10.462	-0.01576
	7.8711	15.152	
3	7.8600	15.129	-0.01443
	7.7906	19.938	
4	7.9184	10.550	-0.01458
	7.8503	15.222	

5.2.4.2 Temperature difference inside and outside the sensor

Because the sensor produces heat from the pump movements and the LED light emission, the temperature inside the sensor chip is always higher than the *in situ* water temperature. The difference can be determined by comparing the sensor thermistor's reading and the CTD reading. For NOC-pH-14, the average difference was +1.988°C. However, for NOC-pH-16, the difference was +2.862°C at the beginning when the measurement frequency was one measurement every ten minutes, but reduced to +1.307°C when the measurement frequency was reduced to one measurement every half-hour. These temperature offsets are not affected by the seawater temperature significantly. Figure 5-3 shows the heat production inside the sensor, and that it reaches a stable state after a couple of hours.

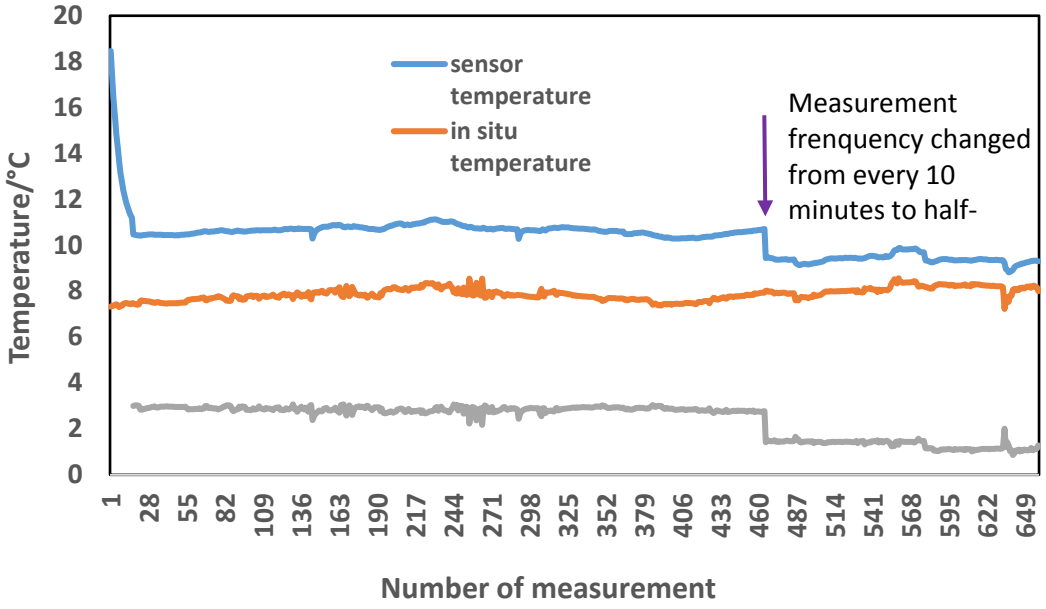

Figure 5-3: The temperature gap observed in February 2017.

The quantification of the temperature difference is important. First it makes it possible to quantitatively assess a few methods that can mitigate the temperature difference. NOC-pH-16 was oil-filled in the housing while NOC-pH-14 was not, so it is likely that the oil filling improved the heat exchange rate between the inner part of the sensor and the surrounding seawater. It makes sense because air is more heat-insulating compared to liquid. Lower frequency also helps to reduce the heat. Nevertheless, the temperature difference is still significant. Therefore it is clear that accurate temperature measurements, i.e. good, reliable thermistors, inside the sensor chip is vital for the pH sensor.

5.2.4.3 In situ deployment data

Figure 5-4 shows the result from the first deployment in December 2015. The average offset of the sensor pH measurements from spectrophotometric result is -0.010 pH units. The pH signal is positively correlated to the tide height, with two peaks a day. This is because the seawater is more alkaline than the fresh water in

nearby River Itchen and River Test. There is a slight delay in the pH signal compared to the tide height, and it is because of the slightly offset of the tide record spot from the sensor deployment place.

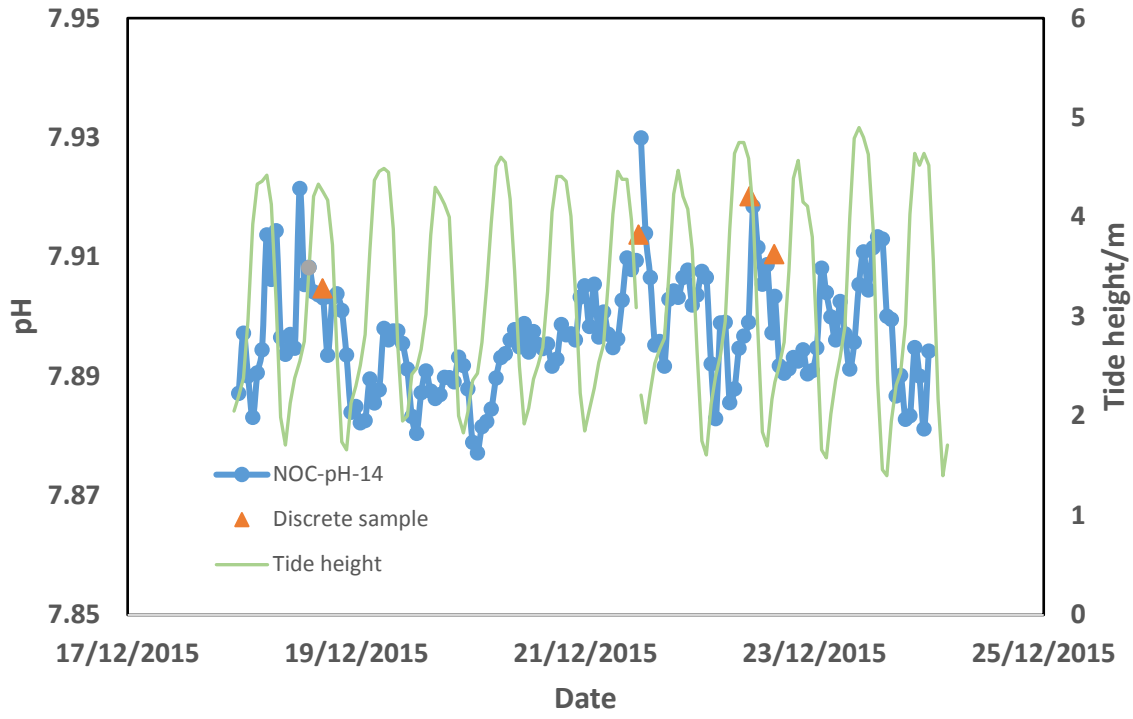

Figure 5-4: The dock deployment, December 2015.

Calculations based on the relationship between seawater carbonate system parameterscould help to distinguish between biological processes, mixing of waters and air-sea exchange. Atamanchuk et al. (2015) used salinity-derived alkalinity and pCO2 to calculate the fjord water DIC, and used O_2 optodes (Tengberg et al., 2006) to obtain O_2 concentration in the water. According to the Redfield ratio (Anderson and Sarmiento, 1994; Redfield, 1934; Redfield, 1963), on average, production or respiration of organic matter in the sea leads to changes of oxygen and carbon in a certain molar ratio, which could be 138:106 (1.30) as Redfield initially suggested or 170:117 (1.45) as modified in later years. Atamanchuk et al. (2015) examined the

changes of oxygen and carbon in the fjord deployment to find that the ratios of changes in different time were parallel, i.e. comparable to each other around a certain constant, when biological processes dominated the environment,. In Atamanchuk's case, the two comparable ratios were -1.38±0.02 and -1.21±0.02 (negative sign means the c of DIC correlates to the accumulation of O_2). Hence the primary production baseline could be determined. Deviations from the Redfield ratio indicated other dynamic processes in the environment. For example, a ratio of -1.95±0.05 means oversaturation of the water with respect to oxygen, which could possibly be facilitated by higher light availability, rapid onset of the bloom and lack of ventilation. Although air-sea gas exchange was excluded in their assumptions, large mixing events, such as a winter storm, could be seen from sudden spikes of oxygen followed by slow changes in DIC. Such events could be identified more precisely if other ancillary data are available, for instance, current speed, wave height, and ambient light information (PAR) and chlorophyll a concentration.

However, similar calculations in the NOC-pH sensor dock deployments are impossible, because two necessary datasets are lacking. The alkalinity-salinity relationship needs to be established *in situ*, i.e. water samples for alkalinity measurements should be collected during deployments, because the alkalinity-salinity relationship could vary in different time periods. In addition, the oxygen data are only available from the first deployment (one week long) and were not available in the second deployment.

The second deployment on the dock pontoon lasts for nearly three months (Figure 5-5). The accuracy was 0.003 pH units in the first two weeks (n=7). However, as the

weather gets warmer and finer, the sensor shows distinct daily cycles. They reached the peak at noon each day and fell during night, despite the salinity data indicated that there were two tides every day. Is it possible that the primary productivity in this area in this time of year was so high that even the tide signal was covered? Discrete sample analyses showed that the seawater pH in April in daytime was 0.02 pH units higher than the pH value in February. But the sensor measurements were 0.03 to 0.08 pH units higher than the benchtop analyses. This means that the filter on the sample inlet of the sensor was prone to biofouling. This inference is also supported by the fact that the pH signal daily cycles after every change of filter became much milder. The biofouling could significantly affect the sensor within three days in fine weather. The third evidence of biofouling is that in cloudy and stormy days (when the salinity signal was noisy, rather than distinct two cycles a day) in early May, after ten days since the change of the filter, the sensor measured the pH value 0.02 pH units higher than benchtop spectrophotometer did, which was a narrower error than in April.

The deployment in the winter and the spring of 2017 shows that the sensor can reach a good accuracy (0.003 pH units) in the first three weeks of deployment, but the filter used on the sensor is prone to biofouling. The next work for this sensor is to introduce anti-biofouling measures on the filter.

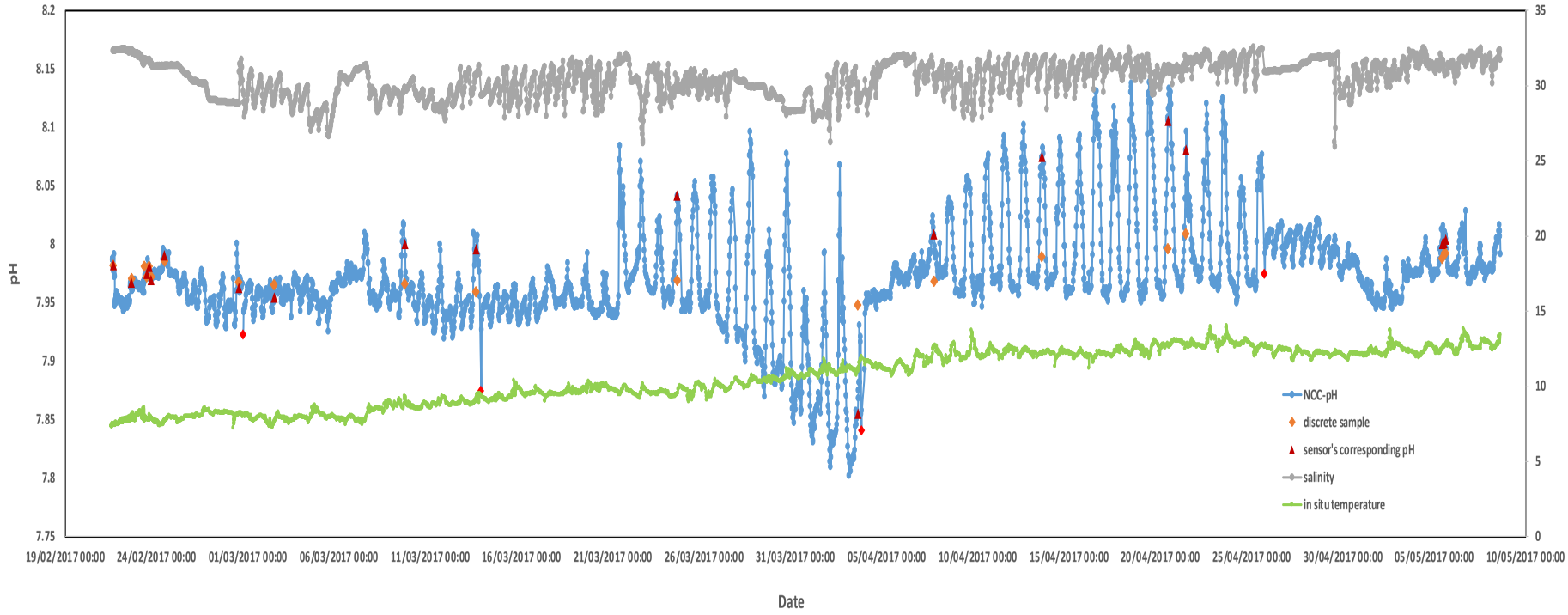

Figure 5-5: The dock pontoon deployment, February 2017. The yellow diamonds represents the pH value obtained from discrete samples measured on a spectrophotometer. The red triangles highlight the corresponding pH value that the sensor measured. The red diamonds marks when the filter was changed.

At the end of the three-month deployment, a non-equimolar Tris buffer with a pH value of 7.7 at 25°C (see Chapter 4.2 for the preparation) was used to test the accuracy drift of the sensor. The Tris buffer and the sensor were placed in the dock overnight for the buffer to reach the *in situ* temperature. Results are shown in Figure 5-6. The sensor basically reflected the pH change of the Tris buffer, but there was an average offset of -0.013 pH units between them, which can be regarded as the accuracy drift of the sensor.

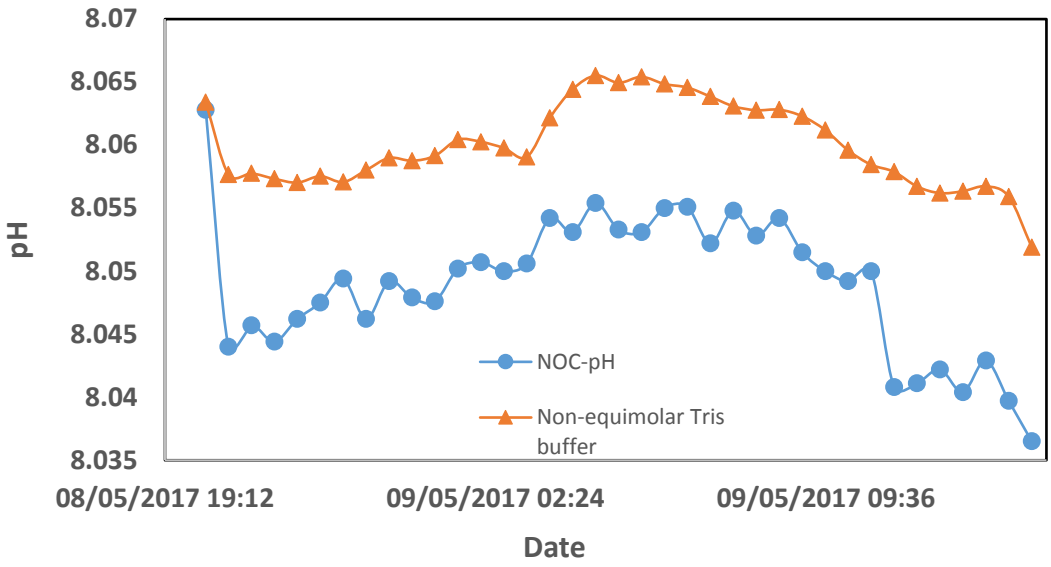

Figure 5-6: The accuracy drift test of the sensor. The blue round points are the measurements of NOC-pH sensor, and the red triangle points are the theoretically calculated pH value of the Tris buffer at the corresponding time and temperature.

The drift might be caused by several factors. First, the indicator dye might have got bleached during the deployment, though this should be unlikely because the dye was carefully wrapped with aluminium foil and placed inside the housing to protect it from bleaching. Second, despite the 0.45 µm filter, there might have some particles or biomass had passed it and contaminated the absorption cell. This hypothesis is supported by the blank intensity decrease (the photodiode-received signal dropped

from 4.5 voltage to 3.0 voltage) during the deployment. The intensity decrease might also have affect the measurement resolution and thus affect the accuracy of the measurement. These are some hypothesis, and to reveal the real reason, further investigation needs to be done in the future.

5.3 SenseOCEAN deployment

SenseOCEAN is an EU Seventh Framework Programme project to develop highly integrated multifunction and cost-effective *in situ* marine sensors. As part of this project, NOC sensors, including the pH sensor, took part in a costal deployment in Kiel, Germany, in September 2016.

5.3.1 Profiling

The sensor was first deployed during a costal cruise of the research vessel *Littoria* between 12th and 14th, September 2016. Two profile data sets were successfully collected on 13th and 14th of September.

5.3.1.1 Method

The sensor was fixed on a frame with a CTD and other SenseOCEAN sensors. The profile started from the bottom depth, i.e. 24 metres. Then it stopped at each depth for 1 hour, for 4 steps in total. The NOC pH sensor takes ten minutes to obtain the data for each measurement, thus six measurements were taken for each depth step. Water samples were also collected from the Niskin bottles and analysed two weeks later in the laboratory of GEOMAR. For each depth step, two samples were collected: 1) DIC&TA, 2) pH.

Figure 5-7: The NOC-pH sensor (front centre) with CTD and rosette sampler

5.3.1.2 Data

The pH data of Niskin water samples are currently unavailable, so the validated pH was calculated from the analysed DIC and TA data.

At each depth, the first measurement point of the sensor is usually different from the validated pH (Figures 5-8 and 5-9). This is because the sensor starts a rinse cycle immediately after the previous measurement when it was still at the previous depth step. Hence, the first sample from each depth step was in a mixture of two steps. Complete rinsing of the sensor may take two measurement steps because the filter

used in this deployment requires additional rinsing to replace all of the previous sample.

This profile deployment was the first time the sensor was filled with oil and deployed to a pressure equal to 24 metres depth. The sensor worked during the first three days of the cruise, but both thermistors stopped working after the profiling. Investigation of the thermistors later in NOCS laboratory showed crash damage to the head of the thermistors. This may have been caused by the pressure change during this depth profile, which pushed the thermistors deep into the channel and broke them when the sensor was detached and removed from the frame.

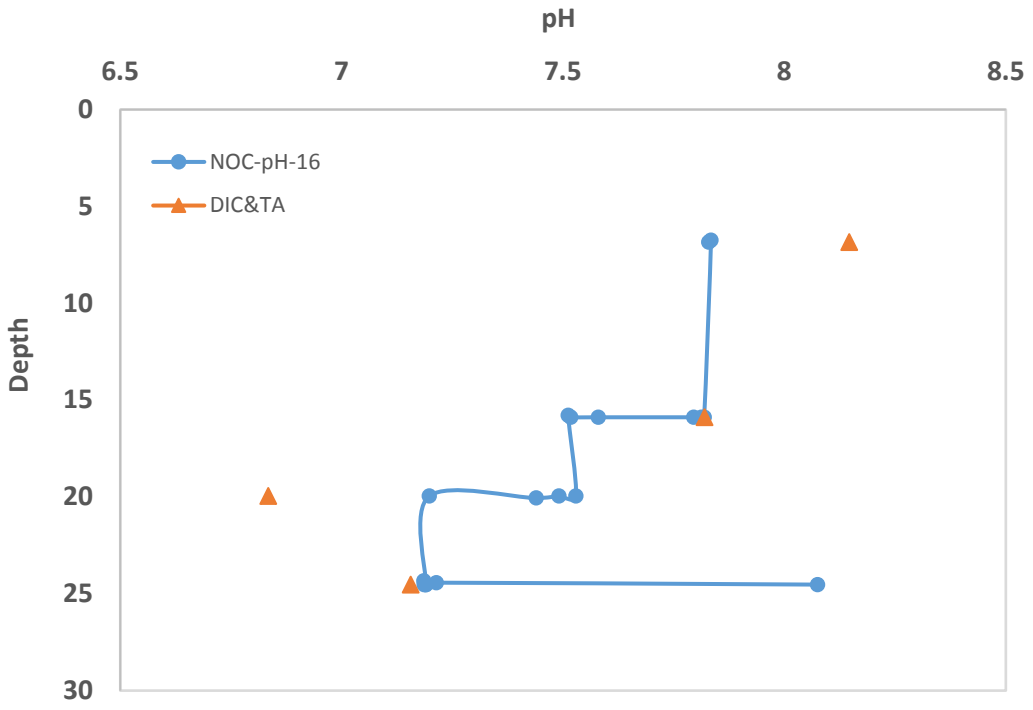

Figure 5-8: The profile data on 13th September 2016

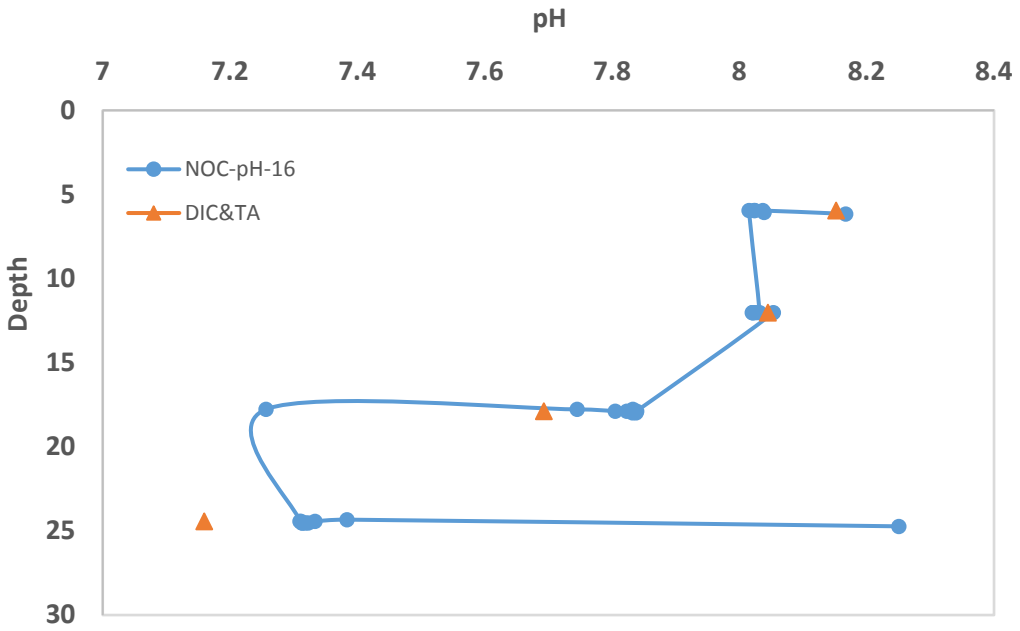

Figure 5-9: The profile data on 14th September 2016

5.3.2 Pontoon deployment

In the second week of SenseOCEAN deployment, the NOC pH sensor was deployed on the pontoon of GEOMAR. This pontoon is located in the port of Kiel, with busy ship movements from research and commercial vessels and tourists ships. The environment is dominated by the port business rather than tidal cycles. The sensor was deployed in the surface water, and co-located with other SenseOCEAN sensors and a CTD. Discrete water samples were collected using a Niskin bottle, and analysed one week later.

The sensor ran for one week, until the end of the SenseOCEAN deployment on 21st September 2016. Both thermistors stopped working at the beginning of the pontoon deployment, so there was no temperature data from within the sensor. Hence the sensor cell temperature was estimated from the CTD data, assuming that the

warming effect in the sensor results in a +1.1°C difference. Using this assumption, the average offset between the sensor and the discrete sample was 0.056 pH units.

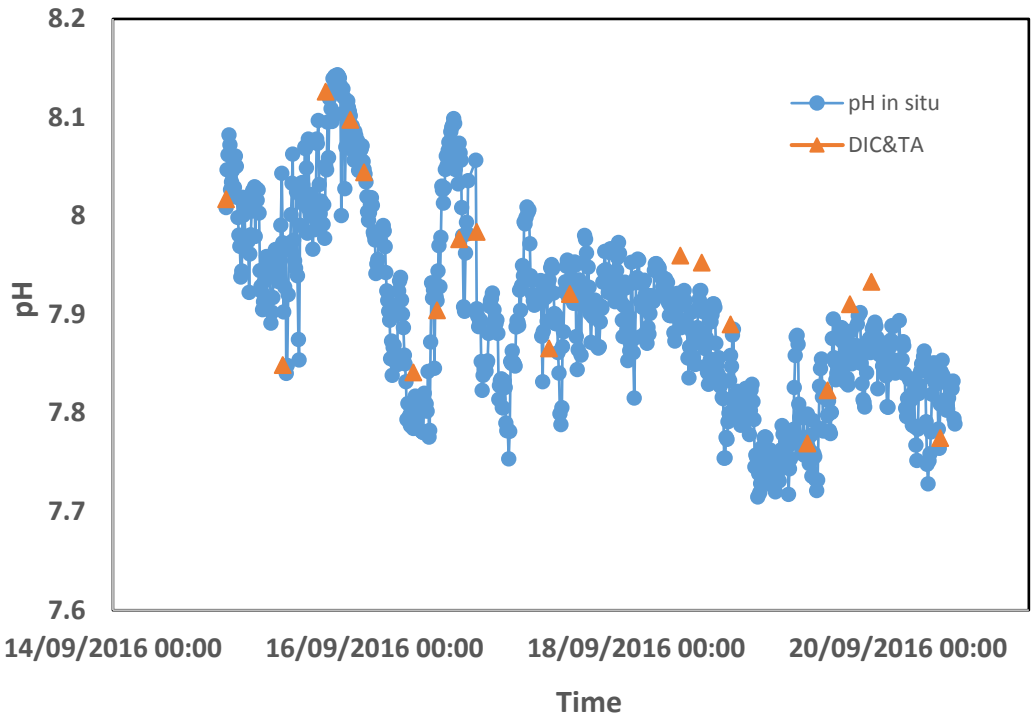

Figure 5-10: The data of the SenseOCEAN deployment on the pontoon of GEOMAR, Kiel, Germany, September 2016

There are several factors that affect the pH accuracy of the sensor measurements. First, the pH sample usually needs to be analysed immediately after collected, as the pCO_2 of the sample changes quickly. Thus, the pH of the discrete sample may have changed during one week interval between collection and analysis. Second, the indicator dye used in the GEOMAR laboratory was not purified. This omission may cause an error of up to 0.015 pH units (Liu et al., 2011). Third, the Niskin bottle was situated about two metres away from the sensor location, and this may also cause a minor error. However, after taking all these three factors into account, there are still

about 0.03 to 0.04 pH units of error that should be considered as the error of the sensor.

Chapter 6 Conclusion and future work

The NOC-pH sensor demonstrated in this thesis, is the first time that the microfluidic lab-on-chip sensors have been made for *in situ* pH measurements of seawater. It has a portable size of ϕ130 × 140 mm of the sensor itself and ϕ150 × 1000 mm as in the housing. It is energy efficient (3 W, if measuring at the highest frequency, i.e. every ten minutes.) and costs low reagent (2.2 µL per measurement). It is environmental friendly benefiting from its minimum waste volume (1.3 mL per measurement).

Multiple steps were undertaken to improve the accuracy and precision of the sensor. An uncertainty analysis were undertaken to reveal the major error sources of the sensor were the temperature measurement inside the sensor and the intensity measurement. Thermistors were then installed and carefully calibrated on the sensor, providing a temperature accuracy of 0.03 K. A novel method of regress absorbance at 434 nm against absorbance at 578 nm was used to eliminate the dye-induced pH perturbation. The R-adjusting calibration method was proved to have an accuracy of better than 0.005 pH units. After these steps were taken, the precision of the pH sensor was improved to 0.0004 pH units and the accuracy between the NOC-pH and Cary UV/Vis had been improved to 0.005 pH units.

Future work to improve this sensor is going to be a new design of the chip, including but not only an addition of a waveguide, a new layout of thermistors and addition of anti-biofouling reagent. To address the temperature and hence time dependent accuracy of calibrations (see chapter 4) which is likely due to LED power and spectral characteristics changing with temperature, the waveguide would direct a portion of the LEDs' emissions directly onto detectors to allow measurement of

intensity drift. The purchase of LEDs with right wavelength or the employment of wavelength filter is also important. Presently the sensor's twin-wavelength LED emits at 425 nm and 596 nm, rather than the mCP dye's maximum absorption wavelength 434 nm and 578 nm. This is due to the lack of commercial availability of such LED. However, with the right wavelength the LED could provide the most efficient output, in which way both reduces power consumption and improves precision. A custom twin-wavelength LED or two LEDs with the right wavelength would be the best solution, but if not available, filters would also be considered. Narrow band spectral filter(s) on the LEDs' output would more completely mitigate spectral changes and more closely match their output to the peaks in the dye absorption spectrum (see chapter 2). Such filters would need to be low-cost (<£250) and able to withstand the ambient pressure in our deployment scenarios. This would offset the effects of temperature variation on LED outputs both due to the environment and heating from within the sensor (see chapter 3) in various conditions and would also enable better calculation of reference baseline and alarms when faults arise. To further address the impact of temperature gradients in the sensor and the optical cell in particular (see chapter 3) the new layout of thermistors would allow the temperature to be measured in the middle or before of the optical cell (as well as at its end as done currently). This would enable a better understanding of the gradient, as well as a more accurate estimation of the temperature inside the cell. Field deployment (see chapter 5) suggests that biofouling could be a serious problem for accurate pH measurement: we observed up to 0.1 pH error attributable to this effect (see chapter 5). To address this the layout of the chip should also be re-design in order to add an ant-biofouling reagent to flush through the chip, and the input filter in particular between measurements. An alternative or additional measure

would be to add electro-chlorination to the filter (Delauney et al., 2015). To implement these enhancements a new state machine that controls the sensor's measurement procedure would certainly be needed. Alongside the additional accuracy drift tests and anti-biofouling study, of the improved sensor, as the sensor has only been tested in coastal waters, an open ocean deployment, as well as hyperbaric testing and deep ocean trial, would also be advised in future work.

Appendix A Matlab script for pH measurement

```
%% Manually input
%load file
file=load('20170327.csv'); % source file
file2=load('sbe37sm-rs232_03711464_2017_04_25.txt');

%result text name
text='test_20170327_CTD_Correct15_December_Calibration.txt';

%% write header of result  text
fid1=fopen(text,'w');
fprintf(fid1,'%4s                 %5s       %1s       %2s    %8s
%9s  %9s     %2s       %2s       %5s      %8s    %9s\r\n','Date','R
unNb','T','pH','nbpoints','Int434ref','Int578ref','T1','T2','D
epth','Salinity','In_situ_T');
fclose(fid1);

%% find temperature and unix_time
th1=file(:,6);th2=file(:,7);
unix_time=file(:,15);

%CTD data
CTD_unix_time=file2(:,7);
CTD_depth=file2(:,2);
CTD_salinity=file2(:,3);
CTD_temp=file2(:,4);

%% find runs
state=file(:,2); % state of the machine is in column 2
stateMeas=find(state==7); % start of measurement
startRun=[stateMeas(1)+10;stateMeas(diff(stateMeas)>1)+10]; %
delay for 10 points to get the fit data and define the start
of each run (i.e. when difference between rown No is >1)
endRun=[stateMeas(diff(stateMeas)>1);stateMeas(end)];

%% for each run, calculate the R0 and T and write to text
% for z=1:size(startRun)
for z=1:30
    RunNb=z;  % Here starts a loop for several runs
    Start=startRun(z);
    End=endRun(z);
    nbdata=End-Start+1;
    Int434=file(Start:End,3); %the data from beginning to end
of state 4
    Int578=file(Start:End,4);

    Int434ref=mean(Int434(400:600));%select ref when signal is
flat
    Int578ref=mean(Int578(400:600));
     %%%%%%%%%%%%%%%%%%%%%%%%%%%%%%%%%%%%%%%%%%%%%%%%%%%%%%%%%%
%%%%%%%%%%%%%%%%%
    %%                             ABSORBANCE
```

```
    %%%%%%%%%%%%%%%%%%%%%%%%%%%%%%%%%%%%%%%%%%%%%%%%%%%%%%%%%%%%%%%%%%%%
%%%%%%%%%%%%%%%%

Ri=NaN(nbdata,1);Abs434=NaN(nbdata,1);Abs578=NaN(nbdata,1); %O
therwise Abs434 will change size every loop

    %calculate absorbance and the ratio
    for i=1:nbdata
        Abs434(i)=-log10(Int434(i)/Int434ref);
        Abs578(i)=-log10(Int578(i)/Int578ref);
        Ri(i)=Abs578(i)/Abs434(i);
    end

    %find the processing data
    [maxAbs578,maxAbs578ROW]=max(Abs578);% Search for maximum
absorbance at 578 and the row which is found

AbsMax=maxAbs578ROW+dsearchn(Abs578(maxAbs578ROW:2400),0.600);
% Search for Maximum absorbance (row) that will be used to
process the data below 1.5 (from the 10th point to the max
abs)

AbsMin=AbsMax+dsearchn(Abs434(AbsMax:2400),0.1000);  %AbsMax-
1;% Search for Minimum absorbance (row) that will be used to
process the data above 0.001
    nbpoints=(AbsMin-AbsMax)+1;% nb of points used to process
the data
    %%%%%%%%%%%%%%%%%%%%%%%%%%%%%%%%%%%%%%%%%%%%%%%%%%%%%%%%%%%%%%%%%%%%
%%%%%%%%%%%%%%%
    %%                      INDICATOR CORRECTION
    %%%%%%%%%%%%%%%%%%%%%%%%%%%%%%%%%%%%%%%%%%%%%%%%%%%%%%%%%%%%%%%%%%%%
%%%%%%%%%%%%%%%
    % Calculate pH corrected from dye addition using Seidel et
al. 2008's method

    if nbpoints>10
        vec=AbsMax:AbsMin;% processing part of data

        x=Abs434(vec);y=Abs578(vec);
        fx=@(b,x)b(1)*x.^2+b(2)*x;% force to set a function
with an intercept of 0.
        b=rand(1,2);
        b=lsqcurvefit(fx,b,x,y);
        Rm=b(2);

        % thermistors' temperature reading
        V1=mean(th1(Start:Start+vec(end))); % the 5th and 7th
row of the file are thermistors' readings
        V2=mean(th2(Start:Start+vec(end)));
        T1=V1^3*0.0683-V1^2*0.3528+V1*7.1159-5.4884; % convert
from voltage to degree Celsius
        T2=V2^3*0.0734-V2^2*0.4119+V2*7.2806-6.3032;
        deltaT=T1-T2; % 1cm between the two thermistors
        if abs(deltaT)<1 % to see if the two thermistors
working well
```

```
            T=mean([T1 T2])+deltaT*2;
        else
            T=T2+0.333;
        end


        Date=datestr(unix_time(Start)/86400 +
datenum(1970,1,1)); %Convert unix time to date
        % look for salinity
        I=find(abs(CTD_unix_time-unix_time(Start))<31);
        [m,n]=size(I);
        if m>1
            I=I(1);
        end
        S=CTD_salinity(I);
        Depth=CTD_depth(I);
        In_situ_T=CTD_temp(I);

        % extinction coefficients by Liu et.al. 2011
        Tm=T+273.15;
        e1=-0.007662+4.5174*0.00001*Tm;
        e3bye2=-0.020813+2.60262*0.0001*Tm+1.0436*0.0001*(S-
35);

        a=-246.64209+0.315971*S+2.8855*0.0001*S^2;
        b=7229.23864-7.098137*S-0.057034*S^2;
        c=44.493382-0.052711*S;
        d=0.0781344;
        pKe2=a+b/Tm+c*log(Tm)-d*Tm;

        Rth=0.9997*Rm+0.0262;
        pH=pKe2+log10((Rth-e1)/(1-Rth*e3bye2));

        % Write the result in a text file
        fid2=fopen(text,'a+');

fprintf(fid2,'%20s %3.0f    %6.4f  %6.4f %6.0f      %6.4f
%6.4f   %6.4f    %6.4f   %6.4f    %6.4f    %6.4f\r\n',Date,Run
Nb,T,pH,nbpoints,Int434ref,Int578ref,T1,T2,Depth,S,In_situ_T);
        fclose(fid2);

        else
    end
    figure;
    subplot(2,1,1);plot((vec),Abs434(vec));hold
on;plot((vec),Abs578(vec),'m');
    subplot(2,1,2);plot(Abs434(vec),Abs578(vec));
end
```

Appendix B Matlab script of error propagation

```
clear all;
%%Input
S=35;
Tm=25; T=273.15+Tm;

uS=0.002; %uS=0.005 precision of TRIS buffer make-
up %uS=0.0028 using SeaBird 4 at 15C

A=0.9997; B=0.0262;
Rm=1.28;
Rth=A*Rm+B;
uA=0.00074;
uB=0.0013;

Iref434=3.207342; Iref578=3.130928;
I434=1.07323; I578=0.55511; %Maximum absorbance point

uIref434=0.00005*Iref434+0.003;
uIref578=0.00005*Iref578+0.003;

uI434=0;
uI578=0;

count=0;
U1=NaN(1,20);
U2=NaN(1,20);
U3=NaN(1,20);
```

```
U4=NaN(1,20);
upH=NaN(1,20);
precT=NaN(1,20);

%uA2 and uA1
uA2=1/log(10)*sqrt((uIref578/Iref578)^2+(uI578/I578)^2);
uA1=1/log(10)*sqrt((uIref434/Iref434)^2+(uI434/I434)^2);

for uT=0.001:0.005:0.1
count=count+1;
precT(count)=uT;

%%upK2e2
%Dissociation constant of purified mCP by Liu et al. 2011
a=-246.64209+0.315971*S+2.8855*0.0001*S^2;
b=7229.23864-7.098137*S-0.057034*S^2;
c=44.493382-0.052711*S;
d=0.0781344;
pK2e2=a+b/T+c*log(T)-d*T;

DT=-b/(T^2)+c/T-d;
DS=(0.0005771-0.114068/T)*S+0.315974-7.098137/T-
0.052711*log(T);

upK2e2=sqrt((DT*uT)^2+(DS*uS)^2);

%%uR
D1=1/log(Iref434/I434)*1/Iref578;
D2=-1/log(Iref434/I434)*1/I578;
D3=-log(Iref578/I578)*1/(Iref434*log(Iref434/I434)^2);
D4=log(Iref578/I578)*1/(I434*log(Iref434/I434)^2);
```

```
uRm=sqrt((D1*uIref578)^2+(D2*uI578)^2+(D3*uIref434)^2+(D4*uI43
4)^2);

% uRth=sqrt((Rm*uA)^2+(A*uRm)^2+uB^2);

uRth=0.02;


%%ue1 and ue4

ue1=0.000045174*uT;

ue4=sqrt((0.000260262*uT)^2+(0.00010436*uS)^2);


%%upH

%ratio of extinction coefficents of purified mCP by Liu et al.
2011

e1=-0.004363+0.00003598*T;

e4=-0.016224+0.000242851*T+0.0000505663*(S-35);

DpK=1;

DRth=1/log(10)*(1-e1*e4)/((1-Rth*e4)*(Rth-e1));

De1=-1/log(10)*1/(Rth-e1);

De4=1/log(10)*Rth/(1-Rth*e4);


upH(count)=sqrt((DpK*upK2e2)^2+(DRth*uRth)^2+(De1*ue1)^2+(De4*
ue4)^2);

U1(count)=DpK*upK2e2;

U2(count)=DRth*uRth;

U3(count)=De1*ue1;

U4(count)=De4*ue4;


end


plot(precT,upH,precT,U1,precT,U2,precT,U3,precT,U4);

xlabel('uncertainty of temperature measurement/K');

ylabel('uncertainty of pH/pH units');
```

```
legend('upH','contribution of upK2e2','contritbution of
uRth','contribution of ue1','contribution of ue4');

title('uncertainty of pH with a salinity measurement precision
of ±0.002');
```

Reference

Adornato, L., Kaltenbacher, E., Byrne, R. H., Liu, X. W., Sharp, J. & Ieee. Development of a Portable Carbon System Sensor for Ocean Acidification Research. *Oceans 2016 Mts/Ieee Monterey*, 7 (2016).

Aigner, D., Borisov, S. M., Orriach Fernandez, F. J., Fernandez Sanchez, J. F., Saf, R. & Klimant, I. New fluorescent pH sensors based on covalently linkable PET rhodamines. *Talanta* **99**, 194-201, doi:10.1016/j.talanta.2012.05.039 (2012).

Aigner, D., Freunberger, S. A., Wilkening, M., Saf, R., Borisov, S. M. & Klimant, I. Enhancing Photoinduced Electron Transfer Efficiency of Fluorescent pH-Probes with Halogenated Phenols. *Analytical chemistry* **86**, 9293-9300 (2014).

Aigner, D., Ungerboeck, B., Mayr, T., Saf, R., Klimant, I. & Borisov, S. M. Fluorescent materials for pH sensing and imaging based on novel 1,4-diketopyrrolo- 3,4-c pyrrole dyes. *Journal of Materials Chemistry C* **1**, 5685-5693, doi:10.1039/c3tc31130a (2013).

Anderson, L. A. & Sarmiento, J. L. Redfield ratios of remineralization determined by nutrient data analysis. *Global biogeochemical cycles* **8**, 65-80 (1994).

Aßmann, S., Frank, C. & Körtzinger, A. Spectrophotometric high-precision seawater pH determination for use in underway measuring systems. *Ocean Science* **7**, 597-607, doi:10.5194/os-7-597-2011 (2011).

Atamanchuk, D., Kononets, M., Thomas, P. J., Hovdenes, J., Tengberg, A. & Hall, P. O. Continuous long-term observations of the carbonate system dynamics in the water column of a temperate fjord. *Journal of Marine Systems* **148**, 272-284 (2015).

Bates, N. R., Best, M. H. P., Neely, K., Garley, R., Dickson, A. G. & Johnson, R. J. Detecting anthropogenic carbon dioxide uptake and ocean acidification in the North Atlantic Ocean. *Biogeosciences* **9**, 2509-2522, doi:10.5194/bg-9-2509-2012 (2012).

Bates, R. & Culberson, C. Hydrogen ions and the thermodynamic state of marine systems. *The Fate of Fossil Fuel CO2 in the Oceans, edited by: Andersen, NR and Malahoff, A., Plenum Press, New York*, 45-61 (1977).

Beaton, A. D., Cardwell, C. L., Thomas, R. S., Sieben, V. J., Legiret, F. E., Waugh, E. M., Statham, P. J., Mowlem, M. C. & Morgan, H. Lab-on-chip measurement of nitrate and nitrite for in situ analysis of natural waters. *Environmental science & technology* **46**, 9548-9556, doi:10.1021/es300419u (2012).

Bellerby, R. G. J., Olsen, A., Johannessen, T. & Croot, P. A high precision spectrophotometric method for on-line shipboard seawater pH

measurements: the automated marine pH sensor (AMpS). *Talanta* **56**, 61-69, doi:10.1016/s0039-9140(01)00541-0 (2002).

Bergveld, P. Thirty years of ISFETOLOGY - What happened in the past 30 years and what may happen in the next 30 years. *Sensors and Actuators B-Chemical* **88**, 1-20, doi:10.1016/s0925-4005(02)00301-5 (2003).

Bockmon, E. E. & Dickson, A. G. An inter-laboratory comparison assessing the quality of seawater carbon dioxide measurements. *Marine Chemistry* **171**, 36-43, doi:10.1016/j.marchem.2015.02.002 (2015).

Bresnahan, P. J., Wirth, T., Martz, T. R., Andersson, A. J., Cyronak, T., D'Angelo, S., Pennise, J., Melville, W. K., Lenain, L. & Statom, N. A sensor package for mapping pH and oxygen from mobile platforms. *Methods in Oceanography* **17**, 1-13 (2016).

Briggs, E. M., Sandoval, S., Erten, A., Takeshita, Y., Kummel, A. C. & Martz, T. R. Solid State Sensor for Simultaneous Measurement of Total Alkalinity and pH of Seawater. *ACS Sens.* **2**, 1302-1309, doi:10.1021/acssensors.7b00305 (2017).

Byrne, M., Ho, M., Wong, E., Soars, N. A., Selvakumaraswamy, P., Shepard-Brennand, H., Dworjanyn, S. A. & Davis, A. R. Unshelled abalone and corrupted urchins: development of marine calcifiers in a changing ocean. *Proc. R. Soc. B-Biol. Sci.* **278**, 2376-2383, doi:10.1098/rspb.2010.2404 (2011).

Byrne, R. H. STANDARDIZATION OF STANDARD BUFFERS BY VISIBLE SPECTROMETRY. *Analytical chemistry* **59**, 1479-1481, doi:10.1021/ac00137a025 (1987).

Byrne, R. H. & Breland, J. A. HIGH-PRECISION MULTIWAVELENGTH PH DETERMINATIONS IN SEAWATER USING CRESOL RED. *Deep-Sea Research Part a-Oceanographic Research Papers* **36**, 803-810, doi:10.1016/0198-0149(89)90152-0 (1989).

Caldeira, K. & Wickett, M. E. Ocean model predictions of chemistry changes from carbon dioxide emissions to the atmosphere and ocean. *Journal of Geophysical Research* **110**, doi:10.1029/2004jc002671 (2005).

Canadell, J. G., Le Quere, C., Raupach, M. R., Field, C. B., Buitenhuis, E. T., Ciais, P., Conway, T. J., Gillett, N. P., Houghton, R. A. & Marland, G. Contributions to accelerating atmospheric CO2 growth from economic activity, carbon intensity, and efficiency of natural sinks. *Proceedings of the National Academy of Sciences of the United States of America* **104**, 18866-18870, doi:10.1073/pnas.0702737104 (2007).

Carter, B. R., Radich, J. A., Doyle, H. L. & Dickson, A. G. An automated system for spectrophotometric seawater pH measurements. *Limnology and Oceanography: Methods* **11**, 16-27, doi:10.4319/lom.2013.11.16 (2013).

Chen, M. *Chemical Oceanography*. (Ocean Press, 2009).

Chou, J. C. & Weng, C. Y. Sensitivity and hysteresis effect in Al2O3 gate pH-ISFET. *Mater. Chem. Phys.* **71**, 120-124, doi:10.1016/s0254-0584(00)00513-7 (2001).

Ciais, P., Sabine, C., Bala, G., Bopp, L., Brovkin, V., Canadell, J., Chhabra, A., DeFries, R., Galloway, J., Heimann, M., Jones, C., Le Quéré, C., Myneni, R. B., Piao, S. & Thornton, P. in *Climate Change 2013: The Physical Science Basis. Contribution of Working Group I to the Fifth Assessment Report of the Intergovernmental Panel on Climate Change* (eds T.F. Stocker *et al.*) Ch. 6, 465–570 (Cambridge University Press, 2013).

Clarke, J. S., Achterberg, E. P., Rerolle, V. M. C., Bey, S. A. K., Floquet, C. F. A. & Mowlem, M. C. Characterisation and deployment of an immobilised pH sensor spot towards surface ocean pH measurements. *Analytica chimica acta* **897**, 69-80, doi:10.1016/j.aca.2015.09.026 (2015).

Clayton, T. D. & Byrne, R. H. SPECTROPHOTOMETRIC SEAWATER PH MEASUREMENTS - TOTAL HYDROGEN-ION CONCENTRATION SCALE CALIBRATION OF M-CRESOL PURPLE AND AT-SEA RESULTS. *Deep-Sea Research Part I-Oceanographic Research Papers* **40**, 2115-2129, doi:10.1016/0967-0637(93)90048-8 (1993).

Delauney, L., Kada, B., Karenn, B., Jean-Yves, C., Mathieu, D., Bertrand, F., Celia, G., Gerard, G., Yves, L., Michel, P., Emmanuel, R. & Ieee. Biofouling protection by electro-chlorination on optical windows for oceanographic sensors and imaging devices. *Oceans 2015 - Genova*, 10 (2015).

DelValls, T. A. & Dickson, A. G. The pH of buffers based on 2-amino-2-hydroxymethyl-1,3-propanediol ('tris') in synthetic sea water. *Deep-Sea Research Part I-Oceanographic Research Papers* **45**, 1541-1554, doi:10.1016/s0967-0637(98)00019-3 (1998).

Dickson, A. G., Sabine, C. L. & Christian, J. R. *Guide to Best Practices for Ocean CO2 Measurements*. Vol. PICES Special Publication 3 (2007).

Dickson, A. G., Sabine, C. L. & Christian, J. R. *Guide to Best Practices for Ocean CO2 Measurements*. (PICES Spec. ed., 2007).

Dore, J. E., Lukas, R., Sadler, D. W., Church, M. J. & Karl, D. M. Physical and biogeochemical modulation of ocean acidification in the central North Pacific. *Proceedings of the National Academy of Sciences of the United States of America* **106**, 12235-12240, doi:10.1073/pnas.0906044106 (2009).

Fages, M., Doizi, D. & Deniau, G. Study and design of an optode for pH measurement. *Optical Sensors 2013* **8774**, 7, doi:10.1117/12.2020771 (2013).

Feely, R. A., Doney, S. C. & Cooley, S. R. Ocean Acidification: Present Conditions and Future Changes in a High-CO2 World. *Oceanography* **22**, 36-47, doi:10.5670/oceanog.2009.95 (2009).

Friis, K., Kortzinger, A. & Wallace, D. W. R. Spectrophotometric pH measurement in the ocean: Requirements, design, and testing of an autonomous charge-coupled device detector system. *Limnol Oceanogr-Meth* **2**, 126-136 (2004).

Gabriel, M., Forja, J., Rubio, J. & Gómez-Parra, A. Temperature and salinity dependence of molar absorptivities of thymol blue: Application to the spectrophotometric determination of pH in estuarine waters. *Ciencias Marinas* **31**, 309-318 (2005).

Gattuso, J.-P. & Hansson, L. *Ocean Acidification*. (Oxford University Press Inc., New York, 2011).

Gonski, S. F., Cai, W. J., Ullman, W. J., Joesoef, A., Main, C. R., Pettay, D. T. & Martz, T. R. Assessment of the suitability of Durafet-based sensors for pH measurement in dynamic estuarine environments. *Estuar Coast Shelf S* **200**, 152-168, doi:10.1016/j.ecss.2017.10.020 (2018).

Gonzalez-Davila, M., Santana-Casiano, J. M., Rueda, M. J. & Llinas, O. The water column distribution of carbonate system variables at the ESTOC site from 1995 to 2004. *Biogeosciences* **7**, 3067-3081, doi:10.5194/bg-7-3067-2010 (2010).

Gray, S. E. C., DeGrandpre, M. D., Moore, T. S., Martz, T. R., Friederich, G. E. & Johnson, K. S. Applications of in situ pH measurements for inorganic carbon calculations. *Marine Chemistry* **125**, 82-90, doi:DOI 10.1016/j.marchem.2011.02.005 (2011).

Hakonen, A., Anderson, L. G., Engelbrektsson, J., Hulth, S. & Karlson, B. A potential tool for high-resolution monitoring of ocean acidification. *Analytica chimica acta* **786**, 1-7, doi:10.1016/j.aca.2013.04.040 (2013).

Hansson, I. The determination of dissociation constants of carbonic acid in synthetic sea water in the salinity range of 20–40‰ and temperature range of 5–30◦ C. *Acta Chem. Scandinavica* **27**, 931-944 (1973).

Hecht, M., Kraus, W. & Rurack, K. A highly fluorescent pH sensing membrane for the alkaline pH range incorporating a BODIPY dye. *The Analyst* **138**, 325-332, doi:10.1039/c2an35860c (2013).

Hemmink, G. J., Oars, J., Weusten, B. L., Bredenoord, A. J., Timmer, R. & Smout, A. Ambulatory Esophageal pH-Impedance Reflux Monitoring: A Comparison Between Antimony, ISFET and Glass pH Electrodes. *Gastroenterology* **136**, A297-A297 (2009).

Hunter, K. A. The temperature dependence of pH in surface seawater. *Deep-Sea Research Part I-Oceanographic Research Papers* **45**, 1919-1930, doi:Doi 10.1016/S0967-0637(98)00047-8 (1998).

Johnson, K. S., Jannasch, H. W., Coletti, L. J., Elrod, V. A., Martz, T. R., Takeshita, Y., Carlson, R. J. & Connery, J. G. Deep-Sea DuraFET: A Pressure Tolerant pH Sensor Designed for Global Sensor Networks. *Analytical chemistry* **88**, 3249-3256, doi:10.1021/acs.analchem.5b04653 (2016).

Jung, W., Jang, A., Bishop, P. L. & Ahn, C. H. A polymer lab chip sensor with microfabricated planar silver electrode for continuous and on-site heavy metal measurement. *Sensors and Actuators B: Chemical* **155**, 145-153 (2011).

Lai, C. Z., DeGrandpre, M. D., Wasser, B. D., Brandon, T. A., Clucas, D. S., Jaqueth, E. J., Benson, Z. D., Beatty, C. M. & Spaulding, R. S. Spectrophotometric measurement of freshwater pH with purified meta-cresol purple and phenol red. *Limnology and Oceanography: Methods* **14**, 864-873 (2016).

Le Quéré, C., Moriarty, R., Andrew, R. M., Peters, G. P., Ciais, P., Friedlingstein, P., Jones, S. D., Sitch, S., Tans, P. & Arneth, A. Global carbon budget 2014. *Earth System Science Data* **7**, 47-85 (2015).

Liu, X., Patsavas, M. C. & Byrne, R. H. Purification and characterization of meta-cresol purple for spectrophotometric seawater pH measurements. *Environmental science & technology* **45**, 4862-4868, doi:10.1021/es200665d (2011).

Lueker, T. J., Dickson, A. G. & Keeling, C. D. Ocean pCO(2) calculated from dissolved inorganic carbon, alkalinity, and equations for K-1 and K-2: validation based on laboratory measurements of CO2 in gas and seawater at equilibrium. *Marine Chemistry* **70**, 105-119, doi:10.1016/s0304-4203(00)00022-0 (2000).

Martz, T. R., Carr, J. J., French, C. R. & DeGrandpre, M. D. A submersible autonomous sensor for spectrophotometric pH measurements of natural waters. *Analytical chemistry* **75**, 1844-1850, doi:Doi 10.1021/Ac020568l (2003).

Martz, T. R., Connery, J. G. & Johnson, K. S. Testing the Honeywell Durafet for seawater pH applications. *Limnology and Oceanography: Methods* **8**, 172-184, doi:10.4319/lom.2010.8.172 (2010).

McClendon, J. The standardization of a new colorimetric method for the determination of the hydrogen ion concentration, CO2 tension, and CO2 and O2 content of sea water, of animal heat, and of CO2 of the air, with a summary of similar data on bicarbonate solutions in general. *Journal of Biological Chemistry* **30**, 265-288 (1917).

McElligott, S., Byrne, R. H., Lee, K., Wanninkhof, R., Millero, F. J. & Feely, R. A. Discrete water column measurements of CO2 fugacity and pH(T) in seawater: A comparison of direct measurements and thermodynamic calculations. *Marine Chemistry* **60**, 63-73, doi:10.1016/s0304-4203(97)00080-7 (1998).

McLaughlin, K., Dickson, A., Weisberg, S. B., Coale, K., Elrod, V., Hunter, C., Johnson, K. S., Kram, S., Kudela, R., Martz, T., Negrey, K., Passow, U., Shaughnessy, F., Smith, J. E., Tadesse, D., Washburn, L. & Weis, K. R. An evaluation of ISFET sensors for coastal pH monitoring applications. *Reg. Stud. Mar. Sci.* **12**, 11-18, doi:10.1016/j.rsma.2017.02.008 (2017).

Milani, A., Statham, P. J., Mowlem, M. C. & Connelly, D. P. Development and application of a microfluidic in-situ analyzer for dissolved Fe and Mn in natural waters. *Talanta* **136**, 15-22, doi:10.1016/j.talanta.2014.12.045 (2015).

Nakamura, M., Ohki, S., Suzuki, A. & Sakai, K. Coral Larvae under Ocean Acidification: Survival, Metabolism, and Metamorphosis. *PLoS One* **6**, 7, doi:10.1371/journal.pone.0014521 (2011).

Nakano, Y., Kimoto, H., Watanabe, S., Harada, K. & Watanabe, Y. W. Simultaneous vertical measurements of in situ pH and CO2 in the sea using spectrophotometric profilers. *J. Oceanogr.* **62**, 71-81, doi:10.1007/s10872-006-0033-y (2006).

Nemzer, B. V. & Dickson, A. G. The stability and reproducibility of Tris buffers in synthetic seawater. *Marine Chemistry* **96**, 237-242, doi:http://doi.org/10.1016/j.marchem.2005.01.004 (2005).

Ogilvie, I. R., Sieben, V. J., Mowlem, M. C. & Morgan, H. Temporal optimization of microfluidic colorimetric sensors by use of multiplexed stop-flow architecture. *Analytical chemistry* **83**, 4814-4821, doi:10.1021/ac200463y (2011).

Ogilvie, I. R. G., Sieben, V. J., Floquet, C. F. A., Zmijan, R., Mowlem, M. C. & Morgan, H. Reduction of surface roughness for optical quality microfluidic devices in PMMA and COC. *J. Micromech. Microeng.* **20**, 8, doi:10.1088/0960-1317/20/6/065016 (2010).

Okazaki, R. R., Sutton, A. J., Feely, R. A., Dickson, A. G., Alin, S. R., Sabine, C. L., Bunje, P. M. E. & Virmani, J. I. Evaluation of marine pH sensors under controlled and natural conditions for the Wendy Schmidt Ocean Health XPRIZE. *Limnol Oceanogr-Meth* **15**, 586-600, doi:10.1002/lom3.10189 (2017).

Patsavas, M. C., Byrne, R. H. & Liu, X. W. Purification of meta-cresol purple and cresol red by flash chromatography: Procedures for ensuring accurate spectrophotometric seawater pH measurements. *Marine Chemistry* **150**, 19-24, doi:10.1016/j.marchem.2013.01.004 (2013).

Perez de Vargas Sansalvador, I. M., Fay, C. D., Cleary, J., Nightingale, A. M., Mowlem, M. C. & Diamond, D. Autonomous reagent-based microfluidic pH sensor platform. *Sensors and Actuators B: Chemical* **225**, 369-376, doi:10.1016/j.snb.2015.11.057 (2016).

MS Excel Program Developed for CO2 System Calculations (Analysis Center, Oak Ridge National Laboratory, U.S. Department of Energy, Oak Ridge, Tennessee, 2006).

Pörtner, H.-O., Karl, D. M., Boyd, P. W., Cheung, W. W. L., Lluch-Cota, S. E., Nojiri, Y., Schmidt, D. N. & Zavialov, P. O. in *Climate Change 2014: Impacts, Adaptation, and Vulnerability. Part A: Global and Sectoral Aspects. Contribution of Working Group II to the Fifth Assessment Report of the Intergovernmental Panel on Climate Change* (eds C.B. Field *et al.*) Ch. 6, 411-484 (Cambridge University Press, 2014).

Pratt, K. W. Measurement of pHT values of Tris buffers in artificial seawater at varying mole ratios of Tris:Tris·HCl. *Marine Chemistry* **162**, 89-95, doi:10.1016/j.marchem.2014.03.003 (2014).

Redfield, A. C. On the proportions of organic derivatives in sea water and their relation to the composition of plankton. *James Johnstone memorial volume*, 176-192 (1934).

Redfield, A. C. The influence of organisms on the composition of seawater. *The sea* **2**, 26-77 (1963).

Rérolle, V. *Development and Deployment of an in situ Sensor for Seawater pH Based on the Spectrophotometric Method* PhD thesis, University of Southampton, (2013).

Rérolle, V. M., Floquet, C. F., Harris, A. J., Mowlem, M. C., Bellerby, R. R. & Achterberg, E. P. Development of a colorimetric microfluidic pH sensor for autonomous seawater measurements. *Analytica chimica acta* **786**, 124-131, doi:10.1016/j.aca.2013.05.008 (2013).

Robertbaldo, G. L., Morris, M. J. & Byrne, R. H. SPECTROPHOTOMETRIC DETERMINATION OF SEAWATER PH USING PHENOL RED. *Analytical chemistry* **57**, 2564-2567, doi:10.1021/ac00290a030 (1985).

Seidel, M. P. A sensor for in situ spectrophotometric measurements of seawater pH. (2006).

Seidel, M. P., DeGrandpre, M. D. & Dickson, A. G. A sensor for in situ indicator-based measurements of seawater pH. *Marine Chemistry* **109**, 18-28, doi:DOI 10.1016/j.marchem.2007.11.013 (2008).

Seiter, J. C. & DeGrandpre, M. D. Redundant chemical sensors for calibration-impossible applications. *Talanta* **54**, 99-106, doi:10.1016/s0039-9140(00)00635-4 (2001).

Spaulding, R., DeGrandpre, M. & Harris, K. Autonomous pH and pCO(2) Measurements in Marine Environments Quantifying the Inorganic Carbon System With In-Situ SAMI Technology. *Sea Technol* **52**, 15-+ (2011).

Takahashi, T., Sutherland, S. C., Wanninkhof, R., Sweeney, C., Feely, R. A., Chipman, D. W., Hales, B., Friederich, G., Chavez, F., Sabine, C., Watson, A., Bakker, D. C. E., Schuster, U., Metzl, N., Yoshikawa-Inoue, H., Ishii, M., Midorikawa, T., Nojiri, Y., Kortzinger, A., Steinhoff, T., Hoppema, M., Olafsson, J., Arnarson, T. S., Tilbrook, B., Johannessen, T., Olsen, A., Bellerby, R., Wong, C. S., Delille, B., Bates, N. R. & de Baar, H. J. W. Climatological mean and decadal change in surface ocean pCO(2), and net sea-air CO2 flux over the global oceans. *Deep-Sea Res Pt Ii* **56**, 554-577, doi:10.1016/j.dsr2.2008.12.009 (2009).

Tengberg, A., Hovdenes, J., Andersson, H. J., Brocandel, O., Diaz, R., Hebert, D., Arnerich, T., Huber, C., Körtzinger, A. & Khripounoff, A. Evaluation of a lifetime-based optode to measure oxygen in aquatic systems. *Limnology and Oceanography: Methods* **4**, 7-17 (2006).

Tou, Z. Q., Chan, C. C. & Leong, S. A fiber-optic pH sensor based on polyelectrolyte multilayers embedded with gold nanoparticles. *Measurement Science & Technology* **25**, doi:10.1088/0957-0233/25/7/075102 (2014).

Wang, Z. A., Sonnichsen, F. N., Bradley, A. M., Hoering, K. A., Lanagan, T. M., Chu, S. N., Hammar, T. R. & Camilli, R. In Situ Sensor Technology for Simultaneous Spectrophotometric Measurements of Seawater Total Dissolved Inorganic Carbon and pH. *Environmental science & technology*, doi:10.1021/es504893n (2015).

Wang, Z. H. A., Liu, X. W., Byrne, R. H., Wanninkhof, R., Bernstein, R. E., Kaltenbacher, E. A. & Patten, J. Simultaneous spectrophotometric flow-through measurements of pH, carbon dioxide fugacity, and total inorganic carbon in seawater. *Analytica chimica acta* **596**, 23-36, doi:10.1016/j.aca.2007.05.048 (2007).

Wencel, D., Abel, T. & McDonagh, C. Optical Chemical pH Sensors. *Analytical Chemistry* **86**, 15-29, doi:10.1021/ac4035168 (2014).

Wong, P. P., Losada, I. J., Gattuso, J.-P., Hinkel, J., Khattabi, A., McInnes, K. L., Saito, Y. & Sallenger, A. in *Climate Change 2014: Impacts, Adaptation, and Vulnerability. Part A: Global and Sectoral Aspects. Contribution of Working Group II to the Fifth Assessment Report of the Intergovernmental Panel on Climate Change* (eds C.B. Field *et al.*) Ch. 5, 361-409 (Cambridge University Press, 2014).

Yang, B., Patsavas, M. C., Byrne, R. H. & Ma, J. Seawater pH measurements in the field: A DIY photometer with 0.01 unit pH accuracy. *Marine Chemistry* **160**, 75-81, doi:10.1016/j.marchem.2014.01.005 (2014).

Yao, W. S. & Byrne, R. H. Spectrophotometric determination of freshwater pH using bromocresol purple and phenol red. *Environmental science & technology* **35**, 1197-1201, doi:10.1021/es001573e (2001).

Yao, W. S., Liu, X. W. & Byrne, R. H. Impurities in indicators used for spectrophotometric seawater pH measurements: Assessment and remedies. *Marine Chemistry* **107**, 167-172, doi:10.1016/j.marchem.2007.06.012 (2007).

Zhang, H. & Byrne, R. H. Spectrophotometric pH measurements of surface seawater at in-situ conditions: absorbance and protonation behavior of thymol blue. *Marine Chemistry* **52**, 17-25, doi:http://dx.doi.org/10.1016/0304-4203(95)00076-3 (1996).

Zou, Z., Jang, A., MacKnight, E. T., Wu, P.-M., Do, J., Shim, J. S., Bishop, P. L. & Ahn, C. H. An on-site heavy metal analyzer with polymer lab-on-a-chips for continuous sampling and monitoring. *IEEE Sens. J.* **9**, 586-594 (2009).